OIPE IAP22 FEB 22 2008 PATENT & TRADEMARK OFFICE

Attorney's Docket No.: 42P17761 Patent

IN THE UNITED STATES PATENT AND TRADEMARK OFFICE

In Re Application of:
Stephen W. Montgomery et al.

U.S. Serial No: 10/773,004

Filed: February 4, 2004

For: THREE-DIMENSIONAL NANOTUBE STRUCTURE

Examiner: McCracken, Daniel

Art Unit: 1793

Commissioner for Patents
P.O. Box 1450
Alexandria, VA 22313-1450

I hereby certify that this correspondence is being deposited with the United States Postal Service as first class mail with sufficient postage in an envelope addressed to the Commissioner for Patents, PO Box 1450, Alexandria, Virginia 22313-1450

on February 20, 2008
Date of Deposit

Teresa Matthy
Name of Person Mailing Correspondence

Teresa Matthy 2/20/08
Signature Date

Declaration Under 37 CFR 1.132

Dear Sir:

I, Stephen W. Montgomery, declare the following:

1. I am an inventor of the above identified patent application, hereinafter "Application."

2. I have a Ph.D. in Mechanical Engineering from Purdue University, 2000. I received a M.S. in Mechanical Engineering from Purdue University, 1996, and a B.S. in Mechanical Engineering from the University of Illinois, 1994.

3. I have worked for the assignee, Intel Corporation, in the capacity of research and development and/or management since 2000. I was a Senior Thermal Architect at Intel Corporation at the inventors, including myself, conceptualized the content of the Application. I am presently employed at Intel Corporation as a design manager and program manager for Integrated Silicon Voltage Regulator (ISVR) Technologies.

4. I have reviewed the Application, including the claims of the Application. The declaration made herein is to establish compliance with the enablement and written description requirements under 35 U.S.C. § 112, first paragraph.

5. The Application teaches and claims in claims 1-10 a method of forming three-dimensional nanotube structures. The connector molecules and three-dimensional nanotube structures taught and claimed in claims 1-10 were conceptualized and devised utilizing HyperChem, a well-known molecular modeling software at the time of the invention.

6. Computer-aided molecular design was widely used in industry at the time of the invention as a method for modeling molecule structures and predicting structure-behavior relationships of molecules. Exhibit A attached herewith provides a list of references demonstrating the use of HyperChem in 2004. Exhibit A demonstrates that HyperChem was widely used in industry at the time of the invention as a method for modeling molecule structures and predicting structure-behavior relationships of molecules.

7. Functionalization of carbon nanotubes was widely studied at the time of the invention. Exhibit B attached herewith provides a list of references demonstrating the attachment of functional groups to carbon nanotubes. Exhibit B demonstrates that several methods of functionalizing carbon nanotubes were widely available at the time of the invention.

8. Based on these observations, it is my professional opinion that one of ordinary skill in the art at the time the invention was made, upon review of the Application, would be able to obtain commercially available nanotube segments, synthesize the connector molecule, and bond it to both the nanotube segments as well as to a plurality of other connector molecules to form a three-dimensional nanotube structure.

9. In addition, it is my professional opinion that the Application conveys with reasonable clarity to those skilled in the art, and particularly those familiar with computer-aided molecular design software such as HyperChem, that as of the filing date sought, the inventors, including myself, had possession of the invention as claimed in all presently pending claims.

10. I declare, to the best of my knowledge, that all statements made in this document are true, and that all statements made on the information and belief are believed to be true; and further that these statements were made with the knowledge that willful false statements and the like so made are punishable by fine or imprisonment, or both, under § 1001 of Title 18 of the United States Code,

and that such willful false statements may jeopardize the validity of the above-identified patent application or any patent issued thereon.

Dated: 2/20/06

Name: Stephen W. Montgomery

Appendix A
HyperChem in 2004

- Jayaseharan Johnsamuel, Youngjoo Byun, Thomas P. Jones, Yasuyuki Endo and Werner Tjarks. "A Convenient Method for the Computer-Aided Molecular Design of Carborane Containing Compounds." Bioorganic & Medicinal Chemistry Letters, Vol. 13, Issue 19, 16 October 2003, Pages 3213-3216.

- Nicolae Hurduc, Mihaela Prajinaru, Bogdan Donose, Dumitru Pavel and Natalia Hurduc. "Thermal behaviour and molecular modelling of some aromatic polyethers containing a hexamethylenic spacer." Polymer Degradation and Stability, Vol. 72, Issue 3, June 2001, Pages 441-445

- Yawei Wang, Xiaojun Yao, Xiaoyun Zhang, Ruisheng Zhang, Mancang Liu, Zhide Hu and Botao Fan. "The prediction for gas chromatographic retention indices of saturated esters on stationary phases of different polarity." Talanta, Vol. 57, Issue 4, 10 June 2002, Pages 641-652

- Jian Fang and Jie Li. "Quantum chemistry study on the relationship between molecular structure and corrosion inhibition efficiency of amides." Journal of Molecular Structure: THEOCHEM, Vol. 593, Issues 1-3, 27 September 2002, Pages 179-185.

Hyperchem in 2004

- A convenient method for the computer-Aided molecular design of carborane containing compounds
  Bioorganic & Medicinal Chemistry Letters, Volume 13, Issue 19, 16 October 2003, Pages 3213-3216
  Jayaseharan Johnsamuel, Youngjoo Byun, Thomas P. Jones, Yasuyuki Endo and Werner Tjarks
  - Noted in their conclusions: ***"In conclusion, the combination of HyperChem and SYBYL generated geometries of the o-, m-, and p-carborane clusters resembled closely those obtained previously using different theoretical and experimental methods."***

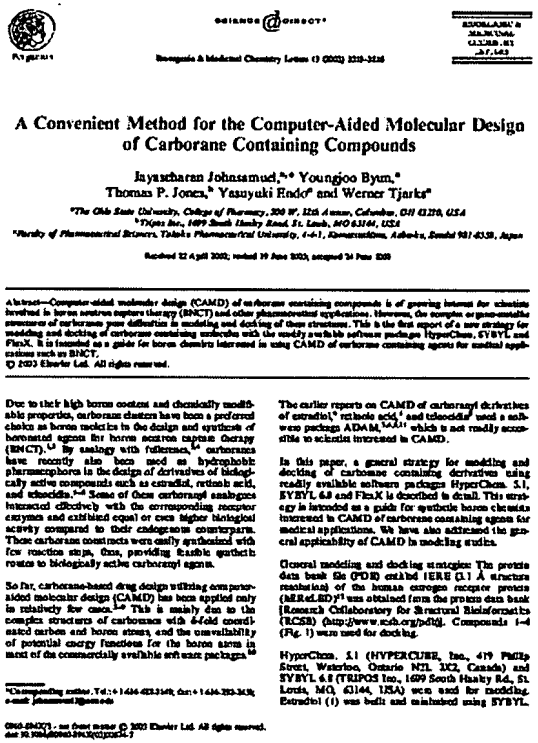

SCIENCE DIRECT®

Bioorganic & Medicinal Chemistry Letters 13 (2003) 3213–3216

A Convenient Method for the Computer-Aided Molecular Design of Carborane Containing Compounds

Jayaseharan Johnsamuel,[a,*] Youngjoo Byun,[a] Thomas P. Jones,[b] Yasuyuki Endo[c] and Werner Tjarks[a]

[a]The Ohio State University, College of Pharmacy, 500 W. 12th Avenue, Columbus, OH 43210, USA
[b]Tripos Inc., 1699 South Hanley Road, St. Louis, MO 63144, USA
[c]Faculty of Pharmaceutical Sciences, Tokushima Pharmaceutical University, 4-6-1, Komatsushima, Aubacho, Tokushima 981-8558, Japan

Received 12 April 2003; revised 19 June 2003; accepted 24 June 2003

Abstract—Computer-aided molecular design (CAMD) of carborane containing compounds is of growing interest for scientists involved in boron neutron capture therapy (BNCT) and other pharmaceutical applications. However, the complex organo-metallic structures of carboranes pose difficulties in modeling and docking of these structures. This is the first report of a new strategy for modeling and docking of carborane containing molecules with the readily available software packages HyperChem, SYBYL and FlexX. It is intended as a guide for boron chemists interested in using CAMD of carborane containing agents for medical applications such as BNCT.
© 2003 Elsevier Ltd. All rights reserved.

Due to their high boron content and chemically modifiable properties, carborane clusters have been a preferred choice as boron molecules in the design and synthesis of heteroatom agents for boron neutron capture therapy (BNCT).[1,2] By analogy with 'ullerenes,[3,4] carboranes have recently also been used as hydrophobic pharmacophores in the design of derivatives of biologically active compounds such as estradiol, retinoic acid, and tiloxicdin.[5–8] Some of these carboranyl analogues interacted effectively with the corresponding receptor enzymes and exhibited equal or even higher biological activity compared to their endogenous counterparts. These carborane constructs were easily synthesized with few reaction steps, thus, providing feasible synthetic routes to biologically active carboranyl agents.

So far, carborane-based drug design utilizing computer-aided molecular design (CAMD) has been applied only in relatively few cases.[5–8] This is mainly due to the complex structures of carboranes with 4-fold coordinated carbon and boron atoms, and the unavailability of potential energy functions for the boron atom in most of the commercially available software packages.[9]

The earlier reports on CAMD of carboranyl derivatives of estradiol,[6] retinoic acid,[7] and tiloxicdin[8] used a software package ADAM,[9,10,11] which is not readily accessible to scientists interested in CAMD.

In this paper, a general strategy for modeling and docking of carborane containing derivatives using readily available software packages HyperChem 5.1, SYBYL 6.8 and FlexX is described in detail. This strategy is intended as a guide for synthetic boron chemists interested in CAMD of carborane containing agents for medical applications. We have also addressed the general applicability of CAMD in modeling studies.

General modeling and docking strategies: The protein data bank file (PDB) entitled 1ERE (2.1 Å structure resolution) of the human estrogen receptor protein (hERα/LBD)[12] was obtained from the protein data bank [Research Collaboratory for Structural Bioinformatics (RCSB) (http://www.rcsb.org/pdb)]. Compounds 1–4 (Fig. 1) were used for docking.

HyperChem. 5.1 (HYPERCUBE, Inc., 419 Phillip Street, Waterloo, Ontario N2L 3X2, Canada) and SYBYL 6.8 (TRIPOS Inc., 1699 South Hanley Rd., St. Louis, MO, 63144, USA) were used for modeling. Estradiol (1) was built and minimized using SYBYL.

*Corresponding author. Tel.: +1-614-292-3149; fax: +1-614-292-3435; e-mail: johnsamuel.1@osu.edu

0960-894X/$ - see front matter © 2003 Elsevier Ltd. All rights reserved.
doi:10.1016/S0960-894X(03)00681-7

Pergamon

SCIENCE DIRECT®

Bioorganic & Medicinal Chemistry Letters 13 (2003) 3213–3216

BIOORGANIC & MEDICINAL CHEMISTRY LETTERS

A Convenient Method for the Computer-Aided Molecular Design of Carborane Containing Compounds

Jayaseharan Johnsamuel,[a,*] Youngjoo Byun,[a] Thomas P. Jones,[b] Yasuyuki Endo[c] and Werner Tjarks[a]

[a]*The Ohio State University, College of Pharmacy, 500 W. 12th Avenue, Columbus, OH 43210, USA*
[b]*Tripos Inc., 1699 South Hanley Road, St. Louis, MO 63144, USA*
[c]*Faculty of Pharmaceutical Sciences, Tohoku Pharmaceutical University, 4-4-1, Komatsushima, Aoba-ku, Sendai 981-8558, Japan*

Received 22 April 2003; revised 19 June 2003; accepted 24 June 2003

Abstract—Computer-aided molecular design (CAMD) of carborane containing compounds is of growing interest for scientists involved in boron neutron capture therapy (BNCT) and other pharmaceutical applications. However, the complex organo-metallic structures of carboranes pose difficulties in modeling and docking of these structures. This is the first report of a new strategy for modeling and docking of carborane containing molecules with the readily available software packages HyperChem, SYBYL and FlexX. It is intended as a guide for boron chemists interested in using CAMD of carborane containing agents for medical applications such as BNCT.
© 2003 Elsevier Ltd. All rights reserved.

Due to their high boron content and chemically modifiable properties, carborane clusters have been a preferred choice as boron moieties in the design and synthesis of boronated agents for boron neutron capture therapy (BNCT).[1,2] By analogy with fullerenes,[3,4] carboranes have recently also been used as hydrophobic pharmacophores in the design of derivatives of biologically active compounds such as estradiol, retinoic acid, and teleocidin.[5–8] Some of these carboranyl analogues interacted effectively with the corresponding receptor enzymes and exhibited equal or even higher biological activity compared to their endogenous counterparts. These carborane constructs were easily synthesized with few reaction steps, thus, providing feasible synthetic routes to biologically active carboranyl agents.

So far, carborane-based drug design utilizing computer-aided molecular design (CAMD) has been applied only in relatively few cases.[5–9] This is mainly due to the complex structures of carboranes with 6-fold coordinated carbon and boron atoms, and the unavailability of potential energy functions for the boron atom in most of the commercially available software packages.[10]

*Corresponding author. Tel.: +1-614-688-3149; fax: +1-614-292-2435; e-mail: johnsamuel.1@osu.edu

0960-894X/$ - see front matter © 2003 Elsevier Ltd. All rights reserved.
doi:10.1016/S0960-894X(03)00674-7

The earlier reports on CAMD of carboranyl derivatives of estradiol,[6] retinoic acid,[5] and teleocidin[8] used a software package ADAM,[5,6,8,11] which is not readily accessible to scientist interested in CAMD.

In this paper, a general strategy for modeling and docking of carborane containing derivatives using readily available software packages HyperChem. 5.1, SYBYL 6.8 and FlexX is described in detail. This strategy is intended as a guide for synthetic boron chemists interested in CAMD of carborane containing agents for medical applications. We have also addressed the general applicability of CAMD in modeling studies.

General modeling and docking strategies: The protein data bank file (PDB) entitled 1ERE (3.1 Å structure resolution) of the human estrogen receptor protein (hERαLBD)[12] was obtained from the protein data bank [Research Collaboratory for Structural Bioinformatics (RCSB) (http://www.rcsb.org/pdb)]. Compounds **1–4** (Fig. 1) were used for docking.

HyperChem. 5.1 (HYPERCUBE, Inc., 419 Phillip Street, Waterloo, Ontario N2L 3X2, Canada) and SYBYL 6.8 (TRIPOS Inc., 1699 South Hanley Rd., St. Louis, MO, 63144, USA) were used for modeling. Estradiol (**1**) was built and minimized using SYBYL.

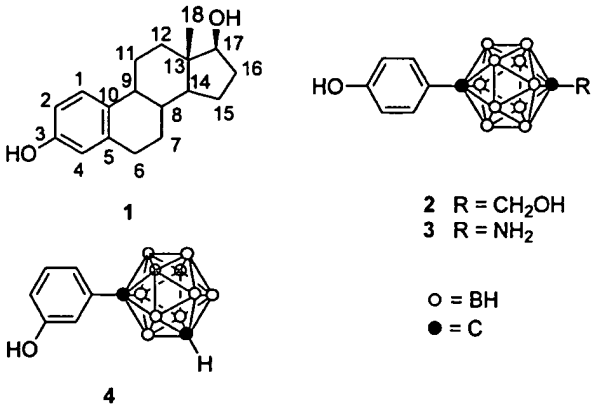

Figure 1. Structures of ligands 1–4.

The atomic point charges were calculated using the Gasteiger–Hückel method. The molecule was minimized using the Maximin2 minimizer and the TRIPOS force field/parameters until an energy gradient of 0.005 *K*cal/mol was reached.

The carboranyl estradiol derivatives **2–4** (Fig. 1) and *o*-, *m*-, and *p*-carborane were constructed on the HyperChem platform and were minimized by the semi-empirical AM1 method to an energy gradient of 0.005 *K*cal/mol. The atomic point charges of *o*-, *m*-, and *p*-carborane as well as compounds **2–4** were re-calculated using the MOPAC interface of SYBYL applying the semi-empirical AM1 method after import of their PDB files generated by Hyperchem.

Docking of ligands **1–4** into the active site of estrogen receptor was performed using FlexX (TRIPOS Inc., 1699 South Hanley Road, St. Louis, MO 63144, USA). Docking produced 30 possible docked conformations for each of the ligands **1–4** and the Cscore™ program of SYBYL scored each conformation. Cscore™ scoring functions include rmsd values,[13] ChemScore,[14] Dock_score,[15] G-score,[16] FlexX_score,[17] and PMF_score.[18] Among the 30 conformational solutions of ligands 1–4, the ones with the best FlexX_score (rank 1) were chosen as the optimal conformational poses[13] in all docking experiment. The rank 1 conformations showed better binding interactions compared to other solutions. SYBYL was used to generate dynamic hydrogen bonds between the best-docked conformational pose of a ligand and the amino acid residues in the active site of the protein. The same software package was used to visualize the binding mode of the docked protein–ligand complexes by generating a Connolly-type MOLCAD surfaces for estradiol with a probe sphere diameter of 1.4 Å based on the X-ray structures from the PDB file, 1ERE. The MOLCAD surface of estradiol was superimposed on the best-docked conformations of ligands 1–4 to visualize the binding of 1–4 within the active sites.

Results and Discussion

HyperChem, but not Insight II or SYBYL, provided a convenient way for generating and minimizing *o*-, *m*-, and *p*-carborane as well as compounds **2–4** using the Allow Ions option and geometry optimization with the semi-empirical AM1 method. The obtained geometries of *o*-, *m*-, and *p*-carborane correlated sufficiently with those obtained from ab initio calculations at the Hartree–Fock/6-31G* level[19] and experimental electron diffraction data.[20]

Unfortunately, HyperChem does not provide any platform for docking operations. Thus, modeling of **2–4** and their docking into the active site of estrogen receptor had to be carried out using SYBYL and FlexX, respectively. PDB files of compounds **2–4**, generated by HyperChem, were imported into SYBYL, partially reconstructed, and saved as 'mol2' files. All boron atoms 'B' in ligands **2–4** were subsequently changed to carbon atoms 'C.3' using the Built/Edit option in SYBYL. The geometries, bond lengths, bond angles, dihedral angles, and atomic point charges of the structures, obtained from semi-empirical AM1 calculations based on carboranyl structures, did not change during this operation. After docking, boron atoms were re-colored to green for easier identification (Fig. 2). This simple but effective modification circumvents the fact that both SYBYL and FlexX do not contain the empirical potential energy functions for the boron atom.[21] We did not notice any limitation of this modification on docking processes and we are not aware of any limitation on extending this methodology to other modeling studies.

The estrogen receptor protein (hERαLBD) contains six ligand binding domains.[12] Each domain contains one receptor site and the amino acid residues, sequences, and active sites are conserved in all domains. In order to simplify the docking process, five of the six domains of the estrogen receptor protein[22–24] were truncated using SYBYL and the resulting monomeric ligand binding domain was used for docking of ligands **1–4**. The minimized structure of estradiol (**1**) was docked first with the estrogen receptor site and the structure of the resulting protein-ligand complex was compared with that of the X-ray crystallograpically determined structure of the same complex. The X-ray structure showed hydrogen-bonding interactions of the hydroxyl groups at positions **3** and **17** of estradiol with the amino group of the arginine residue (R394) and the imino group of the histidine residue (H524), respectively. The optimal conformational pose corresponded to the highest FlexX_score value (rank 1) and the lowest rmsd value (0.80 Å). The docked estradiol–estrogen receptor protein complex reproduced native binding interactions as shown in Figure 2A. A rmsd value of ≤ 2 Å for the docked ligand–protein structure also suggests that estradiol was appropriately docked within the active site of the estrogen receptor.

FlexX docking of ligands **2–4** was carried out using the Run One Ligand option of FlexX. The structures of optimal conformational poses of ligands **2–4** (Table 1) within the active site of the estrogen receptor and the superimposed MOLCAD surface of the X-ray geometry of estradiol were visually examined for binding interactions.

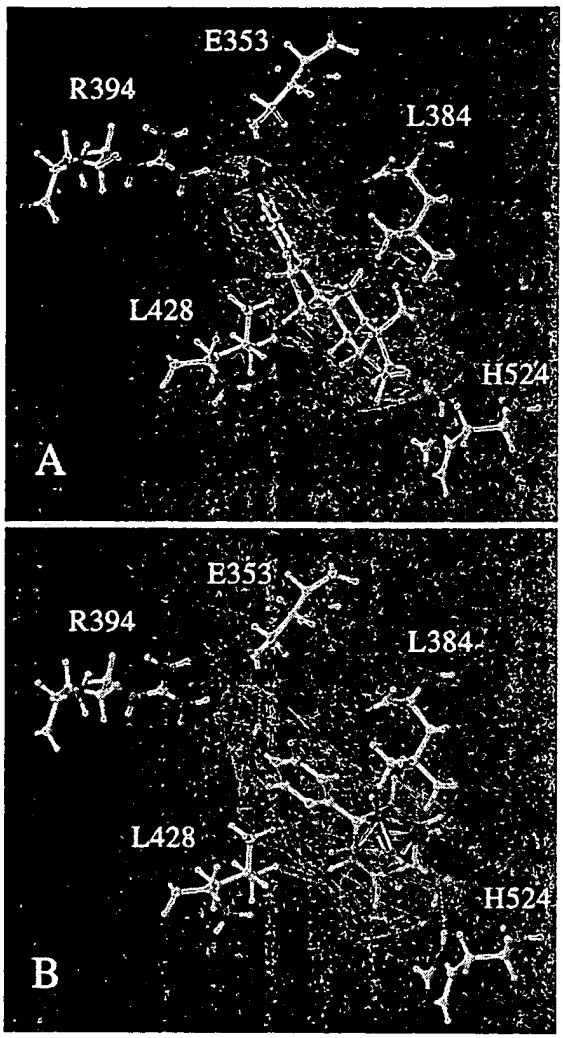

Figure 2. Binding modes of the optimal conformational poses of ligands, 1 (A) and 3 (B), with the active site of the estrogen receptor. The yellow line represents hydrogen bond (≤3.3 Å). The pink grid represents the MOLCAD surface of X-ray geometry of estradiol.

All poses of the ligands **2–4** fitted within the MOLCAD surface area of the X-ray geometry of estradiol as demonstrated by the example of compounds **1** and **3** (Fig. 2A and B). The ligands showed hydrogen bondings between either the alcoholic group (2) or carboranyl amino group (3), and the imino group of the histidine residue (H524) while the phenolic hydroxyl group in these structures interacted with either the amino group of the arginine residue (R394) (**2–3**) or the carboxylic function of the glutamate residue (E353) (**4**). The bulky carborane clusters of ligands **2–4** were positioned in the active site similar to the decahydronaphthalene portion of estradiol and showed hydrophobic interactions with the isobutyl group of the leucine residues (L384 and L428) as illustrated in Figure 2B.

Various scoring values of ligands **2–4** are listed in Table 1 by comparison with the estrogenic activity of these compounds[6] in order to evaluate the effectiveness of the Cscore™ scoring functions for the estrogen receptor protein–ligand complexes. Among the Cscore™ scoring functions, FlexX_score[17] (based on empirical functions), PMF_score[18] (based on statistical ligand–receptor atom-pair interaction potentials), D_score[15] (based on both electrostatic and hydrophobic contributions to the binding energy), and Chemscore[14] (based on a diverse training set of 82 receptor–ligand complexes) produced values for ligands **1–4** that showed some correlation with their respective biological activities. Ligand **4**, with the lowest biological activity of all carboranyl estradiol derivatives, had also the lowest scoring values (Table 1). For G_score,[16] which computes accurately scoring values for ligand–receptor complexes having many polar interactions, no obvious correlation between the scoring values for ligands **1–4** and respective biological activities could be observed. A possible explanation could be the presence of the carborane cluster in ligands **2–4**, which interacts strongly with the receptor in a hydrophobic fashion. Similar sub-optimal correlation of values from Cscore™ scoring functions with biological activities has been reported previously in different experimental/computational settings.[13,25–27]

In conclusion, the combination of HyperChem and SYBYL generated geometries of the *o*-, *m*-, and *p*-carborane clusters resembled closely those obtained previously using different theoretical and experimental methods.[19,20,28] FlexX docked ligands 2–4 into the active site of the estrogen receptor within the MOLCAD surface of estradiol and all ligands reproduced native estradiol binding interactions. Similar results were obtained using the software package ADAM for docking compounds **2–4** into the active site of the estrogen receptor. Computed values from Cscore™ scoring functions, except G_score, showed some correlation with the biological activities.

Based on our studies, it appears that computed scoring functions from Cscore,™ visual comparison between

Table 1. Cscore™ scoring values for complexes of the estrogen receptor with optimal conformational poses of ligands **1–4**

Ligand	FlexX	G_score	PMF_score	D_score	Chemscore	Hydrogen bonds	Biological activity[a]	Interaction energy (*Kcal*)[b]
1	−19	−229	−46	−117	−40	E353, R394, H524	xxx	−54.67
2	−19	−164	−42	−208	−39	R394, H524	xxxx	−51.60
3	−18	−177	−36	−175	−36	E353, G521, H524	xxxx	—
4	−14	−199	−27	−153	−35	E353	x	−45.34

[a]Biological activity is defined as the capacity of compounds **1–4** to induce transcriptional activation of COS-1 cells and was estimated from results obtained by Endo et al.[3] xxxx = very high, xxx = high, xx = medium, x = low.
[b]Interaction energies between estrogen receptor protein and ligands **1–4**, generated by ADAM, were taken from ref 6.

geometries of docked ligands and MOLCAD surfaces, and comparison between the binding interactions of docked ligands with those within ligand–receptor protein X-ray structures can be valuable tools for CAMD of carboranyl derivatives.

The lack of CAMD approaches involving carboranes is a major draw back in BNCT compound development. The described strategy for modeling molecules containing carborane clusters with the accessible software packages SYBYL, FlexX, and HyperChem should be of value for synthetic chemists involved in BNCT compound development.

Acknowledgements

This work was funded by US Department of Energy grant DE-FG02-90ER60972. The authors thank Professor Emeritus Albert H. Soloway, College of Pharmacy, The Ohio State University, Professor Christopher M. Hadad, Department of Chemistry, The Ohio State University, and John C. Hackett, graduate student, College of Pharmacy, The Ohio State University, for fruitful comments and discussions on CAMD.

References and Notes

1. Soloway, A. H.; Tjarks, W.; Barnum, B. A.; Rong, F.-G.; Barth, R. F.; Codogni, I. M.; Wilson, J. G. *Chem. Rev.* **1998**, *98*, 2389.
2. Valliant, J. F.; Guenther, K. J.; King, A. S.; Morel, P.; Schaffer, P.; Sogbein, O. O.; Stephenson, K. A. *Coordin. Chem. Rev.* **2002**, *232*, 173.
3. Marcorin, G. L.; Da Ros, T.; Castellano, S.; Stefancich, G.; Bonin, I.; Miertus, S.; Prato, M. *Org. Lett.* **2000**, *2*, 3955.
4. Friedman, S. H.; Ganapathi, P. S.; Rubin, Y.; Kenyon, G. L. *J. Med. Chem.* **1998**, *41*, 2424.
5. Endo, Y.; Iijima, T.; Yaguchi, K.; Kawachi, E.; Inoue, N.; Kagechika, H.; Kubo, A.; Itai, A. *Bioorg. Med. Chem. Lett.* **2001**, *11*, 1307.
6. Endo, Y.; Iijima, T.; Yamakoshi, Y.; Fukasawa, H.; Miyaura, C.; Inada, M.; Kubo, A.; Itai, A. *Chem. Biol.* **2001**, *8*, 341.
7. Endo, Y.; Yaguchi, K.; Tsuji, M.; Yamaguchi, K.; Shudo, K. *Chem. Pharm. Bull.* **1999**, *47*, 699.
8. Endo, Y.; Yoshimi, T.; Kimura, K.; Itai, A. *Bioorg. Med. Chem. Lett.* **1999**, *9*, 2561.
9. Tsuji, M.; Koiso, Y.; Takahashi, H.; Hashimoto, Y.; Endo, Y. *Biol. Pharm. Bull.* **2000**, *23*, 513.
10. Tao, P.; Lai, L. *J. Comput. Aid. Mol. Des.* **2001**, *15*, 429.
11. Mizutani, M. Y.; Tomioka, N.; Itai, A. *J. Mol. Biol.* **1994**, *243*, 310.
12. Brzozowski, A. M.; Pike, A. C.; Dauter, Z.; Hubbard, R. E.; Bonn, T.; Engstrom, O.; Ohman, L.; Greene, G. L.; Gustafsson, J. A.; Carlquist, M. *Nature* **1997**, *389*, 753.
13. Gohlke, H.; Hendlich, M.; Klebe, G. *J. Mol. Biol.* **2000**, *295*, 337.
14. Eldridge, M. D.; Murray, C. W.; Auton, T. R.; Paolini, G. V.; Mee, R. P. *Comput. Aided Mol. Des.* **1997**, *11*, 425.
15. Ewing, T. J. A.; Kuntz, I. D. *J. Comput. Chem.* **1997**, *18*, 1175.
16. Jones, G.; Willett, P.; Glen, R. C.; Leach, A. R.; Taylor, R. *J. Mol. Biol.* **1997**, *267*, 727.
17. Rarey, M.; Kramer, B.; Lengauer, T.; Klebe, G. *J. Mol. Biol.* **1996**, *261*, 470.
18. Muegge, I.; Martin, Y. C. *J. Med. Chem.* **1999**, *42*, 791.
19. Hermansson, K.; Wojcik, M.; Sjoeberg, S. *Inorg. Chem.* **1999**, *38*, 6039.
20. Hnyk, D.; Rankin, D. W. H.; Robertson, H. E.; Hofmann, M.; Schleyer, P. V.; Buhl, M. *Inorg. Chem.* **1994**, *33*, 4781.
21. Cornell, W. D.; Cieplak, P.; Bayly, C. I.; Gould, I. R.; Merz, K. M., Jr.; Ferguson, D. M.; Spellmeyer, D. C.; Fox, T.; Caldwell, J. W.; Kollman, P. A. *J. Am. Chem. Soc.* **1995**, *117*, 5179.
22. Tedesco, R.; Thomas, J. A.; Katzenellenbogen, B. S.; Katzenellenbogen, J. A. *Chem. Biol.* **2001**, *8*, 277.
23. Sippl, W. *Bioorg. Med. Chem.* **2002**, *10*, 3741.
24. Mortensen, D. S.; Rodriguez, A. L.; Carlson, K. E.; Sun, J.; Katzenellenbogen, B. S.; Katzenellenbogen, J. A. *J. Med. Chem.* **2001**, *44*, 3838.
25. Rognan, D.; Bissantz, C.; Dedier, S.; Logean, A.; Reinelt, S. *Chimia* **2000**, *54*, 658.
26. Bissantz, C.; Folkers, G.; Rognan, D. *J. Med. Chem.* **2000**, *43*, 4759.
27. Clark, R. D.; Strizhev, A.; Leonard, J. M.; Blake, J. F.; Matthew, J. B. *J. Mol. Graph. Model.* **2002**, *20*, 281.
28. Davidson, M. G.; Hibbert, T. G.; Howard, J. A. K.; Mackinnon, A.; Wade, K. *J. Chem. Soc., Chem. Commun.* **1996**, *19*, 2285.

Hyperchem in 2004

- Thermal behaviour and molecular modelling of some aromatic polyethers containing a hexamethylenic spacer
  Polymer Degradation and Stability, Volume 72, Issue 3, June 2001, Pages 441-445
  Nicolae Hurduc, Mihaela Prajinaru, Bogdan Donose, Dumitru Pavel and Natalia Hurduc
  - *"Molecular modeling was used as a complementary analysis method for the best understanding of the relationship between the chain conformation and polarity and the thermal behavior. CERIUS2 and HYPERCHEM programs were used to perform the molecular modeling."*

ELSEVIER

Polymer Degradation and Stability 72 (2001) 441–445

Polymer Degradation and Stability

Thermal behaviour and molecular modelling of some aromatic polyethers containing a hexamethylenic spacer

Nicolae Hurduc [a,*], Mihaela Prajinaru [b], Bogdan Donose [a], Dumitru Pavel [a], Natalia Hurduc [b]

[a] Faculty of Chemical Engineering, Department of Macromolecules, Technical University of Iasi, 71 Bd. Mangeron, 6600-Iasi, Romania
[b] Faculty of Chemistry, Department of Physical and Theoretical Chemistry, "Al.I.Cuza" University, 11 Bd. Copou, 6600-Iasi, Romania
[c] Department of Chemical Engineering, Royal Melbourne Institute of Technology, Melbourne, Victoria 3001, Australia

Received 9 September 2000; accepted 20 November 2000

Abstract

We report a study of the thermal stability of some aromatic copolyethers containing a hexamethylenic spacer. The polymers were synthesized by phase transfer catalysis (in a liquid/liquid system) starting from 1,6-dichlorohexane and different biphenolic 4,4'-dihydroxyazobenzene, 4,4'-dihydroxydiphenyl, bisphenol A and 2,7-dihydroxynaphthalene. Thermal stability was investigated by thermogravimetric analysis, in a static air atmosphere the heating rate being 10°C/min. Molecular modeling was used as a complementary analysis method for the best understanding of the relationship between the chain conformation and polarity and the thermal behavior. CERIUS² and HYPERCHEM programs were used to perform the molecular modelling. All the synthesized polymers present similar values of the starting point of the weight loss. This behavior can be explained by supra-molecular ordering, which is probably more important than the chemical structure. The presence of the hexamethylenic spacer leads to a micro-phase separation, with a favourable influence on the ordering in the solid state. All polymers showed low values of the polar radius, with interchain interactions playing a secondary role in the thermal stability. © 2001 Elsevier Science Ltd. All rights reserved.

Keywords: Thermal stability; Molecular modelling; Liquid crystals; Polyethers

1. Introduction

Liquid crystalline polymers (LCP) represent an interesting research field, due to the unique behavior of these materials, which combine two essential properties: order and mobility [1–6]. The presence of the anisotropic moieties in the chains confers the possibility of using them as optical memory systems. Our studies were focused on the synthesis of aromatic polyethers, some of them having liquid crystalline (LC) properties. The presence of the mesogenic groups in the main chain induces high phase-transition values, near the thermal stability limit. In these circumstances, the thermogravimetric study of the polymers is very important for establishing the parameters of the DSC and optical microscopy investigations. Our synthesis strategy is intended to separate as much as possible the influence of chain conformation, flexibility and inter-chain interactions on the LC behavior. This strategy permitted us to have in view, at the same time, the influence of these factors on the polymers' thermal stability.

The present paper is focused on the thermal behavior study of some oligomers with polyether structure, containing biphenolic moieties connected by a hexamethylenic spacer. The synthesis started from 1,6-dichlorohexane and various biphenols as follows: 4,4'-dihydroxyazobenzene (DHAB), 4,4'-dihydroxydiphenyl (DHD), bisphenol A (BPA) and 2,7-dihydroxynaphthalene (DN). Use of biphenols with different (linear or bent) geometry and structure permitted us to modify the chain conformation and polarity and to correlate the influence of these factors with thermal behaviour. Molecular modeling was used as a complementary analysis method for the best understanding of the relationship between chain conformation, polarity and thermal behaviour.

2. Experimental

The polyethers were synthesized by phase transfer catalysis in a liquid/liquid system. Details of the synthesis and

* Corresponding author.
E-mail address: nhurduc@ch.tuiasi.ro (N. Hurduc).

0141-3910/01/$ - see front matter © 2001 Elsevier Science Ltd. All rights reserved.
PII: S0141-3910(01)00044-1

ELSEVIER

Polymer Degradation and Stability 72 (2001) 441–445

Polymer Degradation and Stability

www.elsevier.nl/locate/polydegstab

Thermal behaviour and molecular modelling of some aromatic polyethers containing a hexamethylenic spacer

Nicolae Hurduc [a,*], Mihaela Prajinaru [b], Bogdan Donose [a], Dumitru Pavel [c], Natalia Hurduc [b]

[a] *Faculty of Chemical Engineering, Department of Macromolecules, Technical University of Iasi, 71 Bd. Mangeron, 6600-Iasi, Romania*
[b] *Faculty of Chemistry, Department of Physical and Theoretical Chemistry, "A.I.Cuza" University, 11 Bd. Copou, 6600-Iasi, Romania*
[c] *Department of Chemical Engineering, Royal Melbourne Institute of Technology, Melbourne, Victoria 3001, Australia*

Received 9 September 2000; accepted 20 November 2000

Abstract

We report a study of the thermal stability of some aromatic copolyethers containing a hexamethylenic spacer. The polymers were synthesized by phase transfer catalysis (in a liquid/liquid system) starting from 1,6-dichlorohexane and different bisphenols: 4,4′-dihydroxyazobenzene, 4,4′-dihydroxydiphenyl, bisphenol A and 2,7-dihydroxynaphthalene. Thermal stability was investigated by thermogravimetric analysis, in a static air atmosphere the heating rate being 10°C/min. Molecular modeling was used as a complementary analysis method for the best understanding of the relationship between the chain conformation and polarity and the thermal behavior. CERIUS^2 and HYPERCHEM programs were used to perform the molecular modelling. All the synthesized polymers present similar values of the starting point of the weight loss. This behavior can be explained by supra-molecular ordering, which is probably more important than the chemical structure. The presence of the hexamethylenic spacer leads to a micro-phase separation, with a favourable influence on the ordering in the solid state. All polymers showed low values of the polar surface, with interchain interactions playing a secondary role in the thermal stability. © 2001 Elsevier Science Ltd. All rights reserved.

Keywords: Thermal stability; Molecular modelling; Liquid crystals; Polyethers

1. Introduction

Liquid crystalline polymers (LCP) represent an interesting research field, due to the unique behavior of these materials, which combine two essential properties: order and mobility [1–6]. The presence of the azobenzenic moieties in the chains confers the possibility of using them as optical memory systems. Our studies were focused on the synthesis of aromatic polyethers, some of them having liquid crystalline (LC) properties. The presence of the mesogenic groups in the main chain induces high phase-transition values, near the thermal stability limit. In these circumstances, the thermogravimetric study of the polymers is very important for establishing the parameters of the DSC and optical microscopy investigations. Our synthesis strategy is intended to separate as much as possible the influence of chain conformation, flexibility and inter-chain interactions on the LC behavior. This strategy permitted us to have in view, at the same time, the influence of these factors on the polymers' thermal stability.

The present paper is focused on the thermal behavior study of some oligomers with polyether structure, containing bisphenolic moieties connected by a hexamethylenic spacer. The synthesis started from 1,6-dicholorohexane and various bisphenols as follows: 4,4′-dihydroxyazobenzene (DHAB), 4,4′-dihydroxydiphenyl (DHD), bisphenol A (BPA) and 2,7-dihydroxynaphthalene (DN). Use of bisphenols with different (linear or bent) geometry and structure permitted us to modify the chain conformation and polarity and to correlate the influence of these factors with thermal behaviour. Molecular modelling was used as a complementary analysis method for the best understanding of the relationship between chain conformation, polarity and thermal behaviour.

2. Experimental

The polyethers were synthesized by phase transfer catalysis in a liquid/liquid system. Details of the synthesis and

* Corresponding author.
E-mail address: nhurduc@ch.tuiasi (N. Hurduc).

0141-3910/01/$ - see front matter © 2001 Elsevier Science Ltd. All rights reserved.
PII: S0141-3910(01)00044-1

characterization of the polymers were reported previously [7,8]. The thermal behavior was investigated on a MOM-Budapest derivatograph. The recordings were effected in static air atmosphere with a heating rate of 10°C/min. The molecular simulations were performed using two programs: CERIUS^2 [9] and HYPERCHEM [10]. HYPERCHEM was used to estimate the chain polar surface (QSAR properties module) and CERIUS^2 to investigate the chain geometry. The initial macromolecular conformation of the simulated polyethers was optimized and the value of the total potential energy of the single chain was obtained. In order to search the real value for minimum energy (not a local minimum), the conformation obtained was followed by a molecular dynamic cycle and re-minimized. The criterion of energy convergence was to obtain a residual root-mean-square force in the simulated system of less than 0.12 kJ/mol Å. Minimization was performed using a conjugate-gradient algorithm described by Fletcher and Reeves. Supplementary information concerning the molecular modeling procedure was reported in our previous studies [11–13].

3. Results and discussion

The copolymers were obtained according to the reaction in Scheme 1. Table 1 presents some characteristics of the synthesized polymers.

The molecular weights of the samples are typical of oligomers. We have developed the study in this range because, in our opinion, the influence of the chain conformation, flexibility and interchain interactions are more evident.

A first general observation is that, for all synthesized products, weight loss begins in a very narrow range (Figs. 1–3) situated between 310 and 330°C (except Sample 4). This behaviour is surprising, because for similar structures containing the same bisphenols but other spacers (e.g. oxetane, propylene, diethylether, etc.), the differences of the starting degradation temperatures were up to 200°C, as a function of the bisphenol chemical structure [14–16]. This behaviour can be explained by taking into consideration the supramolecular ordering. It is well known, for the LCP, that the flexible spacer (above a certain length) imposes a micro phase separation, with a positive influence on the mesophase stability. It is possible, for our polymers too, that the supramolecular aspects may be more important that the

Table 1
Some characteristics of the synthesized polymers

Sample no.	Copolymer composition	M_n	Thermal behavior	Polar surface (%)
1	DHAB/BPA = 2.5/1	2150	LC[a]	3.6
2	DHAB/BPA = 1/1.1	2450	SC[b]	3.2
3	DHAB/BPA = 1/3.2	3400	SC	2.6
4	DHD/BPA = 2.7/1	3970	SC	1.7
5	DHD/BPA = 1/1.2	3900	SC	1.8
6	DHD/BPA = 1/3.1	4000	SC	1.9
7	DHAB/DHD = 2.5/1	2030	LC	4.0
8	DHAB/DHD = 1/1.2	2290	LC	3.5
9	DHAB/DHD = 1/3.1	2250	LC	2.6
10	DHAB/DN = 2.9/1	1910	SC	4.4
11	DHAB/DN = 1.2/1	1800	SC	3.8
12	DHAB/DN = 1/2.6	2090	SC	3.0

[a] LC — liquid crystalline.
[b] SC — semi-crystalline.

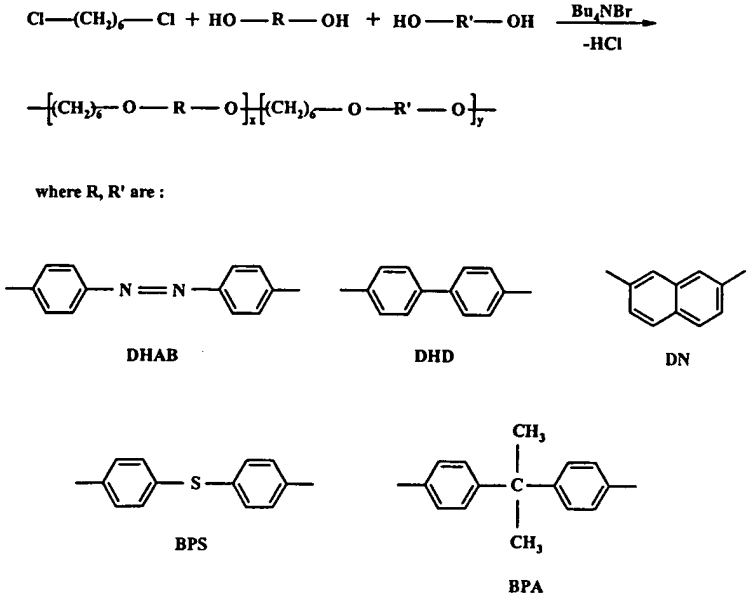

Scheme 1.

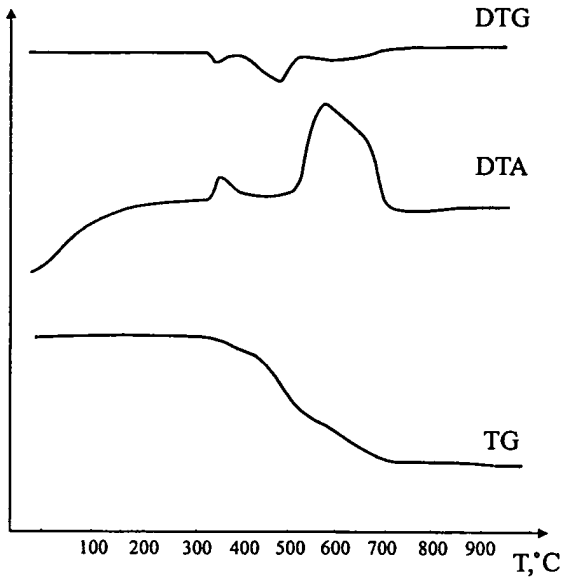

Fig. 1. Thermogram corresponding to Sample 2.

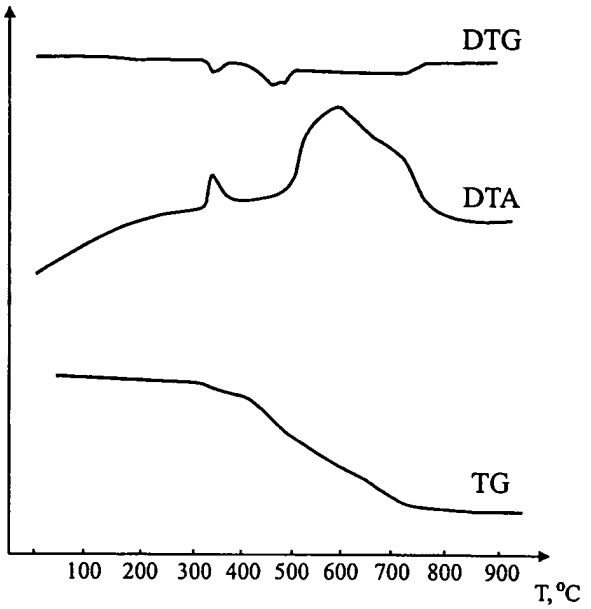

Fig. 3. Thermogram corresponding to Sample 11.

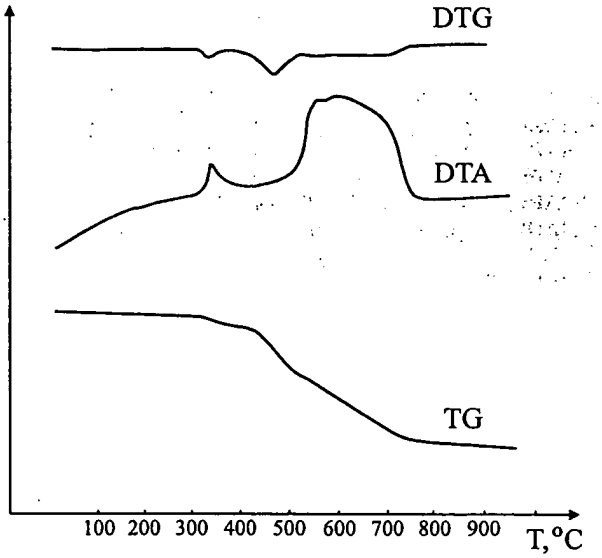

Fig. 2. Thermogram corresponding to Sample 8.

chemical structure. There are many reasons to support this supposition.

The first is the chain geometry. The theoretical conformational studies showed a linear geometry both in the case of homopolymers and copolymers (Figs. 4 and 5). Due to the chain linearity and flexibility, for this polymer group, the sample containing DHAB and BPA (Sample 1) showed a LC behavior. For other flexible spacers, this bisphenol combination does not show a mesophase, the presence of a bent bisphenol consequently causing the loss of LC behaviour.

The second reason is that the presence of different bisphenols in the same chain does not disturb the micro-phase separation. From a geometrical point of view, the bisphenols' lengths are 7.3 Å (DN), 9.7 Å (BPA) 9.8 Å (DHD) and 11.5 Å (DHAB). The length of the flexible spacer is 6.5 Å (from first to the sixth methylenic group). Excepting the combination of DHAB and DN the bisphenol, lengths do not disturb the micro-phase separation.

The presence of the hexamethylenic moiety in the chain leads to low values of the polar surface (due to the hydrophobic character), compared with other flexible spacers. For example in the case of oxetanic or propylenic spacers, the polar surface was up to 8%, compared with 4.4%, the maximum value corresponding to Sample 10. Because of these low polar surface values, the chain polarity does not significantly influence the polymers thermal stability. This observation is in agreement with the results of our previous studies [14–15]. According to these data, a significant influence of the chain polarity upon the polymer thermal stability is recorded only for structures having a polar surface higher than 3–4%.

A general observation that can be made concerning the degradation mechanism is that all of the polymers present three steps of weight loss (Table 2).

The presence of other spacers, with oxetanic, propylenic or diethyether structure, induces differences concerning the degradation mechanism. For example, the polymers with azobenzenic moieties showed three steps of degradation, while all others structures showed only two steps. This also proves the major influence of the supramolecular ordering, in competition with the chemical structure.

The temperature domains corresponding to each degradation step are in the same region. The temperatures of half decomposition, excepting Sample 10, are

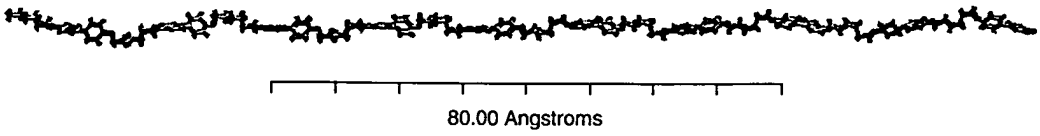

Fig. 4. Chain geometry of the homopolymer with biphenyl mesogenic groups.

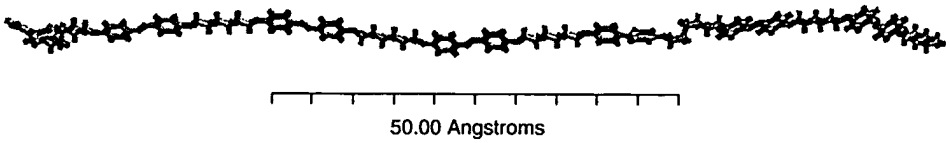

Fig. 5. Chain geometry corresponding to Sample 7.

Table 2
Thermogravimetric characteristics of the synthesized polymers

Sample no.	ΔT_1[a] (°C)	W_1[b] (%)	ΔT_2 (°C)	W_2 (%)	ΔT_3 (°C)	W_3 (%)	T_α[c] (°C)
1	310–380	10.6	380–505	36.2	505–740	53.2	510
2	330–390	8.7	290–520	50.0	520–700	41.3	500
3	330–410	10.2	410–530	55.0	530–680	34.8	500
4	350–440	21.2	440–540	42.3	540–710	36.5	500
5	320–450	19.2	450–550	46.8	550–710	34.0	490
6	320–440	12.5	440–550	62.5	550–675	25.0	500
7	330–400	9.8	400–580	41.2	530–740	49.0	510
8	310–390	12.3	390–520	36.7	520–740	51.0	510
9	320–415	10.9	415–520	41.3	520–720	47.8	505
10	310–360	12.5	370–500	29.2	500–770	58.3	575
11	320–360	8.9	400–490	31.1	490–740	60.0	560
12	305–370	8.3	410–510	45.8	510–730	45.9	510

[a] ΔT — The temperature domain corresponding to the degradation step.
[b] W — The weight loss corresponding to the degradation step.
[c] T_α — The temperature corresponding to 50% weight loss.

all around 500°C. Kinetic parameters were calculated for the second degradation step (Table 3).

Except for Samples 4–6 and 12, the other polymers gave similar values of the reaction order and activation energy of the degradation. The reaction order values suggest that chemical processes play an essential role and the mechanism is similar for all of the products.

The compensation effect was evaluated using the relation $\ln A = f(E)$, the linear dependence confirming similar degradation mechanisms. The resulting equation is:

$$\ln A = 0.16E + 4$$

Another aspect investigated was the modification of the activation energy of the degradation as a function of conversion (Table 4). The modifications of this parameter suggest a complex mechanism probably involving successive reactions:

$$P(\mathrm{s}) \rightarrow I_1(\mathrm{s}) + V \rightarrow I_2(\mathrm{s}) \rightarrow V$$

where P(s) is solid polymer, I (s) is a solid intermediate and V volatile products. The I_2 is probably the same for

Table 3
Kinetic characteristics of the synthesized polymers

Sample no.	ΔT[a] (°C)	n[b]	E (kJ/mol) F.C.[c]	E (kJ/mol) C.R.[d]	ln A[e]	S_p[f]
1	380–505	1	170	176	22.86	6.07
2	390–520	1	159	153	28.39	5.68
3	410–530	1	268	228	45.04	5.95
4	440–540	1	342	244	64.36	6.29
5	450–550	2	322	287	50.96	6.31
6	440–550	0.5	283	229	44.88	3.30
7	400–530	1	181	207	29.58	6.11
8	390–520	1	213	228	37.91	5.62
9	415–520	1	191	206	32.85	5.81
10	370–500	1	177	153	29.86	5.35
11	400–490	1	196	172	34.53	5.56
12	410–510	1	356	273	58.36	6.10

[a] ΔT — Temperature domain.
[b] n — Reaction order.
[c] E — Activation energy corresponding to the degradation step (ΔT) calculated by Freeman–Caroll method.
[d] E — Activation energy corresponding to the degradation step (ΔT) calculated by Coats–Redfern method.
[e] A — Pre-exponential factor.
[f] S_p — Compensation parameter.

Table 4
Dependence of the activation energy (kJ/mol) as a function of the weight loss

Sample no.	10%	20%	30%	40%	50%	60%
2	135	78	–	82	189	193
5	143	78	125	171	–	212
8	161	134	159	172	185	184
10	248	159	143	124	118	122
11	149	151	168	175	111	111
12	290	–	–	238	117	108

all investigated products because in the second step of the degradation process, the activation energy has similar values (Table 4).

4. Conclusions

1. All the synthesized polymers have similar temperature values at the starting point of the weight loss. The azobenzenic structures follow this behavior although in the case of other structures containing flexible or semi-flexible spacers the differences in this temperature value were up to 200°C, as a function of the bisphenolic structure.
2. The small differences between the starting points of the degradation can be explained by the supramolecular ordering, which is more important than the chemical structure. The presence of the hexamethylenic spacer leads to a micro-phase separation with a favorable influence on the supramolecular ordering in the solid state.
3. The conformational studies showed linear chain geometry, also favorable for the micro-phase separation. The differences between bisphenols length do not disturb the micro-phase separation.
4. All polymers had low values of the polar surface, typically below 4%, consequently, interchain interactions play a secondary role in the thermal stability.
5. The degradation mechanism is complex, taking place probably by successive reactions.
6. An equation corresponding to the compensation effect was proposed.

Acknowledgements

The authors wish to acknowledge the Romanian National Agency for Science and Technology (ANSTI) for financial support of this research.

References

[1] Roviello A, Sirigu A. Macromol Chem 1982;183:895.
[2] Zhou QF, Lenz RV. J Polym Sci Polym Chem Ed 1983;21:3313.
[3] Percec V, Nava H, Jonsson H. J Polym Sci Part A: Polym Chem 1987;25:1943.
[4] Shaffer TD, Percec V. J Polym Sci Part A: Polym Chem 1987;25:2755.
[5] Hurduc N, Bulacovschi V, Scutaru D, Barboiu V, Simionescu CI. Eur Polym J 1993;29:1333.
[6] Hurduc N, Daudi A, Buisine JM, Barboiu V, Simionescu CI. Eur Polym J 1998;34:123.
[7] Catanescu O, Hurduc N, Scutaru D, Stoleru A, Simionescu CI. Die Angew Makromol Chem 1999;273:91.
[8] Catanescu O, Hurduc N, Scutaru D, Stoleru A, Simionescu CI. New Polym Materials, in press.
[9] Cerius^2, Molecular simulation software for material science, version 3.5. San Diego CA. Molecular Simulations, 1997.
[10] Hyperchem 4.5, Hypercube Inc (licensed to Constantinescu M).
[11] Pavel D, Ball J, Bhattacharya N, Shanks RA, Hurduc N. Comput Theor Polym Sci 1997;7:7.
[12] Pavel D, Ball J, Bhattacharya N, Shanks RA, Toader V, Bulacovschi V, Hurduc N. Comput Theor Polym Sci 1999;9:1.
[13] Pavel D, Ball J, Bhattacharya N, Shanks RA, Hurduc N. J Polym Sci Part B: Polym Phys 1999;37:2334.
[14] Tarus A, Hurduc N, Catanescu O, Cobzaru C, Hurduc NN. Polym Degrad Stab 2000;68:87.
[15] Hurduc N, Creanga A, Pavel D, Hurduc NN. Polym Degrad Stab 2000;70:277.
[16] Hurduc N, Dragoi N, Ghirvu C, Hurduc NN. J Therm Anal Cal 1999;58:525.

Hyperchem in 2004

- The prediction for gas chromatographic retention indices of saturated esters on stationary phases of different polarity
  Talanta, Volume 57, Issue 4, 10 June 2002, Pages 641-652
  Yawei Wang, Xiaojun Yao, Xiaoyun Zhang, Ruisheng Zhang, Mancang Liu, Zhide Hu and Botao Fan
  - *"A quantitative structure-retention relationship (QSRR) model has been developed for the gas chromatographic Kova´ts indices of 98 saturated esters on seven different polar stationary phases by multiple linear regression analysis (MLR)… Chemical descriptors were calculated from the molecular structures by PM3 of Hyperchem 4.0. … The proposed model had a high multiple square correlation coefficient R2 and low standard error S.E. The result proved the strong predictive power of the model."*

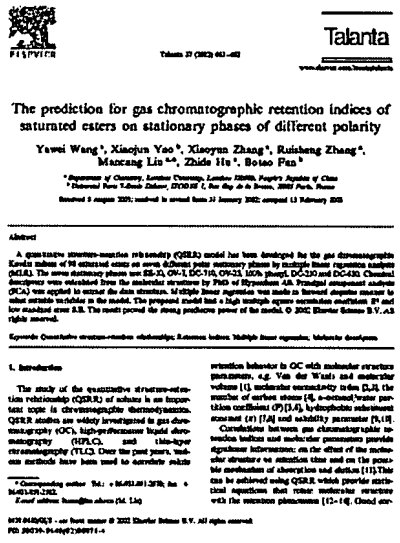

Talanta

The prediction for gas chromatographic retention indices of saturated esters on stationary phases of different polarity

Yawei Wang [a], Xiaojun Yao [b,*], Xiaoyun Zhang [a], Ruisheng Zhang [a], Mancang Liu [a,*], Zhide Hu [a], Botao Fan [b]

[a] Department of Chemistry, Lanzhou University, Lanzhou 730000, People's Republic of China
[b] Université Paris 7-Denis Diderot, ITODYS UMR 7, Rue Guy de la Brosse, 75005 Paris, France

Received 5 August 2001; received in revised form 31 January 2002; accepted 13 February 2002

Abstract

A quantitative structure-retention relationship (QSRR) model has been developed for the gas chromatographic Kovats indices of 98 saturated esters on seven different polar stationary phases by multiple linear regression analysis (MLR). The seven stationary phases were SE-30, OV-1, DC-710, OV-25, 10% phenyl, DC-220 and DC-430. Chemical descriptors were calculated from the molecular structures by PM3 of Hyperchem 4.0. Principal component analysis (PCA) was applied to extract the data structure. Multiple linear regression was made in forward stepwise manner to select suitable variables in the model. The proposed model had a high multiple square correlation coefficient R^2 and low standard error S.E. The result proved the strong predictive power of the model. © 2002 Elsevier Science B.V. All rights reserved.

Keywords: Quantitative structure-retention relationships; Kovats indices; Multiple linear regression; Molecular descriptors

1. Introduction

The study of the quantitative structure-retention relationship (QSRR) of solutes is an important topic in chromatographic thermodynamics. QSRR studies are widely investigated in gas chromatography (GC), high-performance liquid chromatography (HPLC), and thin-layer chromatography (TLC). Over the past years, various methods have been used to correlate solute orientation behavior in GC with molecular structure parameters, e.g. Van der Waals and molecular volume [1], molecular connectivity index [2,3], the number of carbon atoms [4], n-octanol/water partition coefficient (P) [3,5], hydrophobic substituent constant (π) [7,8] and solubility parameter [9,10].

Correlations between gas chromatographic retention indices and molecular parameters provide significant information on the effect of the molecular structure on retention time and on the possible mechanism of absorption and elution [11]. This can be achieved using QSRR which provide statistical equations that relate molecular structure with the retention phenomena [12–14]. Good cor-

* Corresponding author. Tel.: +86-931-891-2578; fax: +86-931-891-2582.
E-mail address: liumc@lzu.edu.cn (M. Liu)

0039-9140/02/$ - see front matter © 2002 Elsevier Science B.V. All rights reserved.
PII: S0039-9140(02)00071-4

ELSEVIER

Talanta 57 (2002) 641–652

Talanta

www.elsevier.com/locate/talanta

The prediction for gas chromatographic retention indices of saturated esters on stationary phases of different polarity

Yawei Wang [a], Xiaojun Yao [b], Xiaoyun Zhang [a], Ruisheng Zhang [a], Mancang Liu [a,*], Zhide Hu [a], Botao Fan [b]

[a] *Department of Chemistry, Lanzhou University, Lanzhou 730000, People's Republic of China*
[b] *Université Paris 7-Denis Diderot, ITODYS 1, Rue Guy de la Brosse, 75005 Paris, France*

Received 8 August 2001; received in revised form 31 January 2002; accepted 15 February 2002

Abstract

A quantitative structure-retention relationship (QSRR) model has been developed for the gas chromatographic Kováts indices of 98 saturated esters on seven different polar stationary phases by multiple linear regression analysis (MLR). The seven stationary phases are: SE-30, OV-7, DC-710, OV-25, 100% phenyl, DC-230 and DC-530. Chemical descriptors were calculated from the molecular structures by PM3 of Hyperchem 4.0. Principal component analysis (PCA) was applied to extract the data structure. Multiple linear regression was made in forward stepwise manner to select suitable variables in the model. The proposed model had a high multiple square correlation coefficient R^2 and low standard error S.E. The result proved the strong predictive power of the model. © 2002 Elsevier Science B.V. All rights reserved.

Keywords: Quantitative structure-retention relationships; Retention indices; Multiple linear regression; Molecular descriptors

1. Introduction

The study of the quantitative structure-retention relationship (QSRR) of solutes is an important topic in chromatographic thermodynamics. QSRR studies are widely investigated in gas chromatography (GC), high-performance liquid chromatography (HPLC), and thin-layer chromatography (TLC). Over the past years, various methods have been used to correlate solute retention behavior in GC with molecular structure parameters, e.g. Van der Waals and molecular volume [1], molecular connectivity index [2,3], the number of carbon atoms [4], *n*-octanol/water partition coefficient (P) [5,6], hydrophobic substituent constant (π) [7,8] and solubility parameter [9,10].

Correlations between gas chromatographic retention indices and molecular parameters provide significant information: on the effect of the molecular structure on retention time and on the possible mechanism of absorption and elution [11].This can be achieved using QSRR which provide statistical equations that relate molecular structure with the retention phenomena [12–16]. Good cor-

* Corresponding author. Tel.: +86-931-891-2578; fax: +86-931-891-2582.
E-mail address: liumc@lzu.edu.cn (M. Liu).

0039-9140/02/$ - see front matter © 2002 Elsevier Science B.V. All rights reserved.
PII: S0039-9140(02)00078-4

relations have been obtained between RI and theoretically calculated data for molecules with different functional groups: alkanes [17], dialkylhydrazones [18], alkenes [19], alkybenzenes and naphthalenes [20], phenol derivatives [21], azo compounds [19], primary, secondary and tertiary amines [22], etc. Several works have been done, but the QSRR on different polar stationary phases of esters has not been reported.

The goal of our present study was to characterize chromatographic retention on different polar stationary phases by topological descriptors and quantum chemical descriptors. The molecular structures of solutes were represented using CHI-0A, CHI-0AV, CHI-2A, CHI-2AV, WA, LUMO, QMAX, QTOT and DIP. Seven stationary phases selected were: SE-30, OV-7, DC-710, OV-25, 100% phenyl, DC-230 and DC-530. We hoped that the dependence of retention of these compounds from stationary phase polarity would be better explained using these descriptors.

2. Theory

2.1. Descriptor generation

To obtain a QSRR model, compounds must be represented using molecular descriptors and retain structure information. Here two types of descriptors were used: topological and quantum-chemical descriptors. The quantum-chemical descriptors were calculated using semi-empirical quantum-chemical method PM3 in Hyperchem 4.0 software: energy of the lowest unoccupied molecular obitals (LUMO, unit:ev), dipole moment (DIP, unit:debye), the maximum of the net atomic charge on the C atom (QMAX), the sum of positive charge on C atoms (QTOT). The molecular structures were generated with the molecular builder inside Hyperchem and optimized by following the Polak Ribiere algorithm until RMS gradient 0.01 kal Å mol^{-1}. Their minimum were supported by the positive definiteness of the force matrix. The quantum-chemical descriptors were obtained from the thermodynamically most stable molecules. The topological descriptors (CHI-2, CHI-0AV, CHI-2AV, CHI-0A, CHI-2A) were calculated by the method proposed by Randic [23] and the wiener index (WA) by the method proposed by Wiener [24].

2.2. Principles of PCA

Application of principal component analysis (PCA) has become a popular method in the last decades. It can provide information: classification, searching similarities, finding relationships, finding physical significance to principal components, etc. The principles of PCA can be seen the work by Héberger and Görgényi [25].

2.3. Principles of MLR

Multiple linear regression (MLR) is a common method used in QSRR study. The QSRR equations were obtained by forward stepwise multiple regression techniques following the multilinear forms: $RI = b_0 + b_1D_1 + b_2D_2 + \ldots b_nD_n$, where RI was the retention index, D_1, D_2 and D_n were the descriptors, the intercept (b_0) and the regression coefficients of the descriptors ($b_1, b_2 \ldots b_n$) were determined by using the least squares method and n was the number of the descriptors. The statistical evaluation of the data was obtained by the software SPSS.

In MLR analysis, the descriptors in the regression equation must be orthogonal. So, in order to reduce the number of the descriptors and minimize the information overlap in the descriptors, the concept of non-redundant descriptors (NRD) [26,27] was used. When the linear correlation coefficients value of two descriptors are larger than 0.9, they are correlated. Then they are not available in one equation. The best regression equation is selected on basis of the highest multiple correlation coefficient (R), F value and the lowest standard error of estimation (S.E.).

3. Experiment and methodology

3.1. Retention indices

The Kováts indices of esters compounds on

seven stationary phases in this paper were taken from the report of Ashes and Haken [28]. The compounds included C_1–C_6 saturated acids esters. The esters and their retention indices were shown in Table 1. The retention data was obtained isothermally at 150 °C using 12 ft. × 1/4 in O.D. aluminum columns packed with 10% stationary phase on 62–72 mesh acid-washed and silanized celatom. Flame ionization detection was used under the following conditions: injection temperature, 190°; detector temperature, 220°; carrier gas, helium; flow rate, 30 ml min^{-1} with an inlet pressure of 310.05 kPa.

3.2. Stationary phases

The stationary phases used all polysiloxanes and could be separated into two basic classes depending on the type of substituent group. Class 1 consisted of non-polar phases, primarily containing alkyl groups, class 2 of the low- to medium-polarity donor phases, containing groups capable of exhibiting donor properties. The degree and type of substitution, as well as the classification of polarity in terms of Rohrschneider constants, for the polysiloxanes used were shown in Table 2.

3.3. Model developing

MLR forward stepwise regression manner was used to select suitable variables in the model. The final model selection was accomplished through the following statistical validation techniques. At first, the RI values of esters on seven different stationary phases were regressed versus each one of the descriptors. Then another descriptor was selected for higher-order regression treatments. In the successive step, according to the stepwise multilinear regression method, the noncolinear descriptors were selected and regressed against RI. Table 4 showed these selected descriptors. And the best model was selected based on the multiple square correlation coefficient (R^2) and the standard error of estimation (S.E.).

4. Result and discussion

4.1. PCA of descriptors variables

The original matrix was decomposed into loadings and scores matrix by PCA. Table 3 showed the result, which supported that the original variables were not strongly correlated. The first factor explained 47.7%, the second 22.5%, the third 11.4%, the forth 8.6%, the fifth 5.9% and the sixth 4.9% of the total variance. Using the first six factors could explain 95.8% of the total variance in the data. In Table 3, the significant values were put in bold (the loading were >0.7000) [29]). The first factor correlated well with CHI-0A, CHI-2A, CHI-0AV, CHI-2AV, WA, QTOT. The second factor correlated with QMAX, DIP. The third factor correlated with LUMO.

4.2. Results of MLR

The value of the calculated quantum-chemical descriptors and the topological indices were summarized in Table 5. The correlation coefficient matrix of the parameters were shown in Table 6 which proved that the descriptors selected were non-linear. These data served as a basis for further statistical analysis. Seven of the best regression equations were selected from each of the stationary phases and a summary of these models was given in Table 4. The results had a high value of R^2 and F value and a low S.E. Then it indicated that these equations represented good model for the two types of descriptors.

If comparing the fitting parameters in the equations above and the polarity of the stationary phases the following qualitative statements could be made.

As could be seen from Table 4 that the topological index WA, CHI-2A and calculated quantum-chemical descriptor LUMO were included in seven equations, QMAX was included in four equations (SE-30, OV-7 and OC-25 except). It could be seen that WA, CHI-2A, LUMO and QMAX had good correlation with RI.

Table 1
The retention indices of different compounds on different stationary phases [28]

No.	Compounds	SE-30	OV-7	DC-710	OV-25	100% phenyl	DC-230	DC-530
1	Methyl formate	386	453	496	571	618	419	488
2	Ethyl formate	495	552	586	655	715	521	587
3	Propyl formate	602	667	696	756	813	626	686
4	Butyl formate	707	774	804	852	907	734	792
5	Pentyl formate	810	879	912	952	998	835	885
6	Hexyl formate	907	976	1011	1047	1092	937	980
7	Isopropyl formate	552	604	635	686	754	553	622
8	Isobutyl formate	670	731	766	803	858	684	739
9	Isopentyl formate	777	840	872	915	958	795	849
10	Methyl acetate	509	559	609	693	732	519	569
11	Ethyl acetate	592	648	690	760	895	704	747
12	Butyl acetate	794	855	895	949	991	810	846
13	Pentyl acetate	891	958	996	1044	1081	914	942
14	Hexyl acetate	988	1056	1092	1113	1174	1012	1040
15	Isopropyl acetate	643	686	722	782	846	635	672
16	Isobutyl acetate	750	810	846	898	942	770	820
17	Isopentyl acetate	859	922	955	1001	1042	880	917
18	Methyl propionate	617	667	710	775	829	610	663
19	Ethyl propionate	692	743	783	845	885	692	740
20	Propyl propionate	789	851	884	934	977	792	835
21	Butyl propionate	886	949	984	1032	1069	896	934
22	Pentyl propionate	980	1047	1082	1125	1166	1003	1031
23	Hexyl propionate	1074	1142	1176	1115	1255	1100	1126
24	Isopropyl propionate	733	785	817	971	894	736	777
25	Isobutyl propionate	848	909	938	985	1010	857	895
26	Isopentyl propionate	948	1014	1042	1086	1118	963	1003
27	Methyl butyrate	702	767	803	868	907	719	757
28	Ethyl butyrate	778	840	876	931	968	794	828
29	Protyl butyrate	875	938	973	1022	1056	896	924
30	Butyl butyrate	969	1036	1069	1114	1147	994	1021
31	Pentyl butyrate	1062	1131	1164	1208	1241	1091	1116
32	Hexyl butyrate	1156	1225	1258	1292	1331	1186	1209
33	Isopropyl butyrate	820	878	905	955	983	835	864
34	Isobuyl butyrate	933	993	1023	1065	1093	955	981
35	Isopentyl butyrate	1029	1093	1124	1163	1196	1056	1080
36	Methyl pentanoate	807	871	907	961	1001	821	863
37	Ethyl pentanoate	876	941	975	1014	1060	896	930
38	Protyl pentanoate	971	1036	1069	1111	1147	994	1023
39	Butyl pentanoate	1063	1130	1163	1205	1237	1089	1116
40	Pentyl pentanoate	1155	1222	1257	1204	1329	1185	1210
41	Hexyl pentanoate	1247	1316	1349	1382	1420	1287	1304
42	Isopropyl pentanoate	915	971	1000	1046	1079	932	961
43	Isobutyl pentanoate	1027	1087	1117	1156	1187	1051	1077
44	Isopentyl pentanoate	1132	1185	1217	1253	1286	1150	1173
45	Methyl hexanoate	902	974	1006	1056	1091	925	960
46	Ethyl hexanoate	976	1045	1073	1118	1148	995	1026
47	Protyl hexanoate	1064	1138	1164	1207	1239	1090	1119
48	Butyl hexanoate	1156	1231	1256	1295	1329	1184	1209
49	Pentyl hexanoate	1246	1325	1349	1384	1419	1278	1304
50	Hexyl hexanoate	1337	1417	1440	1475	1508	1371	1397
51	Isopropyl hexanoate	1008	1074	1015	1131	1172	1028	1055

Table 1 (*Continued*)

No.	Compounds	SE-30	OV-7	DC-710	OV-25	100% phenyl	DC-230	DC-530
52	Isobutyl hexanoate	1119	1189	1211	1246	1279	1128	1171
53	Isopentyl hexanoate	1212	1287	1308	1342	1376	1228	1266
54	Methyl isobutyrate	665	823	764	812	848	677	708
55	Ethyl isobutyrate	732	893	831	875	906	757	779
56	Propyl isobutyrate	836	891	925	968	994	851	878
57	Butyl isobutyrate	931	987	1019	1059	1091	945	974
58	Pentyl isobutyrate	1024	1082	1115	1155	1180	1045	1070
59	Hexyl isobutyrate	1117	1177	1208	1238	1272	1141	1165
60	Isopropyl isobutyrate	780	829	849	889	927	786	814
61	Isobutyl isobutyrate	899	946	975	1008	1039	913	937
62	Isopentyl isobutyrate	994	1045	1075	1109	1141	1010	1034
63	Methyl isopentanoate	763	823	854	902	945	777	814
64	Ethyl isopentanoate	839	893	925	967	1005	853	881
65	Propyl isopentanoate	929	987	1018	1059	1091	948	976
66	Butyl isopentanoate	1021	1081	1111	1149	1178	1044	1070
67	Pentyl isopentanoate	1112	1174	1204	1238	1272	1139	1164
68	Hexyl isopentanoate	1204	1267	1296	1326	1361	1233	1258
69	Isopropyl isopentanoate	874	923	950	989	1017	889	915
70	Isobutyl isopentanoate	985	1039	1066	1096	1125	1007	1031
71	Isopentyl isopentanoate	1081	1136	1164	1196	1225	1104	1128
72	Methyl isohexanoate	875	936	970	1019	1056	892	927
73	Ethyl isohexanoate	943	1004	1036	1078	1111	963	992
74	Propyl isohexanoate	1035	1094	1128	1165	1202	1056	1083
75	Butyl isohexanoate	1125	1189	1220	1252	1290	1150	1176
76	Pentyl isohexanoate	1215	1281	1313	1340	1381	1244	1268
77	Hexyl isohexanoate	1306	1374	1414	1427	1470	1337	1361
78	Isopropyl isohexanoate	979	1028	1059	1095	1134	988	1020
79	Isobutyl isohexanoate	1089	1147	1175	1200	1240	1110	1135
80	Isopentyl isohexanoate	1181	1244	1272	1298	1337	1209	1231
81	Methyl 2-methylpentanoate	853	908	945	989	1050	864	900
82	Ethyl 2-methylpentanoate	917	973	1006	1053	1097	930	962
83	Propyl 2-methylpentanoate	1009	1064	1096	1136	1184	1026	1055
84	Butyl 2-methylpentanoate	1097	1157	1189	1222	1275	1118	1145
85	Pentyl 2-methylpentanoate	1187	1246	1279	1310	1361	1212	1237
86	Hexyl 2-methylpentanoate	1277	1337	1370	1398	1449	1305	1331
87	Isopropyl 2-methylpentanoate	952	999	1021	1000	1114	960	992
88	Isobutyl 2-methylpentanoate	1064	1116	1144	1179	1120	1081	1109
89	Isopentyl 2-methylpentanoate	1153	1208	1238	1267	1319	1174	1202
90	Methyl 2-ethylbutyrate	845	899	934	979	1043	854	894
91	Ethyl 2-ethylbutyrate	914	969	1000	1037	1092	924	960
92	Propyl 2-ethylbutyrate	1005	1060	1092	1130	1176	1020	1051
93	Butyl 2-ethylbutyrate	1093	1150	1182	1217	1265	1112	1141
94	Pentyl 2-ethylbutyrate	1183	1241	1273	1303	1353	1205	1233
95	Hexyl 2-ethylbutyrate	1273	1332	1364	1393	1441	1298	1326
96	Isopropyl 2-ethylbutyrate	954	996	1022	1058	1104	951	993
97	Isobutyl 2-ethylbutyrate	1060	1112	1139	1167	1216	1075	1107
98	Isopentyl 2-ethylbutyrate	1149	1202	1232	1263	1310	1169	1198

The wiener number is the sum of the graph-theoretical distances between pairs of atoms on the structure. It is related to the steric-branching effects of the molecules. The positive regression coefficients for WA demonstrated that with higher values of them, the molecules would have higher

values of retention index. The value of CHI-2A supported more branches with a molecule, the lower value of it, so, the positive regression coefficients for WA and the negative for CHI-2A (in Table 4), the magnitude of intermolecular interaction about the solute and the stationary phase was related to the degree of the branch of the molecules of the solute.

Another significant factor affecting the retention behavior of the solute is the hydrogen bonding of the molecules. Hydrogen bonding is an electrostatic interaction [30], that atomic charge should be a valid measure of hydrogen bonding ability. QMAX is the maximum of the net atomic charge on the C atom, and hydrogen bonding also has a covalent or charged-transfer component, from the molecular orbital theory of chemical reactivity, LUMO, as electron acceptor, so a combination of QMAX and LUMO should model hydrogen bond donor and acceptor ability. And then in the regression equations of the different stationary phases, QMAX and LUMO had good correlation with RI.

Otherwise, the dipole moment is also important in the interaction of the molecules with apolar and polar stationary phases. The contribution of dipole moment to RI increases with increasing polarity of the stationary phase and the polar interactions become more dominant in the interaction of the solute and stationary phase molecules.

In Table 4 we also saw that the type of the molecular descriptors and the value of them were different on the different stationary phases of different polarity. This illustrated that with the difference of the polarity of the stationary phases, the influence factor to the RI of the solute were always different. But that CHI-2A, LUMO,

Table 2
Composition of stationary phases and Rohrschneider constants

Stationary phase	Class	Methyl replacement	Rohrschneider constants				
			X	Y	Z	U	S
SE-30	1	–	0.16	0.20	0.50	0.85	0.48
OV-7	2	20% phenyl	0.42	0.81	0.85	1.52	0.89
DC-710	2	50% phenyl	1.30	1.66	1.79	2.83	2.47
OV-25	2	75% phenyl	1.76	2.00	2.15	3.34	2.81
100% phenyl	2	100% phenyl	1.81	2.87	2.48	4.35	4.01
DC-230	1	Stearyl	0.42	0.83	0.71	0.96	1.03
DC-530	2	6% aminoalkyl	0.63	2.69	1.29	2.04	1.16

Table 3
Result of the principal component analysis

	Factor loading 1	Factor loading 2	Factor loading 3	Factor loading 4	Factor loading 5
CHI-0A	−0.741	−0.419	−0.208	0.439	−0.125
CHI-2A	−0.783	0.274	−0.0532	0.248	0.442
CHI-0AV	0.744	−0.281	−0.274	0.461	−0.238
CHI-2AV	0.735	0.317	−0.107	0.408	0.350
WA	0.894	0.346	−0.0251	−0.150	0.132
QMAX	0.431	−0.810	0.177	−0.0644	0.285
QTOT	0.878	0.241	−0.313	−0.0395	−0.0930
LUMO	0.510	−0.355	0.726	0.212	−0.0245
DIP	−0.138	0.798	0.462	0.252	−0.192
Explained variance	4.290	2.026	1.003	0.770	0.535
Proportion of the total variance	0.477	0.225	0.114	0.086	0.059

Table 4
The descriptors and regression equations of different stationary phases

Stationary phases	Descriptors	Coefficient	S.E. of coefficients	Standardized coefficients	t	Sig.	F	R^2	S.E.
SE-30 ($n=98$)	b_0	114.524	86.539		1.323	0.189	5406.356	0.996	13.118
	WA	273.494	2.587	0.880	105.739	0.000			
	CHI-2A	−1045.930	71.975	−0.142	−14.532	0.000			
	CHI-0AV	698.497	85.177	0.073	8.201	0.000			
	LUMO	−126.753	37.397	−0.026	−3.389	0.001			
OV-7 ($n=98$)	b_0	−164.845	179.006		−0.921	0.359	1226.873	0.993	16.451
	WA	307.311	5.828	0.986	52.730	0.000			
	CHI-2A	−1478.172	84.170	−0.199	−17.562	0.000			
	CHI-0A	1166.293	193.014	0.114	6.043	0.000			
	LUMO	−169.087	46.993	−0.035	−3.598	0.001			
DC-710 ($n=98$)	b_0	221.441	145.661		1.520	0.132	3039.408	0.995	14.294
	WA	298.848	4.680	0.961	63.850	0.000			
	CHI-2A	−1341.266	81.721	−0.182	−16.413	0.000			
	LUMO	−387.969	62.109	−0.080	−6.247	0.000			
	CHI-0A	726.259	160.945	0.072	4.512	0.000			
	QMAX	528.230	154.461	0.055	3.420	0.001			
	DIP	5.355	2.399	0.032	2.232	0.028			
OV-25 ($n=98$)	b_0	406.111	172.099		2.360	0.020	1237.522	0.985	23.001
	WA	278.120	6.486	0.949	42.881	0.000			
	CHI-2A	−834.923	144.091	−0.120	−5.794	0.000			
	LUMO	−221.383	65.985	−0.049	−3.355	0.001			
	CHI-2AV	−233.326	68.654	−0.076	−3.399	0.001			
	CHI-0AV	657.616	178.585	0.073	3.682	0.000			
100% phenyl ($n=98$)	b_0	848.307	92.851		9.136	0.000	1558.881	0.988	20.318
	WA	282.886	5.565	0.975	50.836	0.000			
	CHI-2A	−934.031	108.610	−0.136	−8.600	0.000			
	CHI-2AV	−236.767	50.726	−0.078	−4.668	0.000			
	LUMO	−278.196	66.089	−0.062	−4.209	0.000			
	QMAX	394.573	130.554	0.044	3.022	0.003			

Table 4 (*Continued*)

Stationary phases	Descriptors	Coefficient	S.E. of coefficients	Standardized coefficients	t	Sig.	F	R^2	S.E.
DC-230 ($n=98$)	b_0	−185.454	172.956		−1.072	0.286	2493.683	0.993	17.517
	WA	311.375	5.713	0.987	54.503	0.000			
	CHI-2A	−1113.335	92.945	−0.149	−11.978	0.000			
	CHI-0A	870.220	187.262	0.085	4.647	0.000			
	LUMO	−194.094	56.720	−0.040	−3.422	0.001			
	QMAX	243.132	114.925	0.025	2.116	0.037			
DC-530 ($n=98$)	b_0	419.688	93.119		4.507	0.000	2272.074	0.992	17.608
	WA	265.465	6.636	0.876	40.006	0.000			
	CHI-2A	−788.180	102.636	−0.110	−7.679	0.000			
	QTOT	24.578	9.223	0.063	2.665	0.009			
	QMAX	335.114	113.947	0.036	2.941	0.004			
	LUMO	−148.667	59.461	−0.032	−2.500	0.014			

Table 5
The value of the descriptors of the compounds

No.	CHI-0A	CHI-2A	CHI-0AV	CHI-2AV	WA	QMAX	QTOT	LUMO	DIP
1	0.85	0.50	0.60	0.33	1.67	0.25	1.27	0.92	3.95
2	0.82	0.45	0.62	0.37	2.00	0.35	1.43	1.09	3.91
3	0.81	0.43	0.64	0.48	2.33	0.35	1.63	1.09	3.91
4	0.79	0.41	0.65	0.53	2.67	0.35	1.83	1.09	3.91
5	0.78	0.40	0.65	0.56	3.00	0.35	2.03	1.09	3.91
6	0.77	0.40	0.66	0.58	3.33	0.35	2.24	1.09	3.91
7	0.83	0.44	0.66	0.51	2.13	0.35	1.73	1.14	4.02
8	0.81	0.42	0.67	0.61	2.48	0.35	1.81	1.10	3.85
9	0.80	0.41	0.67	0.61	2.82	0.35	2.03	1.10	3.93
10	0.86	0.45	0.66	0.35	1.80	0.37	1.54	1.01	1.83
11	0.83	0.44	0.67	0.37	2.13	0.38	1.80	1.06	1.89
12	0.80	0.41	0.68	0.48	2.82	0.35	2.08	1.06	4.15
13	0.79	0.41	0.68	0.51	3.17	0.35	2.28	1.06	4.15
14	0.78	0.40	0.69	0.53	3.51	0.37	2.59	1.04	1.92
15	0.84	0.43	0.70	0.47	2.29	0.35	1.98	1.10	4.28
16	0.82	0.42	0.70	0.55	2.64	0.30	2.73	0.95	4.21
17	0.81	0.41	0.70	0.56	3.00	0.30	3.05	0.95	4.31
18	0.83	0.38	0.67	0.37	2.07	0.37	1.71	1.05	1.76
19	0.81	0.38	0.68	0.39	2.38	0.37	1.97	1.09	1.83
20	0.80	0.38	0.68	0.45	2.71	0.37	2.15	1.09	1.98
21	0.79	0.38	0.68	0.48	3.06	0.37	2.36	1.09	1.98
22	0.78	0.37	0.69	0.51	3.40	0.37	2.56	1.09	1.98
23	0.78	0.37	0.69	0.53	3.75	0.35	2.69	1.10	4.25
24	0.82	0.39	0.70	0.47	2.54	0.37	2.25	1.11	1.78
25	0.81	0.39	0.70	0.54	2.89	0.37	2.32	1.08	1.92
26	0.80	0.38	0.70	0.55	3.24	0.37	2.55	1.07	1.84
27	0.81	0.38	0.68	0.44	2.38	0.37	1.92	1.05	1.75
28	0.80	0.38	0.68	0.44	2.68	0.35	2.05	1.10	4.12
29	0.79	0.38	0.68	0.49	3.00	0.35	2.24	1.10	4.11
30	0.78	0.38	0.69	0.52	3.33	0.35	2.48	1.11	4.30
31	0.78	0.37	0.69	0.54	3.67	0.35	2.69	1.11	4.30
32	0.77	0.37	0.69	0.55	4.01	0.30	4.01	1.00	4.39
33	0.81	0.39	0.70	0.51	2.83	0.35	2.37	1.14	4.24
34	0.80	0.39	0.70	0.56	3.18	0.35	2.44	1.08	4.17
35	0.79	0.38	0.70	0.57	3.53	0.35	2.66	1.08	4.25
36	0.80	0.38	0.68	0.48	2.71	0.37	2.12	1.05	1.74
37	0.79	0.38	0.68	0.48	3.00	0.37	2.38	1.09	1.80
38	0.78	0.38	0.69	0.52	3.31	0.35	2.44	1.10	4.10
39	0.78	0.37	0.69	0.54	3.64	0.35	2.64	1.10	4.09
40	0.77	0.37	0.69	0.55	3.97	0.35	2.89	1.11	4.33
41	0.77	0.37	0.69	0.56	4.31	0.35	3.07	1.07	4.25
42	0.80	0.39	0.70	0.53	3.16	0.35	2.57	1.14	4.23
43	0.79	0.38	0.70	0.58	3.49	0.35	2.62	1.11	4.03
44	0.78	0.38	0.70	0.58	3.83	0.35	2.86	1.08	4.27
45	0.79	0.38	0.68	0.51	3.06	0.37	2.32	1.05	1.74
46	0.78	0.38	0.69	0.50	3.33	0.35	2.45	1.10	4.11
47	0.78	0.37	0.69	0.54	3.64	0.35	2.65	1.10	4.09
48	0.77	0.37	0.69	0.55	3.96	0.35	2.89	1.11	4.36
49	0.77	0.37	0.69	0.56	4.28	0.35	3.07	1.07	4.26
50	0.76	0.37	0.69	0.57	4.62	0.35	3.30	1.11	4.36
51	0.79	0.39	0.70	0.55	3.49	0.35	2.79	1.14	4.20

QMAX were included most of the regression equations showed that the retention was primarily influenced by size, steric factors and polar effects. And the results of this work suggested that the role of the steric factors must be more important in the retention than the

Table 5 (*Continued*)

No.	CHI-0A	CHI-2A	CHI-0AV	CHI-2AV	WA	QMAX	QTOT	LUMO	DIP
52	0.78	0.38	0.70	0.59	3.82	0.35	2.84	1.08	4.20
53	0.78	0.38	0.70	0.59	4.15	0.35	3.06	1.08	4.28
54	0.84	0.38	0.70	0.48	2.19	0.37	1.87	1.07	1.70
55	0.82	0.38	0.70	0.48	2.50	0.37	2.13	1.10	1.99
56	0.81	0.37	0.70	0.52	2.83	0.37	2.31	1.10	1.99
57	0.80	0.37	0.70	0.54	3.18	0.37	2.52	1.10	1.99
58	0.79	0.37	0.70	0.55	3.53	0.35	2.66	1.11	4.23
59	0.78	0.37	0.70	0.56	3.88	0.37	2.93	1.10	1.77
60	0.83	0.39	0.72	0.53	2.67	0.38	2.43	1.14	1.67
61	0.82	0.38	0.72	0.58	3.02	0.37	2.50	1.11	2.02
62	0.81	0.38	0.72	0.58	3.38	0.35	2.65	1.12	4.26
63	0.82	0.39	0.70	0.54	2.54	0.37	2.11	1.04	1.84
64	0.81	0.39	0.70	0.53	2.83	0.30	3.11	0.96	1.84
65	0.80	0.39	0.70	0.56	3.16	0.37	2.55	1.07	1.93
66	0.79	0.39	0.70	0.58	3.49	0.35	2.66	1.09	4.19
67	0.78	0.38	0.70	0.59	3.83	0.38	2.97	1.08	1.80
68	0.78	0.38	0.70	0.60	4.18	0.38	3.17	1.08	1.80
69	0.82	0.40	0.72	0.57	3.00	0.38	2.66	1.10	1.83
70	0.81	0.39	0.72	0.61	3.35	0.35	2.64	1.09	4.13
71	0.80	0.39	0.72	0.62	3.70	0.37	2.97	1.09	1.76
72	0.81	0.39	0.70	0.56	2.89	0.37	2.33	1.04	1.90
73	0.80	0.39	0.70	0.55	3.18	0.38	2.59	1.08	1.96
74	0.79	0.38	0.70	0.57	3.49	0.35	2.75	1.10	4.35
75	0.78	0.38	0.70	0.58	3.82	0.38	3.00	1.09	1.85
76	0.78	0.38	0.70	0.59	4.15	0.38	3.20	1.09	1.84
77	0.77	0.38	0.70	0.60	4.50	0.38	3.41	1.09	1.84
78	0.81	0.39	0.72	0.58	3.35	0.35	2.83	1.13	4.45
79	0.80	0.39	0.72	0.62	3.68	0.38	2.98	1.10	1.88
80	0.79	0.39	0.72	0.62	4.03	0.38	3.20	1.10	1.81
81	0.81	0.35	0.70	0.49	2.72	0.37	2.30	1.06	1.97
82	0.80	0.35	0.70	0.49	3.00	0.37	2.56	1.10	2.05
83	0.79	0.35	0.70	0.52	3.31	0.35	2.67	1.12	4.20
84	0.78	0.35	0.70	0.54	3.64	0.37	2.99	1.09	1.59
85	0.78	0.35	0.70	0.55	3.97	0.37	3.14	1.11	1.76
86	0.77	0.35	0.70	0.56	4.32	0.37	3.34	1.11	1.76
87	0.81	0.36	0.72	0.53	3.16	0.38	2.84	1.14	1.90
88	0.80	0.36	0.72	0.57	3.50	0.37	2.93	1.12	1.83
89	0.79	0.36	0.72	0.58	3.85	0.37	3.14	1.12	1.72
90	0.81	0.33	0.70	0.45	2.61	0.37	2.30	1.07	1.95
91	0.80	0.33	0.70	0.45	2.89	0.37	2.56	1.11	2.02
92	0.79	0.34	0.70	0.49	3.20	0.36	2.68	1.15	4.17
93	0.78	0.34	0.70	0.51	3.53	0.38	2.95	1.13	1.77
94	0.78	0.34	0.70	0.52	3.87	0.38	3.17	1.12	1.80
95	0.77	0.34	0.70	0.54	4.22	0.37	3.41	1.11	1.60
96	0.81	0.35	0.72	0.50	3.06	0.38	2.86	1.16	1.88
97	0.80	0.35	0.72	0.54	3.39	0.38	2.97	1.12	1.62
98	0.79	0.35	0.72	0.55	3.74	0.37	3.17	1.12	1.76

Table 6
Correlation coefficient matrix of ten parameters

	CHI-0A	CHI-2A	CHI-0AV	CHI-2AV	WA	QMAX	QTOT	LUMO	DIP
CHI-0A	1.0000	0.5401	−0.1570	−0.5319	−0.8633	−0.8506	−0.6690	−0.2699	−0.1978
CHI-2A	0.5401	1.0000	−0.6230	−0.2797	−0.5522	−0.4575	−0.6114	−0.4695	0.2784
CHI-0AV	−0.1570	−0.6230	1.0000	0.5745	0.4800	0.4202	0.6654	0.3698	−0.2768
CHI-2AV	−0.5319	−0.2797	0.5745	1.0000	0.7160	0.1018	0.6651	0.2473	0.1287
WA	−0.8633	−0.5522	0.4800	0.7216	1.0000	0.1548	0.8904	0.2902	0.0839
QMAX	−0.8506	−0.4575	0.4202	0.1018	0.1548	0.1000	0.0954	0.5821	−0.6589
QTOT	−0.6690	−0.6114	0.6654	0.6651	0.8904	0.0954	1.0000	0.1662	−0.0753
LUMO	−0.2699	−0.4695	0.3698	0.2473	0.2902	0.5821	0.1662	1.0000	0.1078
DIP	−0.1978	0.2784	−0.2768	0.1287	0.0839	−0.6589	−0.0753	0.1078	1.0000

polar effects on the apolar and low polar stationary phases.

5. Conclusions

Past studies showed that topological and quantum-chemical descriptors were useful in developing models for predicting the gas chromatographic RI of solutes. The strong intercorrelation structural descriptors from a MLR equation might lead to misinterpretation of the corresponding structure-retention model. PCA showed a dominant pattern in descriptors.

On stationary phases of different polarity, the descriptors used in the regression equations showed that the influence factors about the gas chromatographic RI of solute molecules were different to the stationary of different polarity. But Table 2 also told us that the main actors were still related to the degree of the branch of the molecules of the solute and hydrogen bond donor and acceptor ability of the solute molecules.

The good predictive ability of MLR model allows us to estimate retention indices for similar compounds in cases where retention values are not readily available.

Acknowledgements

The authors thank the Association Franco-Chinoise pour la Recherche Scientifique & Technique (AFCRST) for supporting this study (Programme PRA SI 00-05).

References

[1] Y. Feng, P. Zhu, Z. Hu, Chromatographia 25 (1988) 382.
[2] Y.Q. Feng, M.C. Liu, Z.C. Hu, Chin. J. Chromatogr. 4 (1986) 259.
[3] R.M.S. Roca, F.J.G. Albarez, J. Chromatogr. 607 (1992) 91.
[4] W.L. Hinze, S.G. Weber, Anal. Chem. 63 (1991) 1808.
[5] C. Yamagami, T. Oguda, N. Takao, J. Chromatogr. 514 (1990) 123.
[6] A. Kaibara, C. Hohda, N. Hirata, M. Hirose, T. Nakagawa, Chromatographia 29 (1990) 275.
[7] R.M. Smith, J. Chromatogr. A 656 (1993) 381.
[8] B. Law, S. Weir, J. Chromatogr. A 657 (1993) 17.
[9] P.L. Smith, W.T. Cooper, Chromatographia 25 (1988) 55.
[10] H.A.H. Billiet, P.J. Schoenmakers, L.D. Galan, J. Chromatogr. 218 (1981) 443.
[11] T. Körtvélyesi, M. Görgényi, K. Héberger, Anal. Chim. Acta 428 (2001) 73–82.
[12] J. Olivero, T. Gracia, P. Payares, R. Vivas, D. Diaz, E. Daza, P. Geerlings, J. Pharm. Sci. 86 (1997) 625.
[13] P. Payares, D. Diaz, J. Olivero, R. Vivas, I. Gomez, J. Chromatogr. A 771 (1997) 213.
[14] J. Kang, C. Cao, Z. Li, J. Chromatogr. A 799 (1998) 361.
[15] T. Woloszyn, P. Jurs, Anal. Chem. 64 (1992) 3059.
[16] A. Katritzky, E. Ignatchenko, R. Barcock, V. Lobanov, M. Karelson, Anal. Chem. 66 (1994) 1799.
[17] M. Görgényi, Z. Fekete, L. Seres, Chromatographia 27 (1989) 581.
[18] Z. Kiraly, T. Kortvelyesi, L. Seres, Chromatographia 42 (1996) 653.

[19] T. Körtvelyesi, M. Gögényl, L. Seres, Chromatographia 41 (1995) 282.
[20] N. Dimov, A. Osman, Ov. Mekenyan, D. Papazova, Anal. Chim. Acta 298 (1994) 303.
[21] R. Kaliszan, H.-D. Höltje, J. Chromatogr. 234 (1982) 303.
[22] K. Osmialowski, J. Halkiewicz, A. Radecki, R. Kaliszan, J. Chromatogr. 346 (1985) 53.
[23] M. Randic, J. Am. Chem. Soc. 97 (1975) 6609.
[24] H. Wiener, J. Chem. Phys. 15 (1947) 766.
[25] K. Héberger, M. Görgényi, J. Chromatogr. A 845 (1999) 21.
[26] A.R. Katritzky, E. Gordeeva, J. Chem. Inf. Comput. Sci. 33 (1993) 835.
[27] J. Olivero, T. Gracia, P. Payares, R. Vivas, D. Diaz, E. Daza, P. Geerlings, J. Pharm. Sci. 86 (5) (1997) 625.
[28] J.R. Ashes, J.K. Haken, J. Chromatogr. A 101 (1974) 103.
[29] T. Körtvelyesi, M. Gögényl, K. Héberger, Anal. Chim. Acta 428 (2001) 73.
[30] L.Y. Wilson, G.R. Famini, J. Med. Chem. 34 (1991) 1668.

Hyperchem 2004

- Quantum chemistry study on the relationship between molecular structure and corrosion inhibition efficiency of amides
  Journal of Molecular Structure: THEOCHEM, Volume 593, Issues 1-3, 27 September 2002, Pages 179-185
  Jian Fang and Jie Li
  - *"All the study have been carried out using Dewar's LCAO-SCF-MO semiempirical method, MINDO/3 [7], in the commercially available computer program package (HyperChem Pro. Release 6.03 from Hypercube Inc. USA)."*

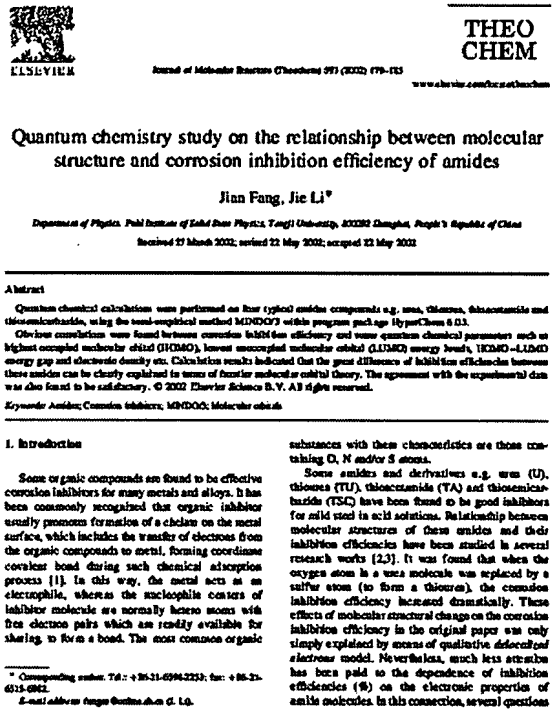

ELSEVIER

THEO CHEM

Journal of Molecular Structure (Theochem) 593 (2002) 179–185

www.elsevier.com/locate/theochem

Quantum chemistry study on the relationship between molecular structure and corrosion inhibition efficiency of amides

Jian Fang, Jie Li*

Department of Physics, Fuhi Institute of Solid State Physics, Tongji University, 200092 Shanghai, People's Republic of China

Received 27 March 2002; revised 22 May 2002; accepted 23 May 2002

Abstract

Quantum chemical calculations were performed on four typical amides compounds e.g. urea, thiourea, thioacetamide and thiosemicarbazide, using the semi-empirical method MINDO/3 within program package HyperChem 6.03.

Obvious correlations were found between corrosion inhibition efficiency and some quantum chemical parameter such as highest occupied molecular orbital (HOMO), lowest unoccupied molecular orbital (LUMO) energy level, HOMO–LUMO energy gap and electronic density etc. Calculation results indicated that the great difference of inhibition efficiencies between these amides can be clearly explained in terms of frontier molecular orbital theory. The agreement with the experimental data was also found to be satisfactory. © 2002 Elsevier Science B.V. All rights reserved.

Keywords: Amides; Corrosion inhibitors; MINDO/3; Molecular orbitals

1. Introduction

Some organic compounds are found to be effective corrosion inhibitors for many metals and alloys. It has been commonly recognized that organic inhibitor usually promotes formation of a chelate on the metal surface, which includes the transfer of electrons from the organic compounds to metal, forming coordinate covalent bond during such chemical adsorption process [1]. In this way, the metal acts as an electrophile, whereas the nucleophile centers of inhibitor molecule are normally hetero atoms with free electron pairs which are readily available for sharing, to form a bond. The most common organic substances with these characteristics are those containing O, N and/or S atoms.

Some amides and derivatives e.g. urea (U), thioures (TU), thioacetamide (TA) and thiosemicarbazide (TSC) have been found to be good inhibitors for mild steel in acid solutions. Relationship between molecular structures of these amides and their inhibition efficiencies have been studied in several research works [2,3]. It was found that when the oxygen atom in a urea molecule was replaced by a sulfur atom (to form a thiourea), the corrosion inhibition efficiency increased dramatically. These effects of molecular structural change on the corrosion inhibition efficiency in the original paper was only simply explained by means of qualitative *delocalized electrons* model. Nevertheless, much less attention has been paid to the dependence of inhibition efficiencies (η) on the electronic properties of amide molecules. In this connection, several questions

* Corresponding author. Tel.: +86-21-6596-2253; fax: +86-21-6513-6862.
E-mail address: fangjian@online.sh.cn (J. Li).

0166-1280/02/$ - see front matter © 2002 Elsevier Science B.V. All rights reserved.
PII: S0166-1280(02)00316-0

ELSEVIER

Journal of Molecular Structure (Theochem) 593 (2002) 179–185

THEO CHEM

www.elsevier.com/locate/theochem

Quantum chemistry study on the relationship between molecular structure and corrosion inhibition efficiency of amides

Jian Fang, Jie Li*

Department of Physics, Pohl Institute of Solid State Physics, Tongji University, 200092 Shanghai, People's Republic of China

Received 27 March 2002; revised 22 May 2002; accepted 22 May 2002

Abstract

Quantum chemical calculations were performed on four typical amides compounds e.g. urea, thiourea, thioacetamide and thiosemicarbazide, using the semi-empirical method MINDO/3 within program package HyperChem 6.03.

Obvious correlations were found between corrosion inhibition efficiency and some quantum chemical parameters such as highest occupied molecular obital (HOMO), lowest unoccupied molecular orbital (LUMO) energy levels, HOMO–LUMO energy gap and electronic density etc. Calculation results indicated that the great difference of inhibition efficiencies between these amides can be clearly explained in terms of frontier molecular orbital theory. The agreement with the experimental data was also found to be satisfactory. © 2002 Elsevier Science B.V. All rights reserved.

Keywords: Amides; Corrosion inhibitors; MINDO/3; Molecular orbitals

1. Introduction

Some organic compounds are found to be effective corrosion inhibitors for many metals and alloys. It has been commonly recognized that organic inhibitor usually promotes formation of a chelate on the metal surface, which includes the transfer of electrons from the organic compounds to metal, forming coordinate covalent bond during such chemical adsorption process [1]. In this way, the metal acts as an electrophile, whereas the nucleophile centers of inhibitor molecule are normally hetero atoms with free electron pairs which are readily available for sharing, to form a bond. The most common organic substances with these characteristics are those containing O, N and/or S atoms.

Some amides and derivatives e.g. urea (U), thiourea (TU), thioacetamide (TA) and thiosemicarbazide (TSC) have been found to be good inhibitors for mild steel in acid solutions. Relationship between molecular structures of these amides and their inhibition efficiencies have been studied in several research works [2,3]. It was found that when the oxygen atom in a urea molecule was replaced by a sulfur atom (to form a thiourea), the corrosion inhibition efficiency increased dramatically. These effects of molecular structural change on the corrosion inhibition efficiency in the original paper was only simply explained by means of qualitative *delocalized electrons* model. Nevertheless, much less attention has been paid to the dependence of inhibition efficiencies (%) on the electronic properties of amide molecules. In this connection, several questions

* Corresponding author. Tel.: +86-21-6598-2253; fax: +86-21-6515-6982.

E-mail address: fungee@online.sh.cn (J. Li).

0166-1280/02/$ - see front matter © 2002 Elsevier Science B.V. All rights reserved.
PII: S0166-1280(02)00316-0

Table 1
Molecular structures, abbreviations and molecular weights of the amides used

	Compounds used as inhibitors	Abbreviation	Molecular formula	Molecular weights
1	Urea	U	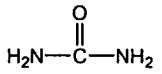	60.0
2	Thiourea	TU	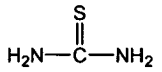	76.0
3	Thioacetamide	TA	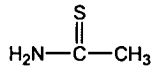	75.0
4	Thiosemicarbazide	TSC	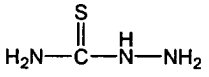	91.0

have been asked e.g. what is the effect on inhibition efficiency, when the amino group of TU is replaced with a methyl group (i.e. to be TA) and/or thiocarbamoyl group (>C=S) replaced by a carbonyl (>C=O). The latter seems especially important for sulfur containing compounds, e.g. thioamides (–CS–NH_2) with excellent inhibition efficiency. Clear comprehension of above questions is helpful to understand the whole inhibition process and the mechanism of adsorption.

On the other hand, quantum chemical studies have been successfully performed to link the corrosion inhibition efficiency with molecular orbitals (MO) energy levels for some kinds of organic compounds, e.g. imidazole [4], cinnamaldehyde [5] and aniline [6], etc.

Following the theoretical analysis procedure mentioned above, we calculated the highest occupied molecular orbital (HOMO), lowest unoccupied molecular orbital (LUMO) energy levels of these amides and its derivatives. Additionally, we also studied their nucleophilic center by calculating the spatial distribution of electronic state density. Our results confirmed the strong correlation between these microscopic electronic properties and corrosion inhibition efficiencies, and gave unambiguous answers to the question about the structure–efficiency relationship of amides, as mentioned above.

2. Calculation method

All the study have been carried out using Dewar's LCAO-SCF-MO semiempirical method, MINDO/3 [7], in the commercially available computer program package (HyperChem Pro. Release 6.03

Table 2
Molecular orbital energy levels of HOMO, LUMO and average inhibition efficiency of amides

	Amides	E (eV)		LUMO–HOMO (eV)	Inhibition efficiency [3] (%)
		HOMO	LUMO		
1	U	−9.945	1.432	11.377	21.98
2	TA	−8.596	0.706	9.302	70.11
3	TU	−8.576	0.755	9.331	70.13
4	TSC	−8.523	0.458	8.981	76.95

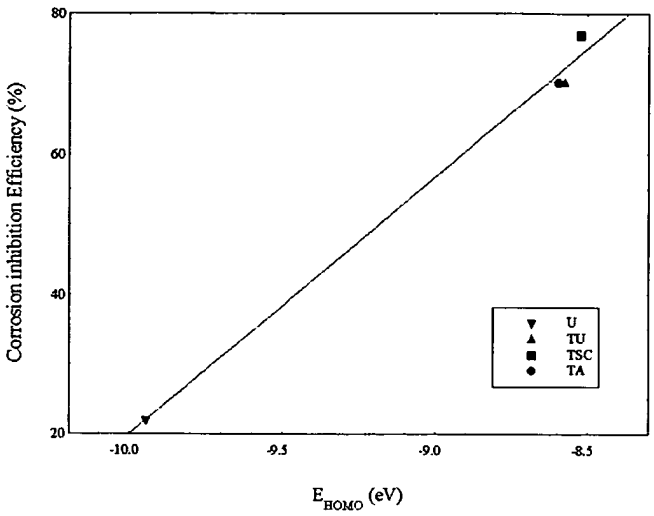

Fig. 1. Plot of E_{HOMO} versus % corrosion inhibition efficiency of amides used.

from Hypercube Inc. USA). The calculation were implemented on an Intel Pentium II 450 MHz computer. MINDO/3 develops the MO on a valence basis set. Molecular structures were optimized to a gradient norm of <0.01 in the vacuo phase. As an optimization procedure, the built-in Polak–Ribiere algorithm was used.

3. Results

Table 1 lists the molecular formula of amide compounds studied in the present work. Urea has a carbonyl group (>C=O) but other three thioamides contain thiocarbamoyl group (>C=S). The difference between TU and TA is that the amino group ($-NH_2$)

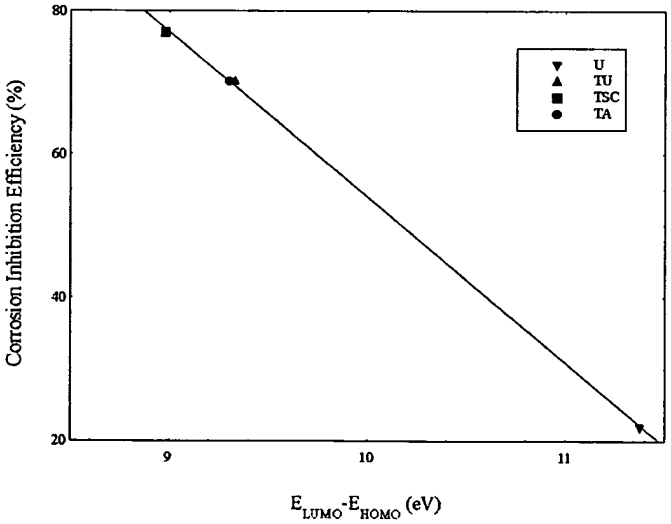

Fig. 2. Plot of HOMO–LUMO energy gap versus % corrosion inhibition efficiency of amides used.

Table 3
Molecular orbital coefficients of HOMO of amides used

		TSC	TU	TA	U
		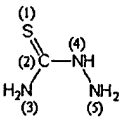	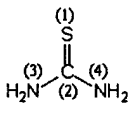	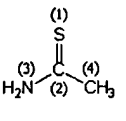	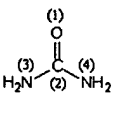
No.	AO	AO coefficients (for HOMO)			
1	2s	0.007	0.000	0.003	0.000
	$2p_x$	0.943	0.970	0.963	0.000
	$2p_y$	−0.110	0.000	−0.014	0.000
	$2p_z$	−0.121	0.000	0.000	0.000
2	2s	−0.017	0.000	0.027	0.000
	$2p_x$	0.006	−0.001	−0.043	0.000
	$2p_y$	0.018	0.000	0.041	0.000
	$2p_z$	0.000	0.000	0.000	0.000
3	2s	−0.091	−0.104	−0.128	0.000
	$2p_x$	0.031	0.042	0.058	0.000
	$2p_y$	0.065	0.083	0.084	0.000
	$2p_z$	−0.003	0.000	0.000	0.707
4	2s	0.110	0.104	0.078	0.000
	$2p_x$	0.021	0.042	0.075	0.000
	$2p_y$	−0.113	−0.083	−0.093	0.000
	$2p_z$	−0.006	0.000	0.000	−0.707
5	2s	0.006	N/A	N/A	N/A
	$2p_x$	0.091			
	$2p_y$	0.160			
	$2p_z$	−0.008			

Molecular orientation definition: use Hyperchem 6.03 built-in Molecular Coordinate System (with x, y, and z Cartesian axes). For four selected amides plotted in the table, x- and y-axes belong to the paper plane and z-axes is perpendicular to the plane of the paper. Molecular Coordinate System was also given in Fig. 3, with relationship to the table above.

in TU is replaced by methyl group ($-CH_3$) in TA. TSC is also a thioamide holding a amino group and a hydrazino ($-NH-NH_2$) group as well.

Table 2 represents calculated energy levels (in eV) of the HOMO and LUMO for the four selected amides. The measured average inhibition efficiencies (%) of these amides were also listed in the table column (these data were measured in 0.05 M HCl acid solutions at 30 °C by using *weight loss technique* [3]).

The relationship between corrosion inhibition efficiencies and HOMO energy levels for these four amides are plotted in Fig. 1. As can be clearly seen from the figure, the inhibition efficiency decreases as the E_{HOMO} level decreases. Urea molecule has the lowest E_{HOMO} value, also has the worst inhibition efficiency. An amount of 1.422 eV energy difference between the E_{HOMO} values of urea and that of TSC which has the highest E_{HOMO} corresponding to 55% change in inhibition efficiency. TU and TA have very close E_{HOMO} values, compared with their very close experimental inhibition efficiencies.

In Fig. 2, inhibition efficiency were plotted against the energy barrier $E_{LUMO} - E_{HOMO}$. TSC has the smallest HOMO–LUMO gap (i.e. 8.981 eV), while U has the highest energy gap (i.e. 11.377 eV). TU and TA also have very close values of energy difference.

Table 3 lists the coefficients (whose squares show the contribution of each atomic orbitals to the density

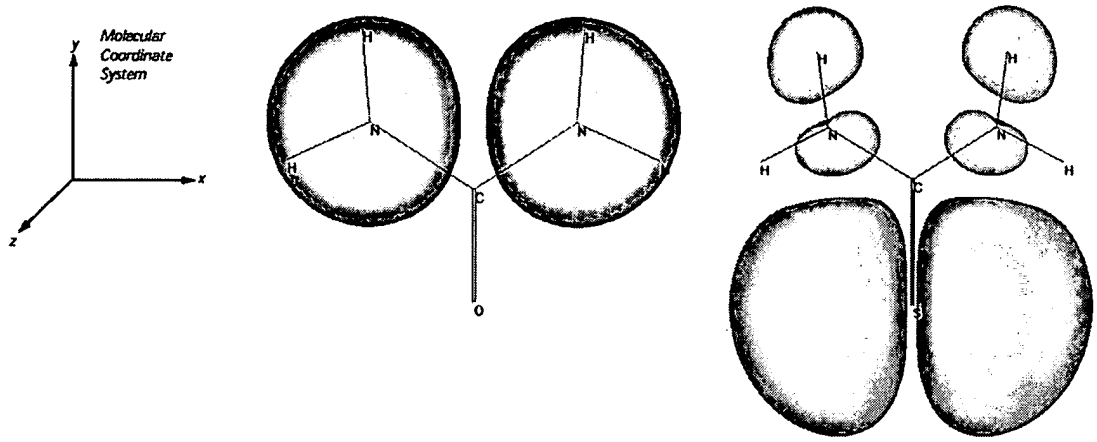

Fig. 3. Plot of HOMO electronic density distribution of U and TU, the HOMO of Urea has most density at each pair of nitrogen atom in amino groups, while transforming to the sulphur atom in the thiocarbamoyl group (>C=S) of TU molecule.

of electron in a given MO [8]) of the development of the HOMO of these four amide molecules. Since MINDO/3 method uses a valence basis set, so that in the development of the MO, only atomic orbitals of the valence shell take a part: 2s, $2p_x$, $2p_y$, $2p_z$ for C, N, O and S, and 1s for H. For brevity's sake, the coefficients corresponding to 1s of H have been omitted in Table 3.

4. Discussion

4.1. Correlation between MO energy level and inhibition efficiency

According to Fukui's frontier orbital approximation [9], interactions happen only between frontier MOs. Therefore, for analysis of the chelate process during chemical adsorption, HOMO and LUMO of both reactants need to be considered. Since due to the inverse dependence of stabilization energy on orbital energy difference, terms involving the frontier MO will provide dominative contribution.

Moreover, another point regarding MO level is the gap between the HOMO and LUMO energy levels for the studied molecules. As was reported [10], Some atoms such as O, N, and S atoms of amides molecules, have unoccupied d orbitals and so exhibit a tendency to obtain electrons; the electrons in the d orbitals can easily be offered because the applied force they affect is small. Excellent corrosion inhibitors are considered to be such organic compounds which not only offer electrons to unoccupied d orbitals of metal surface to form coordinate covalent bond, but also can accept the free electrons from the surface of metal as well, by using their antibond orbital to form feedback bonds in turn.

According to E.E. Ebenso's work [3], when a carbonyl group (>C=O) was substituted by a thiocarbamoyl group (>C=S) (i.e. transform amide to thioamide), the corrosion inhibition efficiency increased significantly. Quantum chemistry calculation reveals that the substitution of (>C=O) by (>C=S) results in a great increase of HOMO energy level (and a great decrease of energy difference, i.e. LUMO–HOMO) obviously. The great increase of inhibition efficiency due to O/S substitution should arise from the great increase of HOMO level, implying the ability of organic molecule to offer free electrons to the metal surface.

Although molecular structures are quite different (i.e. substitution of $-NH_2$ with $-CH_3$), microscopic measurement found that TU and TA have very close values of inhibition efficiency (Table 2), while theoretical calculation obtained that they also have very close values of E_{HOMO} and HOMO–LUMO energy gap as well. Thus TU and TA provides an excellent evidence to confirm the relationship

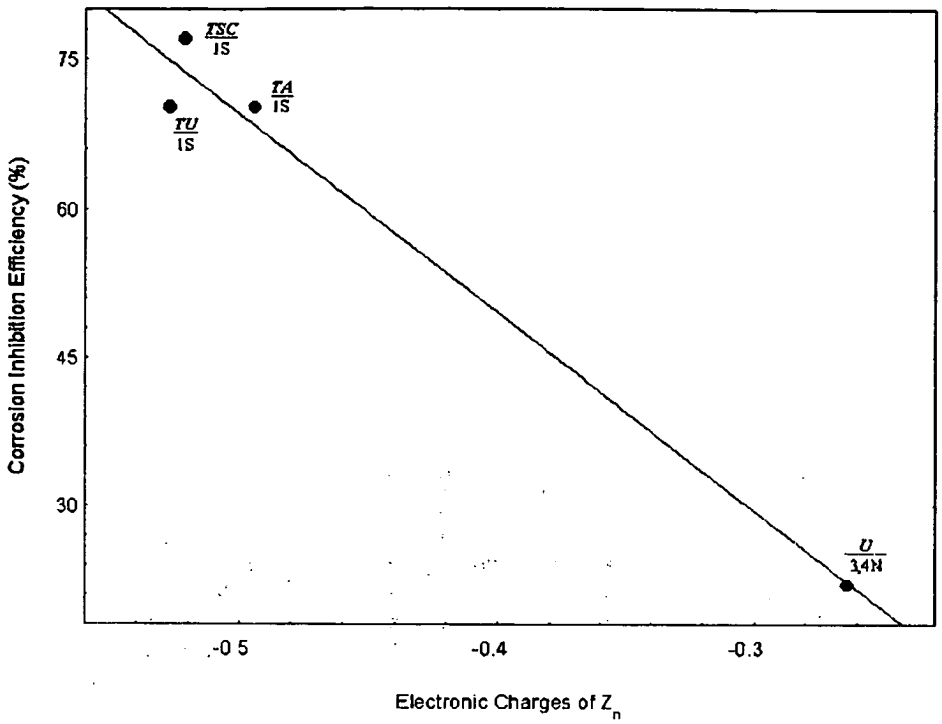

Fig. 4. Plot of electronic charges of specific reactive sites versus % inhibition efficiency of amides used.

between macroscopic properties and their microscopic structures.

Linear correlation between MO energy level and efficiency of amides (Figs. 1 and 2) provides evidence that resulting from the molecular structure, the higher the HOMO energy of the inhibitor, the greater the ease of offering electrons to unoccupied d orbitals of metal surface and the higher the efficiency of the inhibitor for mild steel in HCl acid solutions. The lower the LUMO energy, the easier the acceptance of electrons from metal surface, which decreases HOMO–LUMO energy gap and improves the efficiency of inhibitor.

4.2. Correlation between electronic density and inhibition efficiency

Frontier MO energy level may indicate the tendency of forming a chelate bond with metal surface. Further study on the probable center of chelation site in inhibitors requires knowledge of the spatial distribution of electronic density for given molecules.

From Table 3, the HOMO of three thioamides ($-CS-NH_2$) e.g. TSC, TU, and TA are made up predominantly of $2p_x$ of S atom in the thiocarbamoyl group (>C=S), which contribute respectively 91.6, 94.1, and 92.8% of the electronic charge density of their HOMO levels. This can be associated with the dominative contribution of S atom. According to the Frontier Orbital Approximation, the region of highest density is generally the site of electrophilic attack. Thus, the bond with the chelate from S will be easily formed, rather than C, N atoms.

On the other hand, in the urea molecule, N atom in each amino group contributes 50% of the electronic charge density of HOMO level (Table 3), which is far lower than the contribution of S atom to the HOMO level of thioamide molecules. Therefore, the HOMO is essentially the result of the mixture of the electronic pairs of each N atom. Nevertheless, there seems no MO which may be associated with the O atom in the

carbonyl (>C=O) group. The existence of high coefficients linked to the N atoms guarantees easier formation of the chelate bonds from N by charge transferring, rather than O atom.

Certainly, the analysis of the coefficients reinforces the conclusion in terms of HOMO energy levels that thioamides e.g. TSC, TU, and TA have higher corrosion efficiency than that of non-sulphur containing amide e.g. Urea.

According to the HOMO coefficients listed in Table 3, the HOMO electronic density distribution of Urea and TU are plotted in Fig. 3, clearly indicating the nucleophilic center transforms from each pair of nitrogen atom in Urea to sulphur atom in TU. Similar conclusion was also obtained for other two thioamides, as omitted here.

It is generally true that electrophiles attack molecules at sites of negative charge, which means sites of ionic reactivity can be estimated from the atomic charges in a molecule.

Charges on each probable chelation sites of these amides molecules e.g. $-0.521e$ for S(1) of TSC, $-0.527e$ for S(1) of TU, $-0.494e$ for S(1) of TA and $-0.264e$ for N(3)/N(4) of U, were obtained using MINDO/3 method. Fig. 4 shows the variation of inhibition efficiencies with the charge density of probable electrophilic attack site of each inhibitor molecule. The correlation is linear and efficiency increases as absolute value of charge density increases, which confirms that S atom in the thiocarbamoyl group (>C=S) of thioamide and N atom in the amino group of non-sulphur containing amide are the most probable center of chelation through adsorption via the lone pair of electrons.

5. Conclusions

(I) Strong relationship between HOMO, LUMO levels and corrosion inhibition efficiencies previously reported for some organic compounds was also observed in amide compounds.

(II) Substitution of the carbonyl (>C=O) of some amides (e.g. U) by the group of thiocarbamoyl (>C=S) leads to the transfer of chelation center from each pair of nitrogen atom to the sulphur atom in thiocarbamoyl of thioamide molecules, significantly resulting in the increase of HOMO level and a great reduce of HOMO–LUMO energy difference. This gives a believable explanation for the increase of inhibition efficiency due to the substitution of (>C=O) by (>C=S). That is, thiocarbamoyl group plays predominant role in terms of forming coordinate covalent bonds and/or feedback bonds with metal surface through chemical adsorption.

(III) Analysis of charge density for these four amides also confirmed that nucleophilic center locates on two nitrogen atoms for urea, whereas moves to the sulphur atom for TU.

Acknowledgments

This project is financially supported by the National Natural Science Foundation of China (NO. 20177015).

References

[1] M. Ajmal, A.S. Mideen, M.A. Quaraishi, Corros. Sci. 36 (1994) 79.
[2] B.G. Ateya, B.E. El-Anadouli, F.M.A. El-Nizamy, Bull. Chem. Soc. Jpn 54 (1981) 3157.
[3] E.E. Ebenso, U.J. Ekpe, B.I. Ita, O.E. Offiong, U.J. Ibok, Mater. Chem. Phys. 60 (1999) 79.
[4] G. Bereket, C. Ogretir, A. Yurt, J. Mol. Struct. (Theochem) 571 (2001) 139.
[5] F.B. Growcock, W.W. Frenier, P.A. Andreozzi, Corrosion 45 (1989) 1007.
[6] P.G. Abdul-Ahad, S.H.F. Al-Madfai, Corrosion 45 (1989) 978.
[7] R.C. Bingham, M.J.S. Dewar, D.H. Lo, J. Am. Chem. Soc. 97 (1975) 1285.
[8] J.M. Costa, J.M. Lluch, Corros. Sci. 24 (1984) 929.
[9] H. Fujimoto, S. Kato, S. Yamabe, K. Fukui, J. Chem. Phys. 60 (1974) 572.
[10] S.L. Li, Y.G. Wang, S.H. Chen, R. Yu, S.B. Lei, H.Y. Ma, De X. Liu, Corros. Sci. 41 (1999) 1769.

Appendix B
Functionalization of Nanotubes in 2004

- H. Kuzmany, A. Kukovecz, F. Simon, M. Holzweber, Ch. Kramberger and T. Pichler. "Functionalization of carbon nanotubes." Synthetic Metals, Vol. 141, Issues 1-2, 18 March 2004, Pages 113-122.

- A. A. Koós, Z. E. Horváth, Z. Osváth, L. Tapasztó, K. Niesz, Z. Kónya, I. Kiricsi, N. Grobert, M. Rühle and L. P. Biró. "STM investigation of carbon nanotubes connected by functional groups." Materials Science and Engineering: C, Volume 23, Issues 6-8, 15 December 2003, Pages 1007-1011

- Eugen Unger, Andrew Graham, Franz Kreupl, Maik Liebau and Wolfgang Hoenlein. "Electrochemical functionalization of multi-walled carbon nanotubes for solvation and purification." Current Applied Physics, Vol. 2, Issue 2, April 2002, Pages 107-111.

Functionalization in 2004

- Functionalization of carbon nanotubes *Synthetic Metals*, *Volume 141*, *Issues 1-2*, *18 March 2004*, *Pages 113-122* H. Kuzmany, A. Kukovecz, F. Simon, M. Holzweber, Ch. Kramberger and T. Pichler
  - ***"The functionalization of single wall carbon nanotubes (SWCNTs) is a very actively discussed topic in contemporary nanotube literature because the planned modification of SWCNT properties is believed to open the road towards real nanotechnology applications."***

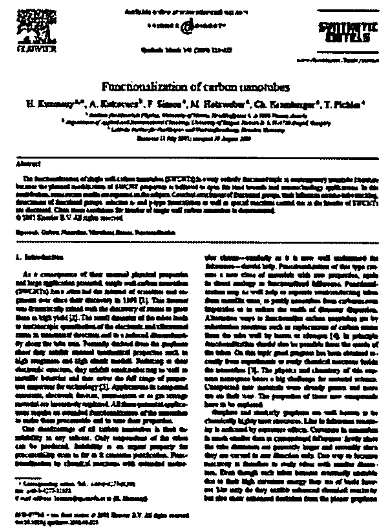
Functionalization of carbon nanotubes

Available online at www.sciencedirect.com
SCIENCE DIRECT
Synthetic Metals 141 (2004) 113–122
SYNTHETIC METALS
www.elsevier.com/locate/synmet

Functionalization of carbon nanotubes

H. Kuzmany[a,*], A. Kukovecz[b], F. Simon[a], M. Holzweber[a], Ch. Kramberger[a], T. Pichler[c]

[a] Institute for Materials Physics, University of Vienna, Strudlhofgasse 4, A-1090 Vienna, Austria
[b] Department of Applied and Environmental Chemistry, University of Szeged, Rerrich B. 1, H-6720 Szeged, Hungary
[c] Leibnitz Institut für Festkörper- und Werkstofforschung, Dresden, Germany

Received 11 July 2003; accepted 19 August 2003

Abstract

The functionalization of single wall carbon nanotubes (SWCNTs) is a very actively discussed topic in contemporary nanotube literature because the planned modification of SWCNT properties is believed to open the road towards real nanotechnology applications. In this contribution, some recent results are reported on the subject. Covalent attachment of functional groups, their influence on tube-tube stacking, detachment of functional groups, selective n- and p-type intercalation as well as special reactions carried out in the interior of SWCNTs are discussed. Clean room conditions for interior of single wall carbon nanotubes is demonstrated.
© 2003 Elsevier B.V. All rights reserved.

Keywords: Carbon; Nanotubes; Vibrations; Raman; Functionalization

1. Introduction

As a consequence of their unusual physical properties and large application potential, single wall carbon nanotubes (SWCNTs) have attracted the interest of scientists and engineers ever since their discovery in 1993 [1]. This interest was dramatically raised with the discovery of routes to grow them in high yield [2]. The small diameter of the tubes leads to macroscopic quantization of the electronic and vibrational states in transversal direction and to a reduced dimensionality along the tube axis. Formally derived from the graphene sheet they exhibit unusual mechanical properties such as high toughness and high elastic moduli. Referring to their electronic structure, they exhibit semiconducting as well as metallic behavior and thus cover the full range of properties important for technology [3]. Applications in compound materials, electronic devices, nanosensors or as gas storage material are intensively explored. All these potential applications require an extended functionalization of the nanotubes to make them processable and to tune their properties.

One disadvantage of all carbon nanotubes is their insolubility in any solvent. Only suspensions of the tubes can be produced. Solubility is an urgent property for processability even as far as it concerns purification. Functionalization by chemical reactions with extended molecular chains—similarly as it is now well understood for fullerenes—should help. Functionalization of this type creates a new class of materials with new properties, again in direct analogy to functionalized fullerenes. Functionalization may as well help to separate semiconducting tubes from metallic ones, to purify nanotubes from carbonaceous impurities or to reduce the width of diameter dispersion. Alternative ways to functionalize carbon nanotubes are by substitution reactions such as replacement of carbon atoms from the tube wall by boron or nitrogen [4]. In principle functionalization should also be possible from the inside of the tubes. On this topic good progress has been obtained recently from experiments to study chemical reactions inside the nanotubes [5]. The physics and chemistry of this concave nanospace bears a big challenge for material science. Unexpected new materials were already grown and more are on their way. The properties of these new compounds have to be explored.

Graphite and similarly graphene are well known to be chemically highly inert structures. Like in fullerenes reactivity is activated by curvature effects. Curvature in nanotubes is much smaller than in conventional fullerenes: firstly since the tube diameters are generally larger and secondly since they are curved in one direction only. One way to increase reactivity is therefore to study tubes with smaller diameters. Even though such tubes become eventually unstable due to their high curvature energy they are of basic interest. Not only do they exhibit enhanced chemical reactivity but also show enhanced deviation from the planar graphene

* Corresponding author. Tel.: +43-1-4277-51306; fax: +43-1-4277-51357.
E-mail address: kuzman@ap.univie.ac.at (H. Kuzmany).

0379-6779/$ – see front matter © 2003 Elsevier B.V. All rights reserved.
doi:10.1016/j.synthmet.2003.08.018

properties. Very narrow tubes were even demonstrated to exhibit superconducting fluctuations up to 15 K.

In this paper, we present some recent results on the chemical functionalization of SWCNT and on chemical reactions and reaction products in the curved nanospace inside the tubes. These reports are preceded by a compilation of SWCNT materials and experimental and analytical procedures used for their study. With respect to the latter particular attention is paid to resonance Raman scattering.

2. Single wall carbon nanotubes

Single wall carbon nanotubes can be understood as rolled up stripes of graphene sheets. Each lattice vector of the sheet determines a particular nanotube by rolling up the sheet in a way that the origin and the top of the lattice vector come to coincidence. This generating vector is called Hamada-vector or folding vector (n, m). Along the tube axis lattice periodicity is provided and the size of the unit cell, including the tube diameter, is determined by the Hamada-vector of the tube. The geometry is depicted in Fig. 1. As long as the carbon–carbon distances are assumed independent from the rolling up process the tube diameter d and the number of carbon atoms per unit cell N can be read directly from the figure as

$$d = \frac{a}{\pi}\sqrt{n^2 + m^2 + nm} \tag{1}$$

$$N = \frac{2(m^2 + n^2 + nm)}{d_R} \tag{2}$$

where $a = 2.41$ Å is the lattice constant of the unrolled honeycomb lattice and d_R is defined as

$$d_R = \begin{cases} d_H & \text{if } (n - m) \text{ is not a multiple of } 3d_H \\ 3d_H & \text{if } (n - m) \text{ is a multiple of } 3d_H \end{cases} \tag{3}$$

where d_H denotes the highest common divisor of n and m.

For small tube diameters Eq. (1) is not valid any more and ab initio density functional calculations are needed to obtain

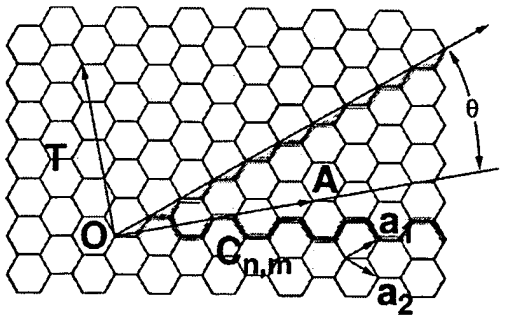

Fig. 1. Basics of SWCNT geometry. Lattice vectors are denoted a_1 and a_2, while the OA vector is the C chiral vector of the (4, 2) tube. The two gray contour lines indicate the cross-sections of the two limiting cases of graphene sheet folding: the zigzag $(n, 0)$ and the armchair (n, n) nanotubes, respectively. The θ angle is the chiral angle of the nanotube.

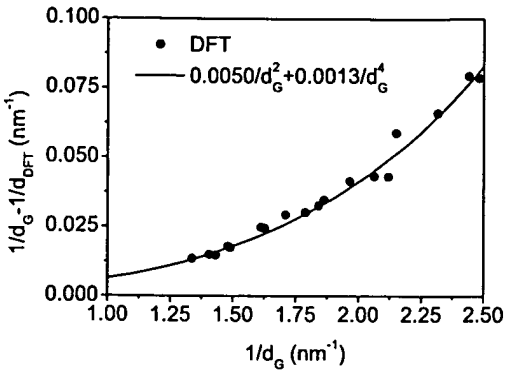

Fig. 2. Difference between inverse tube diameters calculated from density functional theory and zone folding for small tubes vs. inverse zone folding diameters.

the correct tube geometry. Fortunately, the reduced number of carbon atoms in the small tubes allows for such calculations at least up to (5, 6) or $d = 0.75$ nm. Fig. 2 depicts results we have obtained recently from such calculations. For the spectroscopic analysis of small tubes the deviations from the graphene geometry cannot be neglected.

Several SWCNT synthesis methods are available today (see Table 1 for a survey). In general, SWCNTs always grow from carbon plasma in the presence of structure directing agents. The latter are usually in situ formed transition metal (Co, Fe, Ni, V, etc.) nanoparticles, although in special cases (peapod to DWCNT conversion, CNT growth within zeolites) steric limitations can also provide the necessary structure directing constraints. The most important differences between the available methods are (i) the way the plasma is generated, (ii) the way the catalyst metal is introduced, (iii) SWCNT yield, (iv) SWCNT quality and (v) possibilities of up-scaling and commercialization. While at present the majority of the world's SWCNT production comes from the two conventional sources (PLV and dc arc), it is expected that continuous and less power-hungry methods (gas phase decomposition and CCVD) will eventually become the major industrial SWCNT suppliers. The CCVD method is unique since it is the only technique that makes precise spatial SWCNT positioning possible.

One of the classical methods to analyze SWCNT is transmission electron microscopy (TEM). Even though this technique provides direct evidence for some geometrical properties of the tubes it is very site selective and does not give representative results. On the other hand Raman spectroscopy, in particular with its characteristic resonance enhancement, has proven to be an excellent analytical tool [13]. Two spectral ranges are particularly useful for analytical purposes: the range of the radial breathing mode (RBM) between 150 and 450 cm^{-1} and the so called D-line between 1250 and 1400 cm^{-1}.

The RBM is a typical feature of the nanotubes as it does not exist in the graphene plane. Since the mode frequency scales as $1/d$, where d is the tube diameter, it can be used

Table 1
A summary of the contemporary SWCNT synthesis techniques and product description

Short name	Technology of preparation [reference]	Typical mean diameter (nm)	Product description
Laser ablation (PLV)	Ablation from graphite doped with (Fe, Co, Ni, ...) catalyst [2]	1.4 (1–1.8)	High quality, good diameter control, bundled tubes; commercial
dc arc discharge	First reported production. Modified Kratschmer reactor [6]	1.5 (0.9–3.1)	Lesser quality, carbonaceous impurities abundant. CNTs grow bundled
Gas phase decomposition	Decomposition in an oxygen-free environment. Typical: HiPco® (high pressure CO decomposition) [7]	1 (0.9–1.3)	Easy purification, commercial, good quality
CCVD	Catalytic chemical vapor deposition. Supported metal catalysts are used [8]	1.5 (1.3–2)	Cheapest, commercial, up-scalable. Most feasible from the application point of view
Flame pyrolysis	Carbon source + metallocene catalyst, conventional low pressure pyrolysis reactor [9]	2–3	Low yield, bad quality. Still under development. Plant technology available, large commercialization potential
Solar furnace	Solar rays focused on a metal doped graphite target. Growth dynamics similar to PLV [10]	1.4	Good quality CNTs, little amorphous carbon. Spreading not expected in the near future
Inner tubes of DWCNTs	Catalyst free growth from peapods by coalescence of C_{60} molecules [11]	0.7 (0.55–1)	Well shielded, best quality CNTs. Separation from outer tubes is very challenging
Zeolite grown	CNTs grow by thermal decomposition of template molecules within zeolite channels [12]	0.45	Monodisperse diameter distribution, oriented tubes. CNTs metastable outside the channels

to determine tube diameters in principle. Unfortunately, the scaling factor is not known with a high precision. Reported values are between 23 and 48 cm^{-1} [14–16] which allows only an order of magnitude evaluation for absolute values or the evaluation of relative tube diameters and tube diameter distributions [13]. An additional difficulty in the assignment of Raman lines to tube diameters is the high density of geometrically allowed tubes of the order of 15 tubes per nanometer diameter difference or accordingly one tube per wave number difference. This holds at least for standard tube diameters. The resulting overlap of Raman lines is lifted for very small tube diameters as it is demonstrated below. For such tubes the overlap problem is not relevant but now the 1/d law is not well satisfied and ab initio density functional calculations (DFT) are needed to evaluate the tube diameters. On the other hand, as the energy gap between the van Hove singularities in the valance band and in the conduction band also scales with the inverse tube diameter, photoselective resonance scattering is observed [17] and leads to a colorful response in Raman experiments if the spectra are excited with different laser energies [18].

The D-line response is the other important analytical tool. From some very recent work its origin is well understood as a response from the K-point of the graphene Brillouin zone with an enhancement from a triple resonance scattering [19,20]. The scattering process needs an impurity or a defect to be involved for momentum conservation. Therefore the scattering cross section of the D-line depends on the defect concentration and can be used as a measure of the latter. An attractive quantity for this concentration is the relative scattering intensity of the D-line and its overtone, the so called G′ line. The G′ line is also triple resonance enhanced but independent from any defect concentration.

NMR spectroscopy, as such certainly a qualified tool to study functionalization, turned out to be less efficient for long time due to magnetic contamination from catalytic particles. Such particles are difficult to remove since they are often covered up with a carbon layer. Similarly, IR spectroscopy did not provide a good access to SWCNT analysis. However, in the case of chemical functionalization the side groups respond in general well to IR absorption.

Raman spectra recorded in this contribution were obtained on a triple grating Dilor xy spectrometer utilizing a back-thinned CCD detector. Samples for the Raman measurements were in buckypaper form. FT-IR spectra were recorded on a Bruker IFS-66v instrument in reflection absorption geometry.

3. Exohedral chemical functionalization of SWCNTs

The perfect SWCNT is without functional groups and therefore chemically quite inert. Addition-based covalent chemistry on nanotubes is more difficult than transforming fullerenes but is considerably easier than functionalizing graphite. The two main sources of reactivity in SWCNTs are (i) the curvature-induced strain arising from the non-planar geometry of sp^2 carbons and (ii) the misalignment of the π orbitals [21]. The former is more pronounced (i.e. the pyramidalization angle is larger) at the capping fullerene

hemispheres while the latter effects mainly the side-walls. All in all, the most reactive places in any nanotube sample are found in the cap of the thinnest tube and least reactive are the bonds running perpendicular to the axis of the largest diameter SWCNT.

Derivatization reactions can be roughly divided into two categories. In the first case, the required functional groups are attached directly onto the nanotube using 1,3-dipolar cycloaddition [22], the Birch reduction [23] and reactions with nitrenes, radicals and carbenes [24]. When taking the second approach we first build bridgeheads by oxidizing some atoms in the tube wall and then proceed using substitution reactions to change the simple (–F, –OH, –COOH) groups formed. The first reaction step is usually some aggressive treatment, e.g. (i) oxidation in refluxing conc. HNO_3 (yields carboxyl groups) [25–27], (ii) ozone treatment [28,29], (iii) ball milling in reactive atmosphere [30] or together with solid KOH (hydroxyl groups) [31], (iv) HF reaction (–F groups) [32,33]. Then in the second step these bridgeheads are converted to more reactive groups, e.g. carboxyl groups are replaced by acyl chlorides after $SOCl_2$ treatment and finally, conventional organic synthesis reactions like the Grignard reaction [34] are applied to build the desired functionality onto the anchor sp^3 carbon in the nanotube wall.

In the course of the work reported here first the simplest functionalized SWCNTs were studied: nanotubes with –COOH groups formed upon purification treatment in refluxing HNO_3 [35] (see Fig. 3A for a schematic representation of the material). The presence of the carboxyl groups was proved by FT-IR measurements and earlier ^{13}C NMR investigations. In Fig. 4, we present the resonance Raman spectra of the pristine and the functionalized nanotube sample in the RBM region for three selected laser excitation energies. It is interesting to note that the RBM suffers an approx. 8 cm^{-1} up-shift upon functionalization without changing its shape. This phenomenon cannot be explained on the basis of resonant Raman theory alone. Instead, we interpret it as a token of increased stacking interaction within the SWCNT bundles. By analyzing the first and second spectral moments of the RBMs we were able to quantify the extent of this interaction and suggest that the SWCNT bundles after oxidative functionalization contain 6–10 times more nanotubes than before. A possible reason for this behavior could be that the formed carboxyl groups favor the development of intertube H-bonds.

Advancing towards more complex functional groups we investigated the properties of SWCNTs functionalized with the 1,3-dipolar cycloaddition reaction of azomethine yields (see Fig. 3B) [22]. The attachment of the sidechain is evident from the FT-IR spectrum of the material (Fig. 5A) where e.g. the contributions of the ν(N–H), ν(C–H) and ν_{as}(C–O–C) vibrations can be clearly identified at around 3400, 3000 and 1100 cm^{-1}, respectively. In agreement with independent literature reports we have also found the functionalized SWCNT material to be luminescent which prevented direct resonance Raman investigations. The special importance of this functionalization scheme is that the resulting nanotubes become soluble in organic solvents (up to 50 mg/ml in $CHCl_3$) and even in water. Dissolved nanotubes can be separated from impurities by e.g. chromatographic techniques and finally, the original SWCNT structure can be restored by thermal annealing [36]. In Fig. 5B, we present the Raman RBM spectra of the nanotubes before functionalization and after annealing. It is evident from the figure that the RBM modes characteristic for SWCNT samples are recovered by heating.

As demonstrated above, functionalization can affect the constitution of SWCNT bundles when the attached functional groups act as stacking modifiers. Curiously enough, the reverse statement also proved to be valid: the intertube channels are indeed able to affect the functionality of nanotubes by acting as size-selective filters allowing doping species to enter certain bundles and stay clear from others (Fig. 3C) [37]. Fig. 6 depicts present Raman spectra of HiPco® SWCNTs in various stages of potassium intercalation (n-type doping). It can be seen that the RBM lines corresponding to the thinnest and thickest nanotubes are selectively reduced, whereas the modes originating from intermediate tube diameters are not effected that much. Since the diameter of the intertube channels is maximal in the bundles of the thickest nanotubes, the selective reduction of the low wavenumber RBM peaks can be explained simply by geometrical constraints. While not that straightforward, the interpretation of the loss of the peaks corresponding to the thinnest SWCNTs is also possible by realizing that the lattice expansion work required for the potassium dopant to enter the bundle is the smallest in the case of the smallest tube diameters [38]. Very similar trends could be observed in a parallel set of experiments utilizing $FeCl_3$ dopant (p-type doping). The electronic properties of SWCNTs are heavily influenced by both n- and p-type doping. Therefore, the described diameter dependent doping phenomenon may find important applications in nanotube functionalization, especially when high selectivity is required.

4. The concave nanospace inside the tubes as a chemical reactor

4.1. Filling SWCNT with fullerenes

The inside of carbon cages is certainly interesting from a chemical point of view as the distribution of the carbon π orbitals is quite different in comparison to their distribution on the outside. Fig. 7 gives a demonstration for a (7, 7) tube. The smaller the tube diameter the more deviation is established form a clean π–π overlap.

Experimentally very little is known about the interior of carbon cages. The reason is the fact that so far all attempts failed to open the fullerene cages and to inspect the interior chemically by studying reactions in the concave environment of the carbon atoms. Experimentalists were

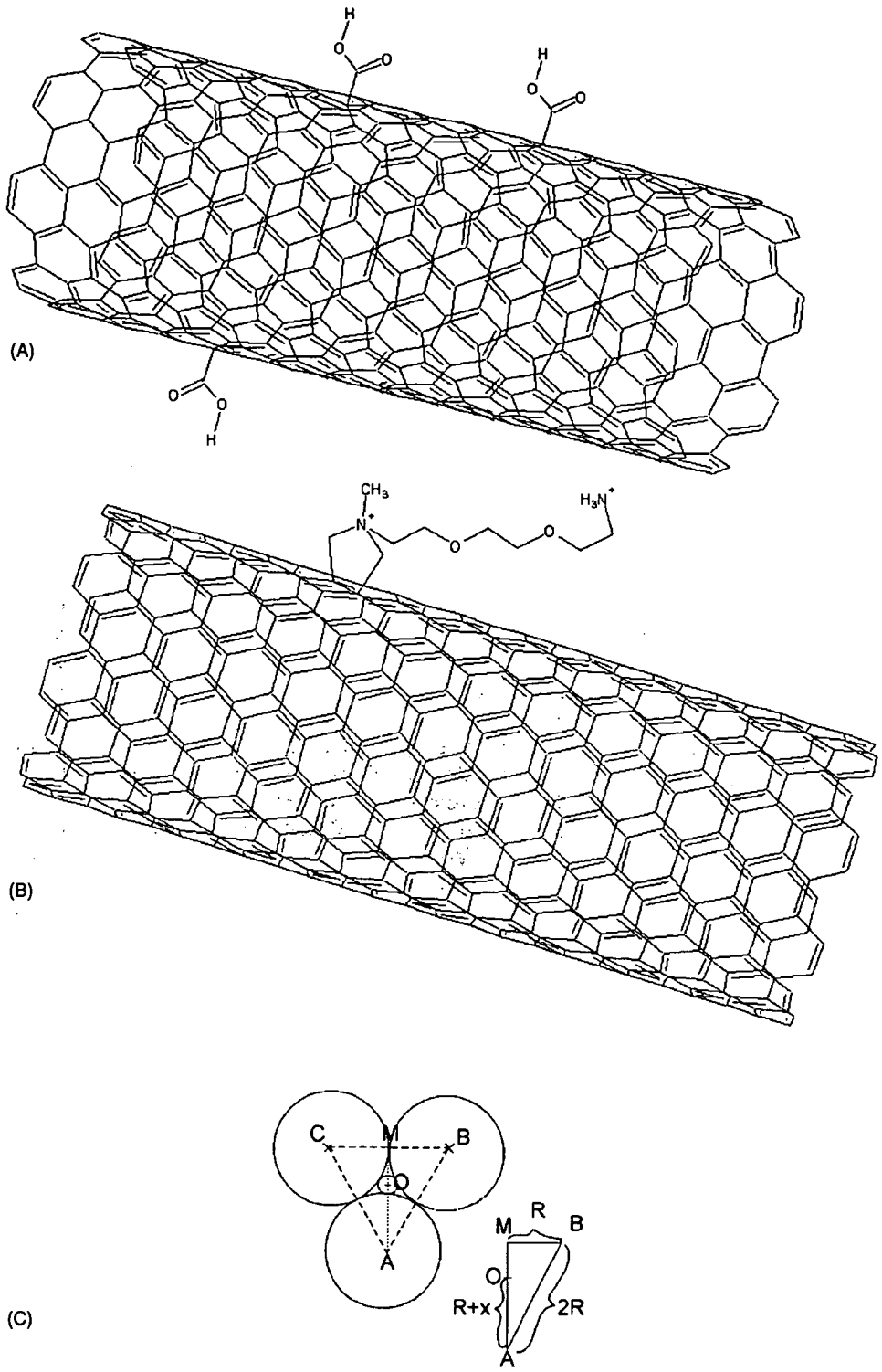

Fig. 3. Visualization of the functionalized SWCNT material studied here: (A) carboxy-functionalized nanotube, (B) solubilized nanotube, (C) basics of calculating the x radius of the intertube channels in a triangular lattice containing r_{NT} radius tubes that have an additional r_{vdW} van der Waals radius around them. $R = r_{NT} + r_{vdW}$. The sides of the ABC triangle are equal, therefore, the O point divides the MA segment in a 1:2 ratio.

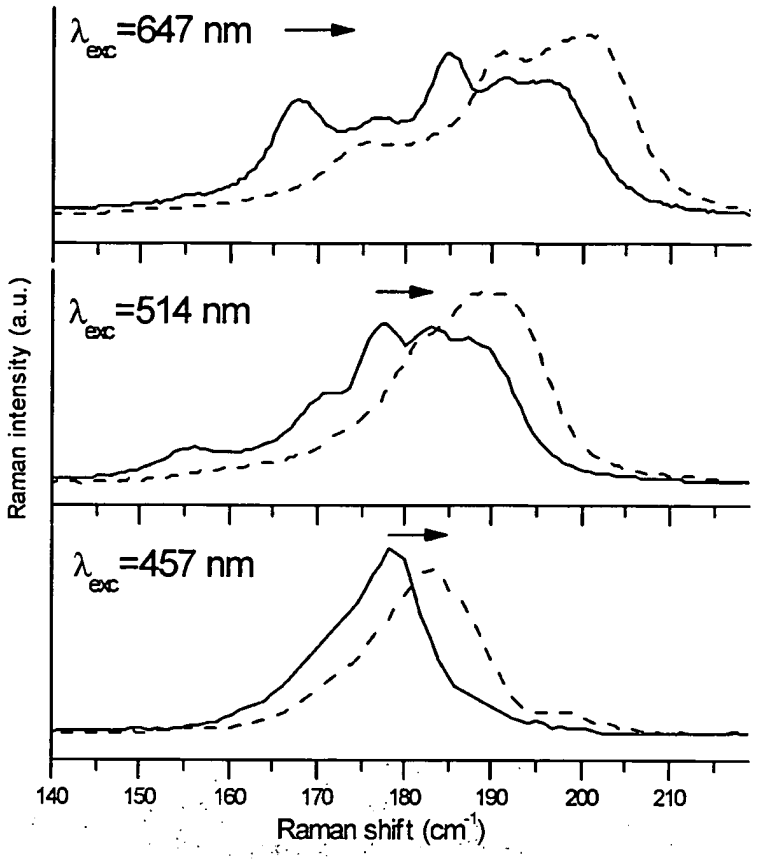

Fig. 4. Resonant Raman spectra of pristine (solid line) and carboxy functionalized (dashed line) SWCNT material in the radial breathing mode region, measured with three different laser lines.

left with the cumbersome purification procedure of material where atoms were incidentally encaged during the growth process. Considerable progress was made recently at this point by discovering a possibility to fill the nanotubes with fullerenes [39] or, more generally, with matter [40]. Particular interest was directed to the filling of single wall carbon nanotubes with C_{60} fullerenes in order to make so called "peapods".

In our experiments commercial SWCNT (Nanocarblab, Moscow, Russia) and fullerenes ('super golden grade' Hoechst AG, Frankfurt, Germany) were used for the production of fullerene peapods. The SWCNT material was prepared by dc arc-discharge and was purified to 50% using repeated high temperature air and acid washing treatments by the manufacturer. Purity was determined from HR-TEM by the supplier and it is consistent with our own studies. The high filling levels discussed below are consistent with the effective tube-end opening side-effect of the SWCNT purification [41]. We found that the other reported tube-end opening procedure, i.e. refluxing in H_2O_2 [42], does not increase the fullerene filling levels. We followed the method of Kataura et al. [42] to fill fullerenes in the vapor phase. This method involves sealing of the SWCNT material with the fullerene in a quartz ampoule and keeping it at 650 °C for 2 h. The resulting material was thoroughly sonicated in toluene in order to remove the non-reacted fullerenes, filtered, and dried from toluene at 400 °C in dynamic vacuum. A 30 min dynamic vacuum treatment at 800 °C is equivalent to this last step in removing non-reacted fullerene particles without observable effect on the peapods.

Both TEM and Raman scattering are excellent tools to analyze the filling of SWCNTs with fullerenes. Fig. 8 is an example for SWCNTs filled with C_{60} (A) and C_{70} (B). As already mentioned above, due to the site selectivity of the TEM technique it is difficult to determine filling concentrations from such experiments. In the Raman response the scattering from the nanotube modes as well as the scattering from the enclosed fullerenes appears [5,42]. In the case of C_{60} a characteristic splitting pattern of the total symmetric modes, the pentagonal pinch mode and the radial breathing mode, is a reliable signature for the C_{60} cages encapsulated into the tubes [43]. The relative intensities of these modes to the RBM mode and to the G mode of the tubes is a quantitative measure for the filling concentration [44]. Absolute values of the filling concentration can be obtained from electron energy loss spectra (EELS) [45]. Results from EELS and Raman are in good agreement and provide therefore reliable numbers for the filling.

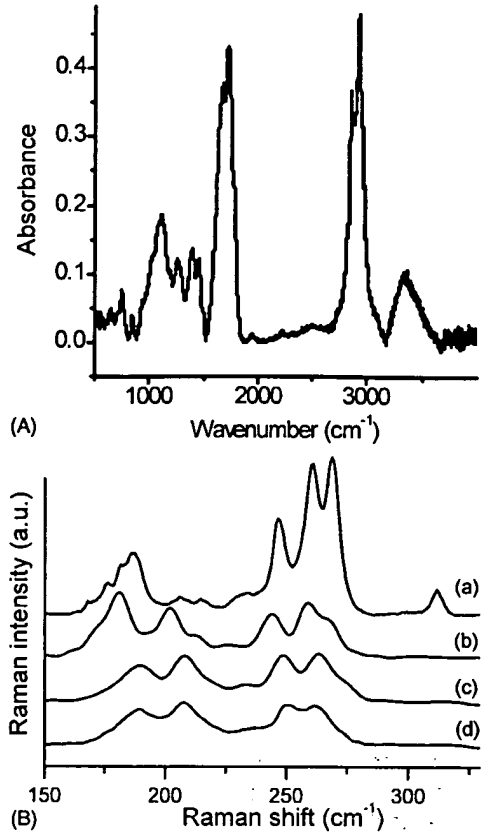

Fig. 5. Spectroscopic study on the solubilized SWCNTs: (A) FT-IR spectrum of the material, (B) resonant Raman spectra of the pristine (a), annealed pristine (b), functionalized and heated (c) and functionalized, heated and annealed (d) SWCNT samples.

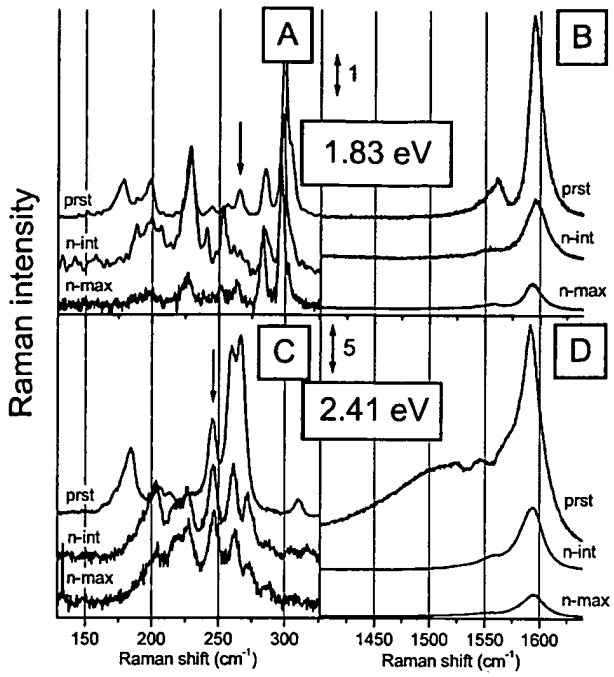

Fig. 6. Development of Raman spectra during the K (n-type) doping of the HiPco® sample. Top row: 1.83 eV excitation. Bottom row: 2.41 eV excitation. Plots (A and C) and (B and D) show the RBM and the G line windows, respectively. In all plots, "prst" marks the spectrum of undoped tubes while "n-int" and "n-max" denote the intermediate and the final stages of the doping process. To make a comparison between relative peak intensities easier, the 1.83 and 2.41 eV RBM spectra are normalized to the intensity of the 265 and 245 cm^{-1} peak, respectively. These peaks are indicated by vertical arrows in the plots. For the G-lines, intensities within one plot are measured on the same scale which is given in the top left corner [38]. Reproduced by permission of the PCCP Owner Societies.

4.2. Polymerization of fullerenes inside the SWCNT

We studied recently two types of chemical reactions of the encaged peas in the nanotubes. One of them is a polymerization of C_{60} fullerenes after heavy doping of the peapod system with electron donors such as alkali metals [5,46]. The results of the doping process on the Raman response are demonstrated in Fig. 9 for potassium doping. The shift of the pentagonal pinch mode of the encapsulated C_{60} as demonstrated in the figure is about 40 cm^{-1}. This means 6 extra electrons are accommodated on the fullerene cage. The results become even more interesting if the response from the radial modes of the C_{60} is analyzed. This response is depicted in Fig. 10 in comparison with the response from C_{60}^{6-} in a crystal and from a typical polymeric phase of C_{60}. The strong features assigned as P at 360 and 620 cm^{-1} are typical signatures from a polymeric phase. These lines have been observed several times in neutral and doped C_{60} polymers. Though slightly shifted they are well pronounced in the selected example of RbC_{60}. A polymeric phase of K_6C_{60} has not been observed so far for C_{60} outside the tubes. From calculation of reaction enthalpies reported by Pekker et al. [47], a linear single bonded C_{60}^{6-} polymeric phase is the second most stable polymeric structure in the system of charged C_{60} molecules. It is thus very likely that the charged C_{60}^{6-} cages have reacted to this structure in the tubes.

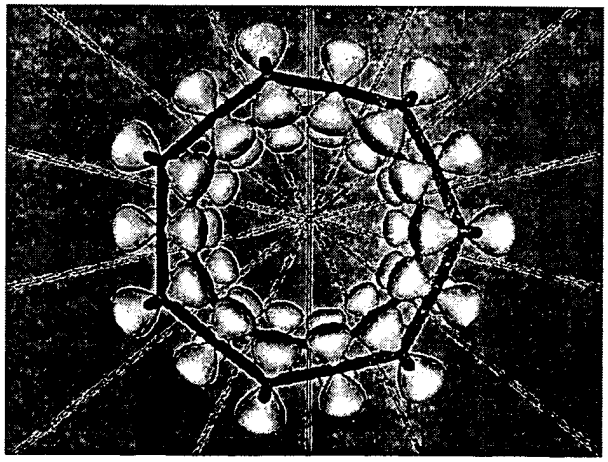

Fig. 7. Schematic view of electronic orbitals inside a (7, 7) single wall carbon nanotube.

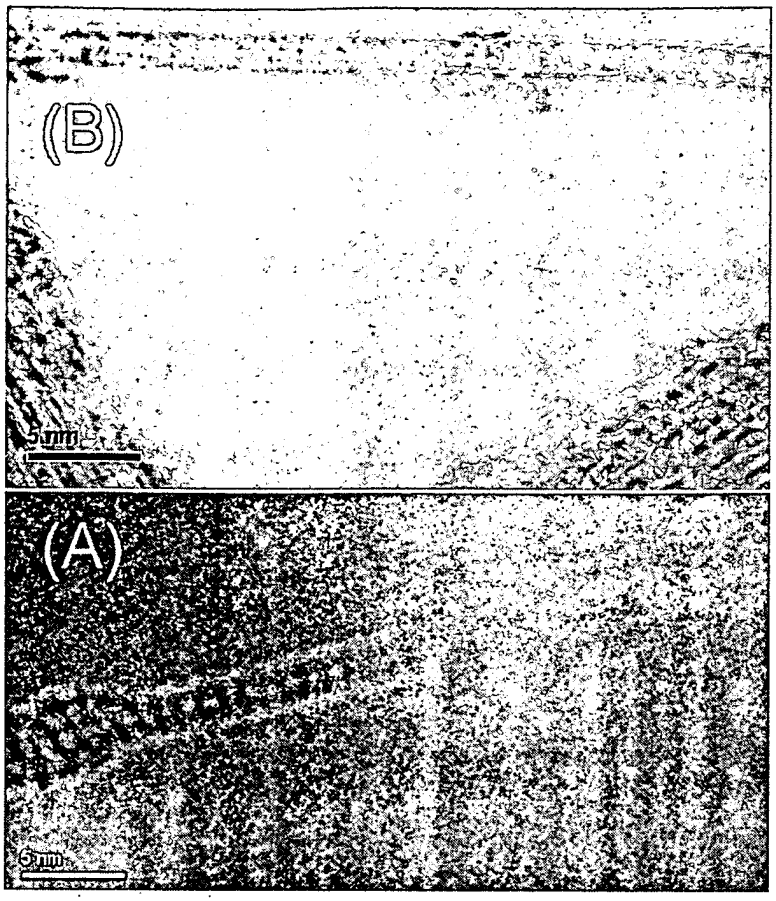

Fig. 8. Transmission electron micrographs of individual tubes filled with C_{60} (A) and C_{70} (B).

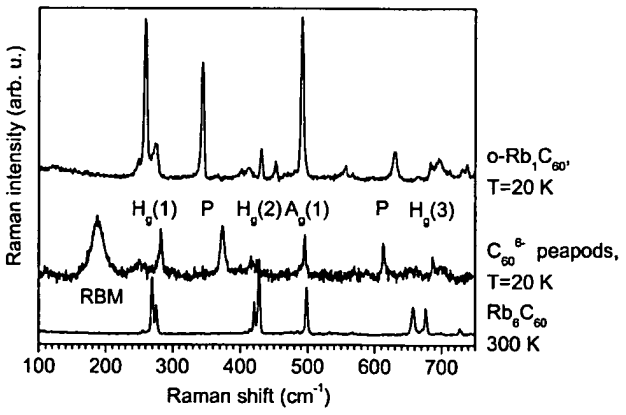

Fig. 9. Raman response of the tangential mode frequency range for potassium doped SWCNTs and potassium doped peapods. Spectra were excited with three different lasers as indicated. The first, third, and fifth spectrum from the bottom are for empty tubes, the second forth and sixth spectrum are for filled tubes. The right arrow assigns the frequency of the pentagonal pinch mode for the uncharged C_{60}, the left arrow marks the frequency after long doping.

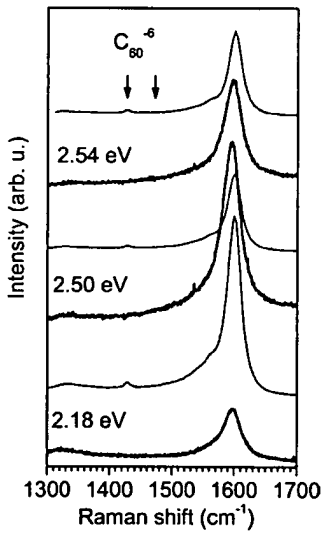

Fig. 10. Raman spectra of the radial part of charged C_{60} as recorded with a green laser line at 514 nm and temperatures as indicated. The spectra at the bottom, in the center, and at the top are for crystalline C_{60}^{6-}, for the heavily doped peapods, and for an one-dimensional polymeric phase of C_{60}^{-}, respectively.

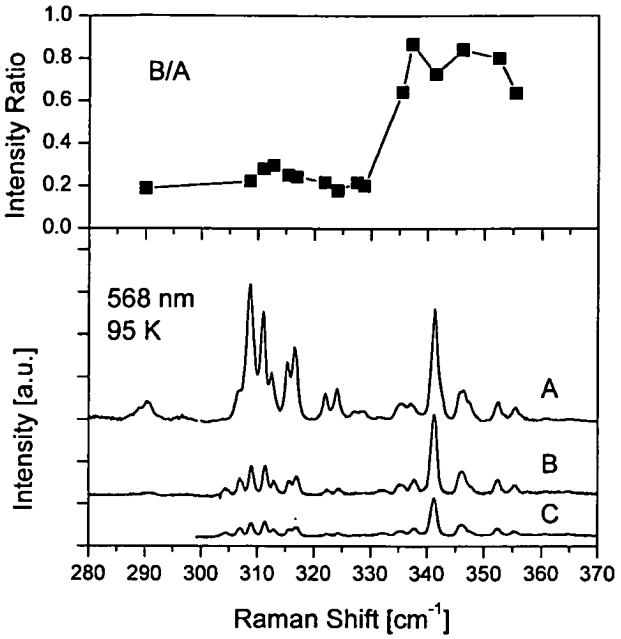

Fig. 11. Growth of DWCNTs from peapods by vacuum annealing at 1520 K. The lower part depicts thee spectra: (C) after 30 min annealing, (B) after 60 min annealing, and (A) after 120 min (saturation) annealing. The upper part depicts the relative intensities of the Raman lines in spectrum B to spectrum (A).

4.3. Generation of double wall carbon nanotubes

The other reaction inside the tube which we have recently investigated is a transformation of the encaged fullerenes to a second inner tube forming the double wall carbon nanotube (DWCNT) system. The creation of DWCNT from the encapsulated fullerene peas was first demonstrated by Bandow et al. by a TEM analysis of high temperature treated peapods [11]. For the growth process several models were proposed. Either the fullerene cages connect via a cyclo-addition process and subsequent Stone-Wales reactions transform the connected cages eventually to an inner tube [48] or the cages break up into small pieces, like e.g. C_2 units, and recondense as an inside tube. Fig. 11 depicts Raman spectra of the radial breathing mode of the inner shell tubes after extended annealing at 1520 K in high vacuum. We demonstrated recently that each (split) peak in the spectrum corresponds to one tube species [49]. The high frequency lines originate from the small tubes with diameters below 0.7 nm. For short annealing times mainly the peas in the narrow tubes transform to the inner shell tube. Only for extended annealing the larger diameter tubes follow. This is explicitly demonstrated in the top part of the figure which exhibits the intensity ratio between the lines in spectrum B to the lines in spectrum A. This result disfavors the cyclo-addition and Stone–Wales transformation model since in the latter high mobility of the peas is requested. Such high mobility is rather provided by the large tubes. The cyclo addition model is also disfavored from our observation that encaged C_{60} and encaged C_{70} molecules give almost the same line pattern after annealing. In other words the same kind of inner tubes are created even though the larger size of the C_{70} molecules does not allow room for a cyclo addition reaction if the tube size is too small for an upright ordering of the elongated C_{70} molecule.

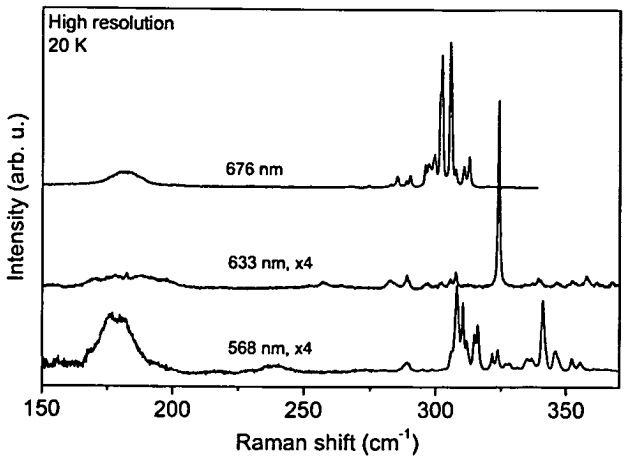

Fig. 12. Raman response of RBMs from outer shell and inner shell tubes in DWCNTs prepared from C_{60} at SWCNT peapods. Inner shell tubes give 10 times higher peaks.

The structural properties of the inner shell tubes in the DWCNT system are interesting by themselves. The widths of the Raman lines from the inner shell RBM response is unusual narrow, of the order of 0.5 cm^{-1} but extends down to even lower values. This means the interior of the primary, outer tubes is highly shielded and the inner tubes exhibit a high degree of perfectness. They are catalyst free grown in a "nano cleanroom". An example for the narrow lines is depicted for three different excitation energies in Fig. 12. The broad lines on the left side represent the response from the outer shell tubes, the narrow lines on the right come from the inner shell. Also, particularly for the excitation with the deep red laser, the peak and total intensities for the scattering from the inner tubes are almost a factor of 10 higher than the scattering from the outer tubes. Very sharp resonances and an enhanced electron-phonon coupling is likely to be the reason for this dramatic behavior. The enhanced electron-phonon coupling for strong curvature carbon surfaces is not unexpected as calculations for small fullerenes have repeatedly demonstrated such effects [50].

5. Summary

The reported results demonstrate that various ways exist to functionalize SWCNT. Functional groups covalently attached to the outer surface of the nanotubes are able to modify the stacking and solvatation properties of nanotubes. An interesting feature of SWCNT bundles is that their n- and p-type intercalation proceeds in a diameter dependent way, thus making it in principle possible to selectively modify

certain nanotubes while leaving others intact. Functionalization inside the tubes in the form of covalent chemical bonds has not yet been demonstrated but chemical reactions which lead to products not observed outside the tubes occur. Such reactions are the polymerization of charged fullerene cages and the catalyst free growth of SWCNTs with a high degree of perfectness. The fullerenes in the smaller tubes exhibit a higher probability for the transformation process as compared to the fullerenes in the larger tubes.

Acknowledgements

The authors acknowledge financial support from the EU RTN FUNCARS (HPRN-CT-1999-00011) and FWF Austria project No. 14386. Valuable discussions with Prof. M. Prato and V. Georgakilas from the University of Trieste are also gratefully acknowledged. A.K. thanks for a support from a Zoltan Magyary fellowship. All authors thank J. Bernardi for the assistance with the TEM studies.

References

[1] S. Iijima, T. Ichihashi, Nature 363 (1993) 603.
[2] T. Guo, P. Nikolaev, A. Thess, D.T. Colbert, R.E. Smalley, Chem. Phys. Lett. 243 (1995) 49.
[3] M.S. Dresselhaus, G. Dresselhaus, P.C. Eklund, Science of Fullerenes and Carbon Nanotubes, Academic Press, San Diego, 1996.
[4] D. Golberg, Y. Bando, W. Han, K. Kurashima, T. Sato, Chem. Phys. Lett. 308 (1999) 337.
[5] T. Pichler, H. Kuzmany, H. Kataura, Y. Achiba, Phys. Rev. Lett. 8726 (2001).
[6] S. Iijima, Nature 354 (1991) 56.
[7] P. Nikolaev, M.J. Bronikowski, R.K. Bradley, F. Rohmund, D.T. Colbert, K.A. Smith, R.E. Smalley, Chem. Phys. Lett. 313 (1999) 91.
[8] J.F. Colomer, C. Stephan, S. Lefrant, G. Van Tendeloo, I. Willems, Z. Konya, A. Fonseca, C. Laurent, J.B. Nagy, Chem. Phys. Lett. 317 (2000) 83.
[9] R.L. Vander Wal, T.M. Ticich, V.E. Curtis, J. Phys. Chem. A 104 (2000) 7209.
[10] D. Laplaze, P. Bernier, W.K. Maser, G. Flamant, T. Guillard, A. Loiseau, Carbon 36 (1998) 685.
[11] S. Bandow, M. Takizawa, K. Hirahara, M. Yudasaka, S. Iijima, Chem. Phys. Lett. 337 (2001) 48.
[12] Z.K. Tang, H.D. Sun, J. Wang, J. Chen, G. Li, Appl. Phys. Lett. 73 (1998) 2287.
[13] H. Kuzmany, W. Plank, M. Hulman, C. Kramberger, A. Grüneis, T. Pichler, H. Peterlik, H. Kataura, Y. Achiba, Eur. Phys. J. B 22 (2001) 307.
[14] S. Bandow, S. Asaka, Y. Saito, A.M. Rao, L. Grigorian, E. Richter, P.C. Eklund, Phys. Rev. Lett. 80 (1998) 3779.
[15] J. Kürti, G. Kresse, H. Kuzmany, Phys. Rev. B 58 (1998) R8869.
[16] A. Jorio, R. Saito, J.H. Hafner, C.M. Lieber, M. Hunter, T. McClure, G. Dresselhaus, M.S. Dresselhaus, Phys. Rev. Lett. 86 (2001) 1118.
[17] A.M. Rao, E. Richter, S. Bandow, B. Chase, P.C. Eklund, K.A. Williams, S. Fang, K.R. Subbaswamy, M. Menon, A. Thess, R.E. Smalley, G. Dresselhaus, M.S. Dresselhaus, Science 275 (1997) 187.
[18] M. Milnera, J. Kurti, M. Hulman, H. Kuzmany, Phys. Rev. Lett. 84 (2000) 1324.
[19] C. Thomsen, S. Reich, Phys. Rev. Lett. 85 (2000) 5214.
[20] V. Zolyomi, J. Kürti, A. Grüneis, H. Kuzmany, Phys. Rev. Lett. 90 (2003) 157401.
[21] S. Niyogi, M.A. Hamon, H. Hu, B. Zhao, P. Bhowmik, R. Sen, M.E. Itkis, R.C. Haddon, Acc. Chem. Res. 35 (2002) 1105.
[22] V. Georgakilas, K. Kordatos, M. Prato, D.M. Guldi, M. Holzinger, A. Hirsch, J. Am. Chem. Soc. 124 (2002) 760.
[23] S. Pekker, J.P. Salvetat, E. Jakab, J.M. Bonard, L. Forro, J. Phys. Chem. B 105 (2001) 7938.
[24] M. Holzinger, O. Vostrowsky, A. Hirsch, F. Hennrich, M. Kappes, R. Weiss, F. Jellen, Angew. Chem. Int. Ed. 40 (2001) 4002.
[25] C.N.R. Rao, A. Govindaraj, B.C. Satishkumar, Chem. Commun. (1996) 1525.
[26] A. Kuznetsova, I. Popova, J.T. Yates, M.J. Bronikowski, C.B. Huffman, J. Liu, R.E. Smalley, H.H. Hwu, J.G.G. Chen, J. Am. Chem. Soc. 123 (2001) 10699.
[27] Z.H. Yu, L.E. Brus, J. Phys. Chem. A 104 (2000) 10995.
[28] D.B. Mawhinney, V. Naumenko, A. Kuznetsova, J.T. Yates, J. Liu, R.E. Smalley, J. Am. Chem. Soc. 122 (2000) 2383.
[29] L.T. Cai, J.L. Bahr, Y.X. Yao, J.M. Tour, Chem. Mater. 14 (2002) 4235.
[30] Z. Konya, I. Vesselenyi, K. Niesz, A. Kukovecz, A. Demortier, A. Fonseca, J. Delhalle, Z. Mekhalif, J.B. Nagy, A.A. Koos, Z. Osvath, A. Kocsonya, L.P. Biro, I. Kiricsi, Chem. Phys. Lett. 360 (2002) 429.
[31] H.L. Pan, L.Q. Liu, Z.X. Guo, L.M. Dai, F.S. Zhang, D.B. Zhu, R. Czerw, D.L. Carroll, Nano Lett. 3 (2003) 29.
[32] E.T. Mickelson, C.B. Huffman, A.G. Rinzler, R.E. Smalley, R.H. Hauge, J.L. Margrave, Chem. Phys. Lett. 296 (1998) 188.
[33] K.F. Kelly, I.W. Chiang, E.T. Mickelson, R.H. Hauge, J.L. Margrave, X. Wang, G.E. Scuseria, C. Radloff, N.J. Halas, Chem. Phys. Lett. 313 (1999) 445.
[34] P.J. Boul, J. Liu, E.T. Mickelson, C.B. Huffman, L.M. Ericson, I.W. Chiang, K.A. Smith, D.T. Colbert, R.H. Hauge, J.L. Margrave, R.E. Smalley, Chem. Phys. Lett. 310 (1999) 367.
[35] A. Kukovecz, C. Kramberger, M. Holzinger, H. Kuzmany, J. Schalko, M. Mannsberger, A. Hirsch, J. Phys. Chem. B 106 (2002) 6374.
[36] V. Georgakilas, D. Voulgaris, E. Vazquez, M. Prato, D.M. Guldi, A. Kukovecz, H. Kuzmany, J. Am. Chem. Soc. 124 (2002) 14318.
[37] A. Kukovecz, T. Pichler, R. Pfeiffer, H. Kuzmany, Chem. Commun. (2002) 1730.
[38] A. Kukovecz, T. Pichler, R. Pfeiffer, C. Kramberger, H. Kuzmany, PCCP Phys. Chem. Chem. Phys. 5 (2003) 582.
[39] B.W. Smith, M. Monthioux, D.E. Luzzi, Nature 396 (1998) 323.
[40] A. Chu, J. Cook, R.J.R. Heesom, J.L. Hutchison, M.L.H. Green, J. Sloan, Chem. Mater. 8 (1996) 2751.
[41] K. Hirahara, S. Bandow, K. Suenaga, H. Kato, T. Okazaki, H. Shinohara, S. Iijima, Phys. Rev. B 6411 (2001) 115420.
[42] H. Kataura, Y. Maniwa, T. Kodama, K. Kikuchi, K. Hirahara, K. Suenaga, S. Iijima, S. Suzuki, Y. Achiba, W. Kratschmer, Synth. Met. 121 (2001) 1195.
[43] R. Pfeiffer, 2003, in press.
[44] H. Kuzmany, R. Pfeiffer, C. Kramberger, T. Pichler, X. Liu, M. Knupfer, J. Fink, H. Kataura, Y. Achiba, B.W. Smith, D.E. Luzzi, Appl. Phys. A: Mater. Sci. Process 76 (2003) 449.
[45] X. Liu, T. Pichler, A. Knupfer, M.S. Golden, J. Fink, H. Kataura, Y. Achiba, K. Hirahara, S. Iijima, Phys. Rev. B 6504 (2002) 045411.
[46] T. Pichler, A. Kukovecz, H. Kuzmany, H. Kataura, Y. Achiba, Phys. Rev. B 67 (2003).
[47] S. Pekker, G. Oszlanyi, G. Faigel, Chem. Phys. Lett. 282 (1998) 435.
[48] D. Tomanek, Personal communication, 2003.
[49] R. Pfeiffer, H. Kuzmany, C. Kramberger, C. Schaman, T. Pichler, H. Kataura, Y. Achiba, J. Kurti, V. Zolyomi, Phys. Rev. Lett. 90 (2003) 225501.
[50] N. Breda, R.A. Broglia, G. Colo, G. Onida, D. Provasi, E. Vigezzi, Phys. Rev. B 62 (2000) 130.

Functionalization in 2004

- STM investigation of carbon nanotubes connected by functional groups
  Materials Science and Engineering: C, Volume 23, Issues 6-8, 15 December 2003, Pages 1007-1011
  A. A. Koós, Z. E. Horváth, Z. Osváth, L. Tapasztó, K. Niesz, Z. Kónya, I. Kiricsi, N. Grobert, M. Rühle and L. P. Biró
  - ***"Chemical functionalization of carbon nanotubes (CNTs) is essential for many applications. Attachment of functional groups to nanotubes can dramatically increase the solubility of the nanotube material. Sidewall functional groups should react with polymers and improve the mechanical properties of nanocomposites. Tubes interconnected by chemical bonds will have a reduced contact resistance and can be used for interconnection purposes in nanoscale circuits."***

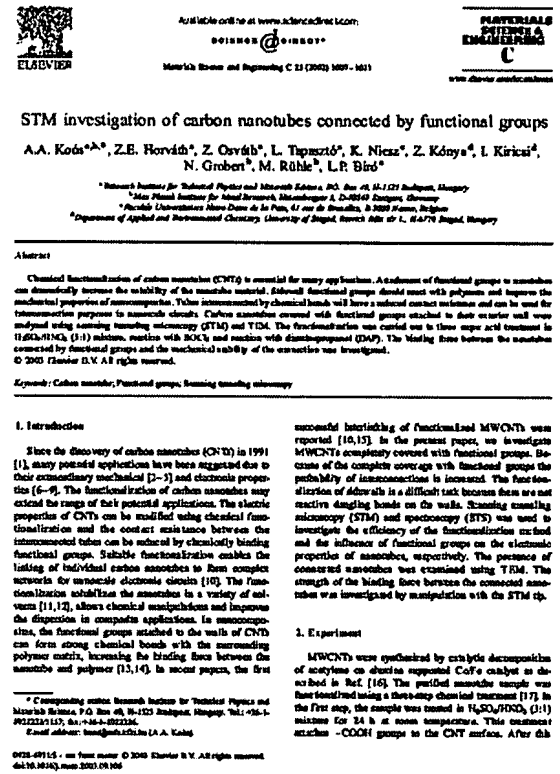

ELSEVIER

Available online at www.sciencedirect.com

SCIENCE DIRECT®

Materials Science and Engineering C 23 (2003) 1007–1011

MATERIALS SCIENCE & ENGINEERING C

www.elsevier.com/locate/msec

STM investigation of carbon nanotubes connected by functional groups

A.A. Koós[a,b], Z.E. Horváth[a], Z. Osváth[a], L. Tapasztó[a], K. Niesz[a], Z. Kónya[a], I. Kiricsi[a], N. Grobert[b], M. Rühle[b], L.P. Biró[a]

[a] Research Institute for Technical Physics and Materials Science, P.O. Box 49, H-1525 Budapest, Hungary
[b] Max Planck Institute for Metal Research, Heisenbergstr. 3, D-70569 Stuttgart, Germany
[c] Facultés Universitaires Notre-Dame de la Paix, 61 rue de Bruxelles, B-5000 Namur, Belgium
[d] Department of Applied and Environmental Chemistry, University of Szeged, Rerrich Béla tér 1, H-6720 Szeged, Hungary

Abstract

Chemical functionalization of carbon nanotubes (CNTs) is essential for many applications. Attachment of functional groups to nanotubes can dramatically increase the solubility of the nanotube material. Sidewall functional groups should react with polymers and improve the mechanical properties of nanocomposites. Tubes interconnected by chemical bonds will have a reduced contact resistance and can be used for interconnection purposes in nanoscale circuits. Carbon nanotubes covered with functional groups attached to their surface wall were analyzed using scanning tunneling microscopy (STM) and TEM. The functionalization was carried out in three steps: acid treatment in H_2SO_4/HNO_3 (3:1) mixture, reaction with $SOCl_2$ and reaction with diaminopropanol (DAP). The binding force between the nanotubes connected by functional groups and the mechanical stability of the connection was investigated.
© 2003 Elsevier B.V. All rights reserved.

Keywords: Carbon nanotubes; Functional groups; Scanning tunneling microscopy

1. Introduction

Since the discovery of carbon nanotubes (CNTs) in 1991 [1], many potential applications have been suggested due to their extraordinary mechanical [2–5] and electronic properties [6–9]. The functionalization of carbon nanotubes may extend the range of their potential applications. The electric properties of CNTs can be modified using chemical functionalization and the contact resistance between the interconnected tubes can be reduced by chemically binding functional groups. Suitable functionalization enables the linking of individual carbon nanotubes to form complex networks for nanoscale electronic circuits [10]. The functionalization solubilizes the nanotubes in a variety of solvents [11,12], allows chemical manipulations and improves the dispersion in composite applications. In nanocomposites, the functional groups attached to the walls of CNTs can form strong chemical bonds with the surrounding polymer matrix, increasing the binding force between the nanotube and polymer [13,14]. In recent papers, the first successful interlinking of functionalized MWCNTs was reported [10,15]. In the present paper, we investigate MWCNTs completely covered with functional groups. Because of the complete coverage with functional groups the probability of interconnections is increased. The functionalization of sidewalls is a difficult task because there are not reactive dangling bonds on the walls. Scanning tunneling microscopy (STM) and spectroscopy (STS) was used to investigate the efficiency of the functionalization method and the influence of functional groups on the electronic properties of nanotubes, respectively. The presence of connected nanotubes was examined using TEM. The strength of the binding force between the connected nanotubes was investigated by manipulation with the STM tip.

2. Experiment

MWCNTs were synthesized by catalytic decomposition of acetylene on alumina supported $CoFe_2O_4$ catalyst as described in Ref. [16]. The purified nanotube sample was functionalized using a three-step chemical treatment [17]. In the first step, the sample was treated in H_2SO_4/HNO_3 (3:1) mixture for 24 h at room temperature. This treatment attaches –COOH groups to the CNT surface. After this

* Corresponding author. Research Institute for Technical Physics and Materials Science, P.O. Box 49, H-1525 Budapest, Hungary. Tel.: +36-1-3922222/1517; fax: +36-1-3922226.
E-mail address: koos@mfa.kfki.hu (A.A. Koós).

0928-4931/$ - see front matter © 2003 Elsevier B.V. All rights reserved.
doi:10.1016/j.msec.2003.09.166

Available online at www.sciencedirect.com
SCIENCE DIRECT®
Materials Science and Engineering C 23 (2003) 1007–1011
MATERIALS SCIENCE & ENGINEERING C
www.elsevier.com/locate/msec

STM investigation of carbon nanotubes connected by functional groups

A.A. Koós[a,b,*], Z.E. Horváth[a], Z. Osváth[a], L. Tapasztó[a], K. Nieszc, Z. Kónya[d], I. Kiricsi[d], N. Grobert[b], M. Rühle[b], L.P. Biró[a]

[a] *Research Institute for Technical Physics and Materials Science, P.O. Box 49, H-1525 Budapest, Hungary*
[b] *Max Planck Institute for Metal Research, Heisenbergstr 3, D-70569 Stuttgart, Germany*
[c] *Facultés Universitaires Notre-Dame de la Paix, 61 rue de Bruxelles, B-5000 Namur, Belgium*
[d] *Department of Applied and Environmental Chemistry, University of Szeged, Rerrich Béla tér 1., H-6720 Szeged, Hungary*

Abstract

Chemical functionalization of carbon nanotubes (CNTs) is essential for many applications. Attachment of functional groups to nanotubes can dramatically increase the solubility of the nanotube material. Sidewall functional groups should react with polymers and improve the mechanical properties of nanocomposites. Tubes interconnected by chemical bonds will have a reduced contact resistance and can be used for interconnection purposes in nanoscale circuits. Carbon nanotubes covered with functional groups attached to their exterior wall were analyzed using scanning tunneling microscopy (STM) and TEM. The functionalization was carried out in three steps: acid treatment in H_2SO_4/HNO_3 (3:1) mixture, reaction with $SOCl_2$ and reaction with diaminopropanol (DAP). The binding force between the nanotubes connected by functional groups and the mechanical stability of the connection was investigated.
© 2003 Elsevier B.V. All rights reserved.

Keywords: Carbon nanotube; Functional groups; Scanning tunneling microscopy

1. Introduction

Since the discovery of carbon nanotubes (CNTs) in 1991 [1], many potential applications have been suggested due to their extraordinary mechanical [2–5] and electronic properties [6–9]. The functionalization of carbon nanotubes may extend the range of their potential applications. The electric properties of CNTs can be modified using chemical functionalization and the contact resistance between the interconnected tubes can be reduced by chemically binding functional groups. Suitable functionalization enables the linking of individual carbon nanotubes to form complex networks for nanoscale electronic circuits [10]. The functionalization solubilizes the nanotubes in a variety of solvents [11,12], allows chemical manipulations and improves the dispersion in composite applications. In nanocomposites, the functional groups attached to the walls of CNTs can form strong chemical bonds with the surrounding polymer matrix, increasing the binding force between the nanotube and polymer [13,14]. In recent papers, the first successful interlinking of functionalized MWCNTs were reported [10,15]. In the present paper, we investigate MWCNTs completely covered with functional groups. Because of the complete coverage with functional groups the probability of interconnections is increased. The functionalization of sidewalls is a difficult task because there are not reactive dangling bonds on the walls. Scanning tunneling microscopy (STM) and spectroscopy (STS) was used to investigate the efficiency of the functionalization method and the influence of functional groups on the electronic properties of nanotubes, respectively. The presence of connected nanotubes was examined using TEM. The strength of the binding force between the connected nanotubes was investigated by manipulation with the STM tip.

2. Experiment

MWCNTs were synthesized by catalytic decomposition of acetylene on alumina supported Co/Fe catalyst as described in Ref. [16]. The purified nanotube sample was functionalized using a three-step chemical treatment [17]. In the first step, the sample was treated in H_2SO_4/HNO_3 (3:1) mixture for 24 h at room temperature. This treatment attaches –COOH groups to the CNT surface. After this

* Corresponding author. Research Institute for Technical Physics and Materials Science, P.O. Box 49, H-1525 Budapest, Hungary. Tel.: +36-1-3922222/1157; fax: +36-1-3922226.
E-mail address: koos@mfa.kfki.hu (A.A. Koós).

0928-4931/$ - see front matter © 2003 Elsevier B.V. All rights reserved.
doi:10.1016/j.msec.2003.09.106

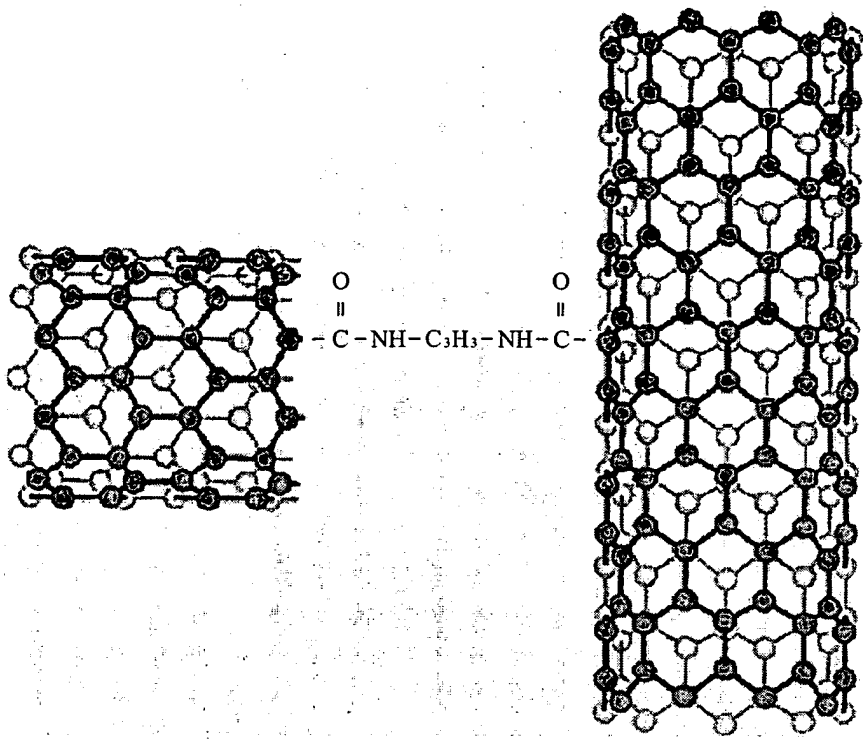

Fig. 1. Schematic representation of an end-to-side junction. The nanotubes are connected via diaminopropane.

treatment, the MWCNTs were mixed in $SOCl_2$ overnight, in order to transform the –COOH groups connected to nanotube surface in –COCl groups. Finally, the nanotube sample was mixed in diaminopropane (DAP) at for 24 h. The diaminopropane connects the functional groups attached to the nanotubes, and in this way interconnects the nanotubes. Fig. 1 shows the schematic representation of an end-to-side junction.

The STM investigation was performed with a DI Nanoscope E STM/AFM instrument in air using commercial Pt/Ir tips with set point currents of 200 pA at a bias of 1 V. The nanotubes were ultrasonicated in isopropanol and droplets

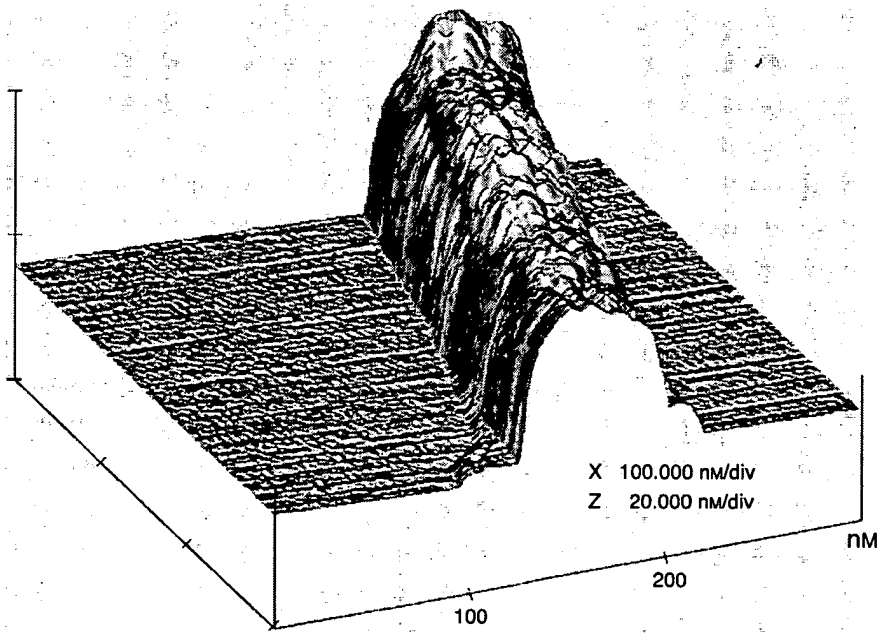

Fig. 2. 3D topographic STM image of MWCNTs covered with functional groups.

of the suspension were placed on highly oriented pyrolytic graphite (HOPG) or Au evaporated onto mica. The connected nanotubes were investigated with a Philips CM 200 (200 kV) TEM.

In order to get insight in the way in which the functionalization took place, the surface of the nanotubes was investigated by STM [18]. Our previous investigations showed that in case of nanotubes functionalized by ball milling in reactive atmosphere the functional groups are attached to defects on the surface in a grouped-together way [19]. The STM investigation of nanotubes after the three-step chemical treatment showed that, opposite to ball milling, the whole surface of the nanotubes was covered with functional groups. The continuous coverage is the consequence of the high density of defect sites on the nanotube surface. Some of these defects may originate from the CVD growth itself, but we have no reason to assume that this would be significantly different from the defect density of the carbon nanotubes used for ball milling experiments. The number of anchoring points for the functional groups incorporated during the CVD process was significantly increased by the applied chemical treatment. The average distance between the defects decreased to a few nanometers; therefore, the "islands" of functional groups are touching each other. A typical nanotube from this sample is shown in Fig. 2.

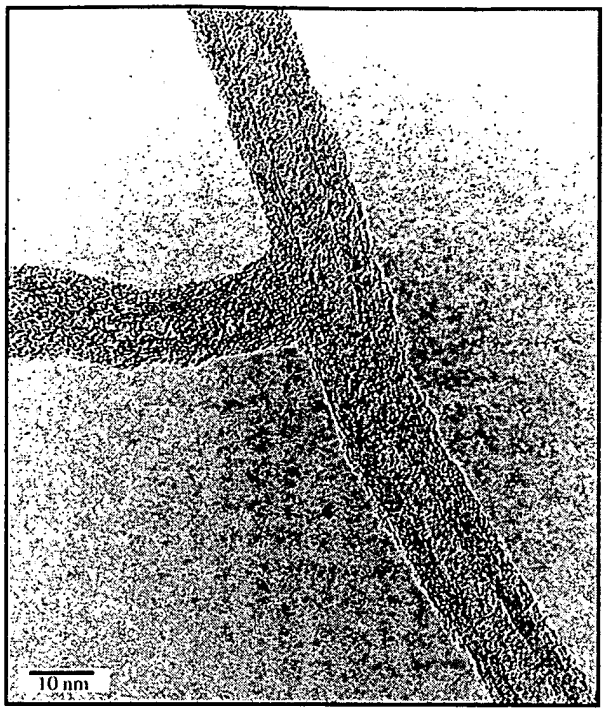

Fig. 4. TEM image of two T-connected nanotubes.

Using STS we investigated the changes in the electronic properties of CNTs. Fig. 3B shows an STS curve recorded on the nanotube shown in Fig. 3A. In order to reduce the noise, 10 current–voltage curves were averaged and after numerical derivation the resulting dI/dV curve was Fourier filtered. The apparent tube diameter determined from Fig. 3A is $d=13$ nm. The nanotube has metallic behavior because the STS curve shows a nonzero density of states at the Fermi energy. For chemically unmodified nanotubes, the distance between the Van Hove singularities should depend only on the diameter [9]. For metallic SWCNTs the singularities appear at energies $E_1=\pm 3\gamma_0 a_{C-C}/d$, $E_2=\pm 6\gamma_0 a_{C-C}/d$ and $E_3=\pm 9\gamma_0 a_{C-C}/d$, where $\gamma_0=2.7$ eV is the C–C tight-binding overlap energy, $a_{C-C}=0.142$ nm is the nearest neighbor C–C distance and d the tube diameter [9,20–22]. Because the interaction between the layers in MWCNT is weak the distance between the Van Hove singularities is not significantly changed compared with SWCNTs [23]. In

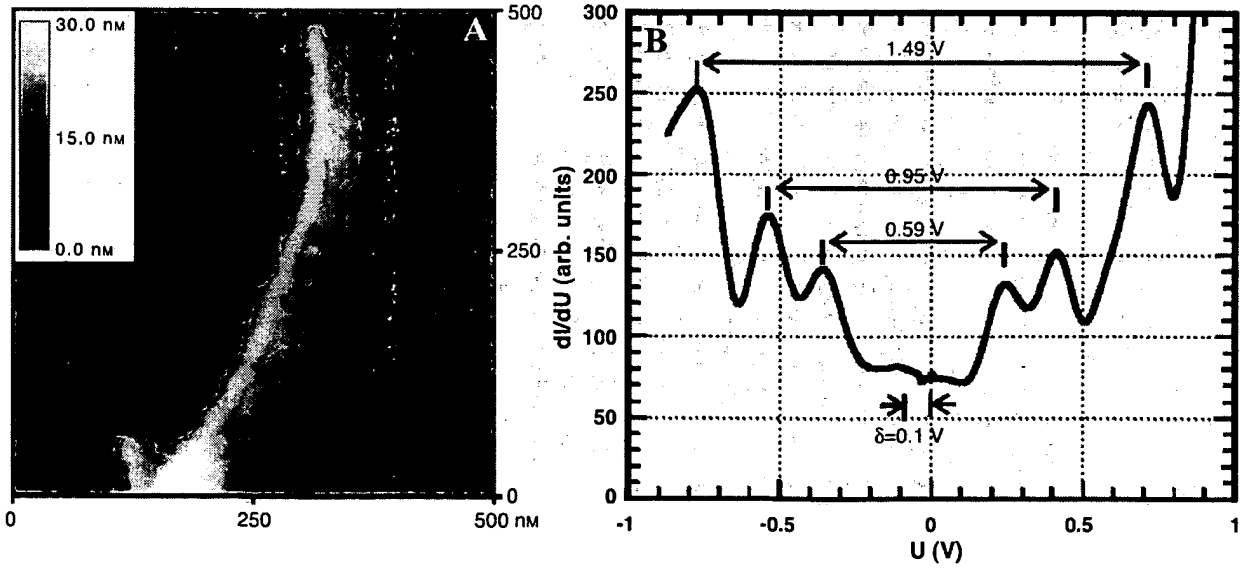

Fig. 3. STM image of a functionalized MWCNT on Au (A) and the STS curve on this tube (B).

our case, the calculated energy gap should be $\Delta E_1 = 0.18$ eV, $\Delta E_2 = 0.35$ eV and $\Delta E_3 = 0.53$. The measured energy gaps are 0.59, 0.95 and 1.49 eV for ΔE_1, ΔE_2 and ΔE_3, respectively, wider than twice the calculated value. Assuming that the functional groups cover the nanotube in one layer only, and they are short as compared with the diameter of the nanotube; this result indicates that the theoretical model used to calculate the position of Van Hove singularities has to be modified in case of functionalized nanotubes. The difference between the calculated and measured energy gaps could be explained only with a significant change in the electronic structure of the nanotube. Furthermore, the Van Hove singularities on the STS curve are not symmetrically positioned around zero bias, the tubes may be doped by the functional groups and possibly by the charge transfer from the Au substrate. The energy levels of not functionalized metallic nanotubes placed on Au surface is shifted by 0.3 eV towards lower energy [9]. The Van Hove singularities on the STS curve are shifted by $\delta = 0.1$ eV to higher energies, which is another difference from the behavior of not functionalized nanotubes. Consequently, functionalization may be used to produce CNTs with modified electronic properties as predicted by theoretical models [24,25].

Because the whole surface of CNTs is covered with functional groups, the probability of interconnections between the nanotubes is higher than in the case of nanotubes functionalized only at their end. The presence of connected nanotubes in the sample was investigated with TEM. A large number of connected nanotubes were found. Approximatively, 10% of the nanotubes were connected in one way or another. Fig. 4 shows a T-like connection of two nanotubes.

The strength of the bonds between the nanotubes was checked using manipulation with the STM tip. This method is able to compare the binding force between the connected nanotubes and the van der Waals interaction between the nanotubes and the HOPG substrate. Fig. 5 shows two consecutive STM images taken in the same region (the same HOPG cleavage step appears on both images). The group of nanotubes on the upper part of the images is moved about 200 nm, while the nanotube on the lower part of the images is rotated with 30°. The nanotubes on the upper part of the images are moved together without the alteration of their global arrangement. This indicates that the binding force between them is larger than the van der Waals interaction between the nanotubes and the substrate. Taking into account that the "dragging force" exerted by the STM tip was acting on only one tube of the group, this indicates a strong enough chemical connection between the nanotubes.

3. Conclusions

The applied functionalization method was able to cover the whole surface of MWCNTs with functional groups. The large number of functional groups on the CNTs surface facilitates the formation of connections between nanotubes; therefore, a large number of connected nanotubes were observed by TEM. This treatment may be useful to improve the mechanical interaction between the nanotubes and the surrounding matrix in composites, too. The functionalization produces significant modifications in the electronic structure of the nanotubes and makes possible to produce nanotubes with modified electronic properties. The binding force between the connected nanotubes was found stronger than the van der Waals interaction between the nanotubes and the graphite substrate, indicating that the electric circuit built from connected nanotubes will be mechanically stable. The carbon nanotube networks connected with functional groups may be used in nanoelectronics.

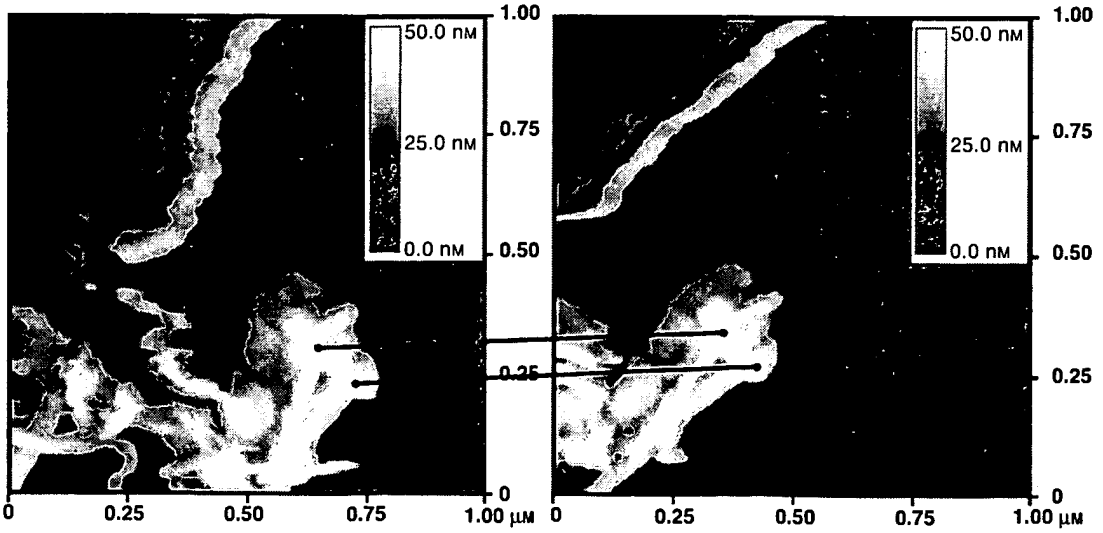

Fig. 5. Consecutive STM images taken in the same region. The nanotubes are moved together without the alteration of their global arrangement.

Acknowledgements

This work was supported by the EC, contract NANOCOMP, HPRT-CT-2000-00037 and HPMT-CT-2000-00051, EU5 Center of Excellence ICAI-CT-2000-70029 and by Hungarian OTKA Grant T 043685.

References

[1] S. Iijima, Nature 354 (1991) 56–58.
[2] M.S. Dresselhaus, G. Dresselhaus, R. Saito, Carbon 33 (1995) 883–891.
[3] M.M. Treacy, T.W. Ebbesen, J.M. Gibson, Nature 381 (1996) 678–680.
[4] E.W. Wong, P.E. Sheehan, C.M. Lieber, Science 277 (1997) 1971–1975.
[5] M.R. Falvo, G.J. Clary, R.M. Taylor II, V. Chi, F.P. Brooks Jr., S. Washburn, R. Superfine, Nature 389 (1997) 582–584.
[6] W.A. de Heer, A. Chatelain, D. Ugarte, Science 270 (1995) 1179–1180.
[7] H. Dai, E.W. Wong, C.M. Lieber, Science 272 (1996) 523–526.
[8] T.W. Ebbesen, H.J. Lezec, H. Hiura, J.W. Bennett, H.F. Ghaemi, T. Thio, Nature 382 (1996) 54–56.
[9] J.W. Wildöer, L.C. Venema, A.G. Rinzler, R.E. Smalley, C. Dekker, Nature 391 (1998) 59–62.
[10] P.W. Chiu, G.S. Duesberg, U. Dettlaff-Weglikowska, S. Roth, Appl. Phys. Lett. 80 (2002) 3811–3813.
[11] J. Chen, M.A. Hamon, H. Hu, Y. Chen, A.M. Rao, P.C. Eklund, R.C. Haddon, Science 282 (1998) 95–98.
[12] E.T. Mickelson, I.W. Chiang, J.L. Zimmerman, P.J. Boul, J. Lozano, J. Liu, R.E. Smalley, R.H. Hauge, J.L. Margrave, J. Phys. Chem., B 103 (1999) 4318–4322.
[13] K.T. Lau, D. Hui, Carbon 40 (2002) 1605–1606.
[14] A. Garg, S.B. Sinnott, Chem. Phys. Lett. 295 (1998) 273–278.
[15] F. Frehill, J.G. Vos, S. Benrezzak, A.A. Koós, Z. Kónya, M.G. Rüther, W.J. Blau, A. Fonseca, J.B. Nagy, L.P. Biró, A.I. Minett, M. Panhuis, J. Am. Chem. Soc. 124 (46) (2002) 13694–13695.
[16] I. Willems, Z. Kónya, J.F. Colomer, G. Van Tendeloo, N. Nagaraju, A. Fonseca, J.B. Nagy, Chem. Phys. Lett. 317 (2000) 71–76.
[17] I. Kiricsi, Z. Kónya, K. Niesz, L.P. Biró, in press..
[18] K.F. Kelly, I.W. Chiang, E.T. Mickelson, R.H. Hauge, J.L. Margrave, X. Wang, G.E. Scuseria, C. Radloff, N.J. Halas, Chem. Phys. Lett. 313 (1999) 445–450.
[19] Z. Kónya, I. Vesselenyi, K. Niesz, A. Kukovecz, A. Demortier, A. Fonseca, J. Delhalle, Z. Mekhalif, J.B. Nagy, A.A. Koós, Z. Osváth, A. Kocsonya, L.P. Biró, I. Kiricsi, Chem. Phys. Lett. 360 (2002) 429–435.
[20] T.W. Odom, J.L. Huang, P. Kim, C.M. Lieber, Nature 391 (1998) 62–64.
[21] J.-C. Charlier, Ph. Lambin, Phys. Rev., B 57 (24) (1998) R15 037–R15 039.
[22] T.W. Odom, J.L. Huang, C.M. Lieber, J. Phys., Condens. Matter 14 (2002) R145–R167.
[23] A. Rubio, Appl. Phys., A 68 (1999) 275–282.
[24] G. Seifert, T. Köhler, T. Frauenheim, App. Phys. Lett. 77 (9) (2000) 1313–1315.
[25] S.B. Fagan, A.J.R. da Silva, R. Mota, R.J. Baierle, A. Fazzio, Phys. Rev., B 67 (2003) 33405.

Functionalization in 2004

- Electrochemical functionalization of multi-walled carbon nanotubes for solvation and purification
  Current Applied Physics, Volume 2, Issue 2, April 2002, Pages 107-111
  Eugen Unger, Andrew Graham, Franz Kreupl, Maik Liebau and Wolfgang Hoenlein

Current Applied Physics

Electrochemical functionalization of multi-walled carbon nanotubes for solvation and purification

Eugen Unger *, Andrew Graham, Franz Kreupl, Maik Liebau, Wolfgang Hoenlein

ELSEVIER

Current Applied Physics 2 (2002) 107–111

Current Applied Physics
Physics, Chemistry and Materials Science

www.elsevier.com/locate/cap

Electrochemical functionalization of multi-walled carbon nanotubes for solvation and purification

Eugen Unger *, Andrew Graham, Franz Kreupl, Maik Liebau, Wolfgang Hoenlein

Infineon Technologies AG, Corporate Research, Otto-Hahn-Ring 6, 81739 Munich, Germany

Accepted 31 October 2001

Abstract

The chemical modification of multi-walled carbon nanotubes using electrolysis is described. It is found that the evolution of the halogens chlorine or bromine on an anode made from a foil of carbon nanotubes couples halogen atoms to the nanotube lattice. Furthermore, oxygen bearing functional groups, such as hydroxyl and carboxyl groups, are formed at the same time aiding solvation of the nanotubes in water or alcohol without any surfactant. Impurities and low grade modified nanotubes remain insoluble. The halogenated carbon nanotubes can be converted with sodium amide or triphenylmethyllithium to add the corresponding functional groups. © 2001 Published by Elsevier Science B.V.

PACS: 81.07.De; 81.20.Yn; 61.46.+w
Keywords: Multiwalled nanotubes; Electrochemical oxidation; Purification; Halogen addition; Derivatisation

1. Introduction

Carbon nanotubes have attracted much attention in the last several years because of their outstanding mechanical and electrical properties. Many useful applications, such as field emission displays, microcircuit wiring, diodes and transistors, sensors, composite polymers, artificial muscles and hydrogen storage [1,2], have already been demonstrated. However, since carbon nanotubes are large molecules with thousands of carbon atoms in an aromatic delocalized system they are practically insoluble in all solvents and are, consequently, difficult to handle. Only very diluted solutions can be obtained using, e.g., DMF or chlorinated hydrocarbons with extensive ultrasonication [3]. The use of surfactants such as dodecylsulfates in aqueous solutions circumvents the problem of insolubility but, as a result, a large amount of additional material is also dissolved which may interfere with, for example, microelectronic applications on the nanometer scale [4]. Furthermore, as deposited carbon nanotubes from an arc or CVD process often contain considerable amounts of soot and other byproducts which must be removed prior to application. Chemical modification of carbon nanotubes can increase the solubility and can aid the purification process but, unfortunately, the carbon nanotubes are very inert due to their delocalized π electron system. In contrast to the well established fullerene chemistry [5], only few reaction pathways have been described to date. Oxidation with molecular fluorine yielded fluorinated carbon nanotubes and treatment with oxidizing acids like nitric and/or sulfuric acid or with an oxygen plasma produced modified nanotubes with carboxylic groups, which could be converted to the corresponding amides with long aliphatic chains, enhancing the solubility in organic solvents [6–9]. In addition, some reactions with carbenes like dichlorocarbene have been described. If such a chemical modification is applied to a single-walled nanotube, the sp^2 structure of the nanotube is interrupted at the functionalization site and, consequently, the electronic properties of the molecule will be altered. This effect can be avoided, or at least minimized, using a non-covalent functionalization of the walls of the nanotubes with smaller aromatic molecules like pyrene derivatives [10]. In the present work we covalently functionalize multi-walled carbon nanotubes (MWNTs)

* Corresponding author.
E-mail address: eugen.unger@infineon.com (E. Unger).

1567-1739/01/$ - see front matter © 2001 Published by Elsevier Science B.V.
PII: S1567-1739(01)00072-4

because, even if the outer wall loses its typical electronic behavior, the non-functionalized inner walls can take over the charge transport.

Functionalization of carbon nanotubes involves processing methods which are very different from normal chemical procedures. In contrast to a chemistry involving defined modification of uniform molecules, every nanotube is unique in size, available reaction sites and reactivity. As a result, all data given are statistical and may vary to some extent from one sample to another. Moreover, if only few additions or substitutions are made to a large carbon molecule, the result may be such a small change of its properties that there is no observable change in its physical or chemical behavior. Therefore, if a change in nanotube properties is observed more than a few sites must have been modified. Many experiments have been described where nanotubes were filled with metal atoms, for example, silver, iron or cobalt, or with molecules like fullerenes [11,12]. Furthermore, it has been shown that gases, in particular hydrogen, can be stored in nanotubes [13,14]. So if elements other than carbon are detected after functionalization of the nanotubes it must also be shown that these atoms are actually covalently bonded to the tubes.

2. Experimental

In this paper we report an electrochemical procedure which uses a thin foil of MWNTs, typically referred to as bucky-paper, as an electrode within an electrolytic cell, as shown in Fig. 1. When current flows through the electrolyte the anions are discharged on the positively charged bucky-paper surface and the reactant generated, for example halogen or oxygen atoms, can react with the nanotube material.

Samples of bucky-paper, both before and after treatment, were analyzed with a scanning electron microscope (SEM) (LEO 1560) equipped with a Noran Vantage energy dispersive X-ray analyzer. Time-of-flight secondary ion mass spectroscopy (SIMS) was performed with an IONTOF-TOFSIMS IV incorporating a 25 kV Ga-source. Elemental analysis was provided by Mikroanalytisches Labor Beller, Göttingen. Infrared spectra were recorded by BIO RAD using the ATR method.

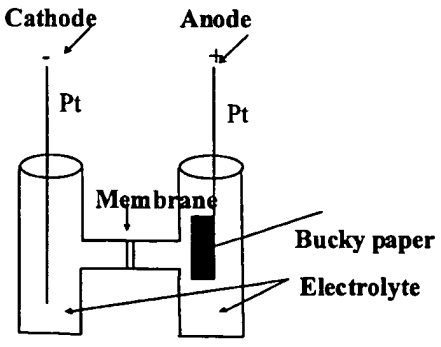

Fig. 1. The electrolytic cell used for the chemical modification of the bucky-papers. The electrolyte is a NaCl or KBr solution. A membrane or cloth plug is inserted in order to seperate the acidic from the basic parts of the electrolyte.

The nanotube material was prepared by a CVD process in a tube furnace as described elsewhere [15]. Briefly, a mixture of 25% hydrogen and 75% acetylene was passed over silicon substrates coated with either a $FeCl_3$ or iron acetylacetonate catalyst in a quartz-tube oven held at a temperature of 700 °C. The nanotubes on the silicon substrates were removed from the furnance at deposition temperature and were cooled rapidly on a stainless steel plate in ambient air. The MWNTs were separated from the silicon by ultrasonic treatment of the silicon substrates in water. The nanotubes were separated from the water by filtration through a PTFE membrane filter, washed with water, isopropyl alcohol and acetone, and allowed to dry. The resulting bucky-paper (typically 8–12 mg) was connected to a platinum wire and incorporated in the electrolytic cell as the anode (Fig. 1).

The electrolytic cell was filled with either a 2 M solution of NaCl or KBr. A constant current of 100 mA was supplied for 16–24 h. After electrolysis the MWNTs were separated from the electrolyte, dispersed in water with a short period of ultrasonic agitation, filtered and washed with water, isopropyl alcohol and acetone. The filtrate was dispersed again in 5 ml of water with an ultrasonic tip for one minute and the mixture centrifuged. The black supernatant was separated, the sediment resuspended in water, centrifuged and the aqueous parts collected. This procedure was repeated until the supernatants became clear. The resulting solutions were filtered again through a PTFE filter and the residue on the filter was washed and dried. The resulting bucky-paper consisted of a lustrous flexible foil which could be easily dissolved in water or alcohol again if freshly prepared. A typical yield from a 12 mg sample was 8.5 mg soluble material following chlorination and 10 mg product after bromine electrolysis. An experiment using a Na_2SO_4 electrolyte yielded only small amounts of soluble nanotubes because the bucky-paper increased drastically in volume after only a few hours and then fell apart in the solution. Therefore, the results from this process will not be discussed here in detail but it is worthwhile noting that the macroscopic properties of the product, i.e. appearance and solubility, were equal to the Cl or Br modified bucky-papers.

The nanotubes used for our experiments were not absolutely pure. A typical sample consisted of 96 wt.% carbon, 1.2% iron (catalyst), 1.2% hydrogen, and 1.36% oxygen. The material could have been oxidized to a small extent when it was removed from the furnace and cooled down in ambient air. Therefore, for nanotubes

not exposed to air at elevated temperatures, the reactivity of the starting material and yield of the electrolysis process may change.

Subsequent reactions with halogenated multi-walled nanotubes were carried out in dry THF in a nitrogen atmosphere. The reaction mixture was hydrolyzed with small amounts of water after stirring one or two days at room temperature. The solutions were filtered and washed with water and acetone and the resulting bucky-paper was dried in vacuum prior to analysis.

Triphenylmethyllithium, used for the reactions with halogenated nanotubes, was prepared from triphenylmethane and an equimolar amount of butyllithium in dry THF under a nitrogen atmosphere by adding the butyllithium hexane solution slowly to the triphenylmethane THF solution. After 1 h of stirring a deep red solution of the lithium salt was obtained.

3. Results

SEM pictures of the bucky-papers made from the soluble part after chlorination and bromination show a network of nanotubes without any graphitic particles (Fig. 2). This material can be redissolved easily in water or alcohol with light ultrasonification. Deep dark solutions are obtained. After storing the bucky-papers for some days the solubility of the material deteriorates. The solutions are stable over weeks, only few flakes precipitate. The sediment obtained from centrifugation of the reaction product still contains a large number of nanotubes as well as some additional byproducts (Fig. 2). This part of the starting material has not been functionalized to a sufficient extent to become soluble.

The infrared spectra from a Cl-bucky-paper show a broad peak near 700 cm^{-1} which can be assigned to C–Cl vibrations. Additional peaks corresponding to the CH_2 and CH_3 vibration modes (2936, 2863 cm^{-1}) as well as CO stretching modes (1750, 1643 cm^{-1}) were observed, indicating that alcohol and carboxylic groups are also present. These findings also agree with an ESCA photoelectron analysis where peaks corresponding to the 1s orbits centered at 284.6 eV (graphitic C), 286.6 eV (C–O) and 289 eV (C–Cl) were found (Fig. 3). The negative fragmentation pattern from the TOF-SI mass spectrum shows Cl-(35, 37 amu), C_6Cl-(107 amu), C_2O-(40 amu), C_7OH-(101 amu) fragments in addition to the typical parts from the nanotube framework: C_9H, $C_{10}H$, $C_{12}H$, $C_{14}H$, $C_{17}H$, etc. EDX analysis indicates a chlorine content of about 7 wt.%. Elemental analysis of a chlorinated bucky-paper sample shows that it is composed of 64.10 wt.% C, 3.55% H, 18.63% O and 8.26% Cl.

Experiments were also undertaken to substitute the covalently bonded chlorine atoms with other functional groups. In the first experiment chlorinated nanotubes were reacted with $NaNH_2$ in dry THF under nitrogen. The product, which was isolated after two days of stirring in THF, has a similar appearance to the starting material but it is almost insoluble in all solvents. The yield was 8.8 mg from 9.5 mg starting material and elemental analysis yielded 69.2% C, 3.8% H and 1.25% N. The EDX spectra show that only a small quantity of chlorine remains in the final product.

Fig. 2. (a) A bucky paper from halogenated carbon nanotubes; the tube structure is fully retained. (b) The insoluble part of a reaction mixture with nanotubes and graphitic byproducts.

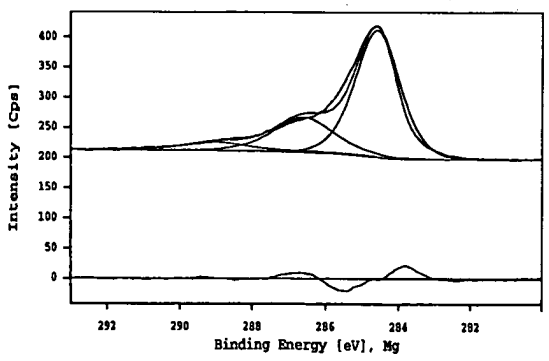

Fig. 3. ESCA spectrum of the chlorinated carbon nanotubes. The 1s C-orbit is observed at 284.6 eV; 1s C–O at 286.6 eV and 1s C–Cl at 289 eV.

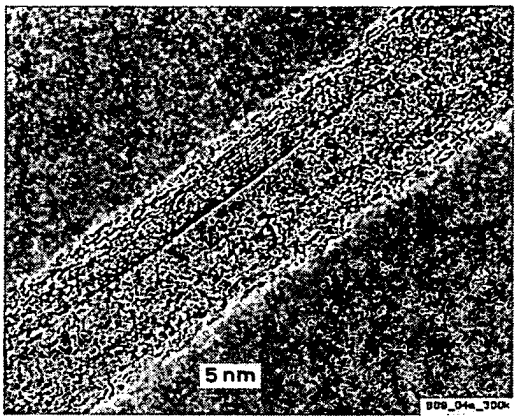

Fig. 4. TEM image of a brominated carbon nanotube. The nanotubes were deposited on a copper grid from an aqueous solution without surfactants.

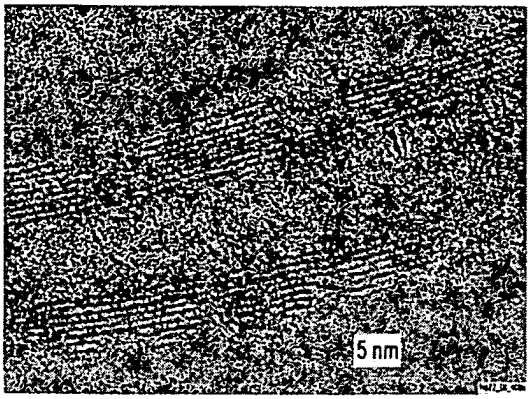

Fig. 5. TEM image of a chlorinated carbon nanotube, the inner diameter is about 5 nm. Attached chlorine atoms are not visible.

The second experiment involved the reaction of chlorinated nanotubes with triphenylmethyllithium $LiC(C_6H_5)_3$. After the reaction no bucky-paper derivative could be filtered from the solution and only some black leaflets were collected. SEM images of the product revealed that only a very few nanotubes survived and all the other material had lost its tube structure to form a soot-like residue.

The bromination of nanotubes results in a derivative which displays the same macroscopic properties as the chlorine compound. The bromine content is, however, significantly lower due to the lower oxidation potential of Br compared with Cl. Elemental analysis resulted in 75.2 wt.% C, 3.8% H, 13% O and 2.8% Br. Hence, the bromine nanotubes contain nearly 180 carbon atoms per Br atom. The TOF-SI mass spectrum shows an equivalent pattern to that obtained from the Cl material, where the Cl and C_6Cl-fragments are replaced by the corresponding Br species. The TEM picture shows an undamaged multi-walled tube (Fig. 4) with more than eight shells.

The subsequent reaction with triphenylmethyllithium gave a product from which a bucky-paper could be obtained. In the mass spectra a triphenylmethyl fragment was found. Infrared absorption peaks were observed at 1560 and near 3000 cm^{-1} and assigned to the phenyl and aromatic C–H vibration modes. The solubility of the freshly prepared triphenylmethyl functionalized nanotubes in water is found to be the same as of the brominated starting material, suggesting that the hydroxylic and carboxylic groups formed within the electrolysis process are responsible for the high solubility.

4. Discussion

Although there is clear evidence that the chlorine is covalently bonded to the nanotubes, the chlorine binding site and environment on the nanotubes cannot be determined from the data. The composition of the chlorinated nanotubes based on the elemental analysis is $C_{23}H_{15}O_5ClFe_{0.43}$. That means that every 23rd carbon atom is bonded to a chlorine atom if all chlorine is incorporated by a chemical reaction. This would be an extremely high chemical modification of the nanotube surface because the inner walls of the nanotube, which compose the bulk of the carbon of the molecule, are only affected by the chemical treatment if there are damages in the structure. Fig. 5 shows a TEM picture of a reacted nanotube and Fig. 6 shows that sometimes such damage is present. Therefore, we believe that a fraction of the chlorine is only physically adsorbed or stored inside of the tube and the remaining part is attached to damaged sites on the tube.

The much lower solubility of the amino nanotubes and the comparatively low content of nitrogen indicates that the chlorine has been substituted not only by amide groups $-NH_2$, but also that other reactions must have

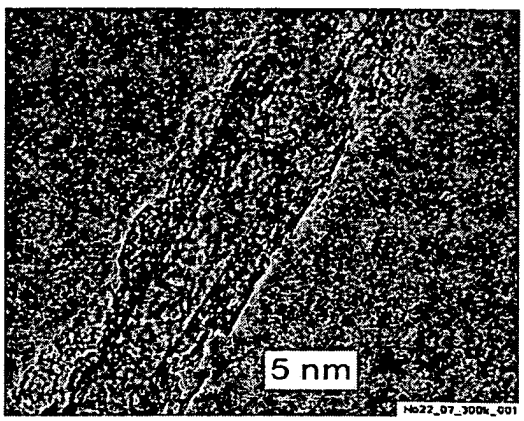

Fig. 6. TEM image of a damaged multi-walled nanotubes obtained after one day of electrolysis. Chlorine atoms may have penetrated the walls of the nanotubes and be located inside the tubes.

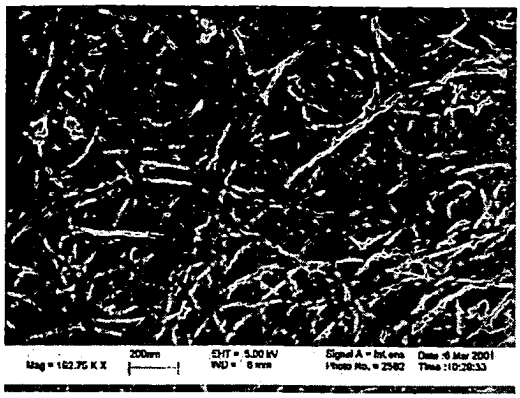

Fig. 7. TEM image of a bucky-paper with amino CNTs. Many nanotubes are linked together and form a complex, insoluble network.

occurred which link the nanotubes together to give big insoluble aggregates. For example:

$$R^*\text{–Cl} + \text{HO–}R^* + NaNH_2 \rightarrow R^*\text{–O–}R^* + NaCl + NH_3$$

$$R^*\text{–}NH_2 + R^*\text{–COOH} \rightarrow R^*\text{–NHCO–}R^* + H_2O$$

$$R^*\text{–}NH_2 + \text{HO–}R^* \rightarrow R^*\text{–}NH_3^+ + {}^-\text{O–}R^*$$

(R^* = MWNT)

The SEM picture in Fig. 7 gives an impression of how the nanotubes form a complex network.

The breakdown of the nanotube structure which occurs during the reaction of chlorinated nanotubes with triphenylmethyllithium may be caused by the great number of reaction sites on the tube surface. The close proximity of the sites does not leave enough space for many of the trityl groups to dock to the tube surface and so steric hindrance may lead to the structural breakdown of the nanotubes. The density of halogen atoms in the brominated nanotubes is lower than in the Cl nanotubes: 23 carbon atoms per Cl atom versus 180 carbon atoms for one Br atom. Therefore, the tube structure of the Br functionalized nanotubes is maintained during the treatment with triphenylmethyllithium and the modified nanotube paper can be recovered.

5. Conclusion

In this work it was demonstrated that "as deposited" MWNTs from a thermal CVD process can be modified by electrochemical treatment. The change in the composition of the nanotubes consists no only of the formation of C–Cl or C–Br bonds but also of the addition of oxygen to the nanotube lattice forming carboxyl and hydroxyl functions. These groups greatly improve the solubility in water or alcohol of the derivatives compared with the pristine nanotubes. The carbon–halogen functions formed can be subject to substitution reactions yielding amino nanotubes or trityl compounds. Since the nanotube structure is maintained the soluble material can be applied in an aqueous system on any surface for electric circuits and measurements. The chlorine and bromine carbon nanotubes offer a pathway to a wide spectrum of nanotube derivatives suitable for numerous applications.

Acknowledgements

The authors thank the working group of S. Roth, MPI Stuttgart for the ESCA spectra, R. Treichler and H. Cerva from Siemens CT for the TOFSIMS and TEM experimental work.

References

[1] P.G. Collins, P. Avouris, Nanotubes for electronics, Sci. Am. 12 (2000) 62.
[2] P.M. Ajayan, Chem. Rev. 99 (1999) 1787.
[3] K.D. Ausman, R. Piner, O. Lourie, R.S. Ruoff, J. Phys. Chem. B. 104 (2000) 8911.
[4] G.S. Duesberg, J. Muster, V. Krstic, M. Burghard, S. Roth, Appl. Phys. A 67 (1998) 117.
[5] A. Hirsch, Angew. Chem. 105 (1993) 1189.
[6] E.T. Mickelson, I.W. Chiang, J.L. Zimmermann, P.J. Boul, J. Lozano, J. Liu, R.E. Smalley, R.H. Hauge, J.L. Margrave, J. Phys. Chem. B 103 (1999) 4318.
[7] J. Liu, A.G. Rinzler, H. Dai, J.H. Hafner, R.K. Bradley, P.J. Boul, A. Lu, T. Iverson, K. Shelimov, C.B. Huffman, F. Rodriguez-Macias, Y.S. Shon, T.R. Lee, D.T. Colbert, R.E. Smalley, Science 280 (1998) 1253.
[8] J. Chen, M.A. Hamon, Y. Hu, Y. Chen, A.M. Rao, P.C. Eklund, R.C. Haddon, Science 282 (1998) 95.
[9] H. Ago, T. Kugler, F. Cacialli, W.R. Salaneck, M.S.P. Shaffer, A.H. Windle, R.H. Friend, J. Phys. Chem. B 103 (1999) 8116.
[10] R.J. Chen, Y. Zhang, D. Wang, H. Dai, J. Am. Chem. Soc. 123 (2001) 3838.
[11] S.C. Tsang, Y.K. Chen, J.F. Harris, M.L.H. Green, Nature 372 (1994) 159.
[12] B.W. Smith, M. Monthioux, D.E. Luzzi, Nature 396 (1998) 323.
[13] Y. Chen, D.T. Shaw, X.D. Bai, E.G. Wang, C. Lund, W.M. Lu, D.D.L. Chung, Appl. Phys. Lett. 78 (2001) 2128.
[14] M. Hirscher, M. Becher, M. Haluska, U. Dettlaff-Weglikowska, A. Quintel, G.S. Duesberg, Y.-M. Choi, P. Downes, M. Hulman, S. Roth, I. Stepanek, P. Bernier, Appl. Phys. A 72 (2001) 129.
[15] X. Xu, G.R. Brandes, Appl. Phys. Lett. 74 (1999) 2549.